Brigham Young University
BYU ScholarsArchive

All Theses and Dissertations

2007-08-15

Design and Fabrication of Out-of-Plane Silicon Microneedles with Integrated Hydrophobic Microchannels

Michael S. Diehl
Brigham Young University - Provo

Follow this and additional works at: https://scholarsarchive.byu.edu/etd

Part of the Mechanical Engineering Commons

BYU ScholarsArchive Citation

Diehl, Michael S., "Design and Fabrication of Out-of-Plane Silicon Microneedles with Integrated Hydrophobic Microchannels" (2007). *All Theses and Dissertations*. 1462.
https://scholarsarchive.byu.edu/etd/1462

This Thesis is brought to you for free and open access by BYU ScholarsArchive. It has been accepted for inclusion in All Theses and Dissertations by an authorized administrator of BYU ScholarsArchive. For more information, please contact scholarsarchive@byu.edu, ellen_amatangelo@byu.edu.

DESIGN AND FABRICATION OF OUT-OF-PLANE SILICON

MICRONEEDLES WITH INTEGRATED HYDROPHOBIC

MICROCHANNELS

by

Michael S. Diehl

A thesis submitted to the faculty of

Brigham Young University

in partial fulfillment of the requirements for the degree of

Master of Science

Department of Mechanical Engineering

Brigham Young University

December 2007

BRIGHAM YOUNG UNIVERSITY

GRADUATE COMMITTEE APPROVAL

of a thesis submitted by

Michael S. Diehl

This thesis has been read by each member of the following graduate committee and by majority vote has been found to be satisfactory.

Date	Brian D. Jensen, Chair
Date	Robert H. Todd
Date	Daniel Maynes

BRIGHAM YOUNG UNIVERSITY

As chair of the candidate's graduate committee, I have read the thesis of Michael S. Diehl in its final form and have found that (1) its format, citations and bibliographical style and consistent and acceptable and fulfill university and department style requirements; (2) its illustrative materials including figures, tables, and charts are in place; and (3) the final manuscript is satisfactory to the graduate committee and is ready for submission to the university library.

______________________	______________________________
Date	Brian D. Jensen Chair, Graduate Committee

Accepted for the Department

______________________	______________________________
Date	Matthew R. Jones Graduate Coordinator

Accepted for the College

______________________	______________________________
Date	Alan R. Parkinson Dean, Ira A. Fulton College of Engineering and Technology

ABSTRACT

INCREASED FLOW RATE IN OUT-OF-PLANE SILICON MICRONEEDLES USING HYDROPHOBIC MICROCHANNELS

Michael S. Diehl

Department of Mechanical Engineering

Master of Science

Microfabricated needles have the potential for inexpensive drug delivery without pain. The ability to deliver medication painlessly to patients will someday be not just hoped for but expected by the general public. The commercialization of this technology will also lead to other valuable technologies, such as systems that continually monitor and control insulin or other drugs in diabetic patients.

This research presents fabrication procedures developed to produce pyramidal-shaped microneedles with microchannels that will allow for fluid delivery. The microchannels are etched into the substrate surface of a [100] silicon wafer using inductively coupled plasma etching. After the channel etch a layer of silicon nitride is deposited onto the inner walls of the microchannels and on the surface of the substrate. The nitride on the

substrate surface provides the hard mask necessary to etch the microneedles, which are wet etched in a bath of potassium hydroxide (KOH). The selectivity of the KOH on [100] silicon is such that octagonal shaped pyramids are etched into the surface of the wafer. The pyramids are aligned with the previously etched microchannels to allow for needles with channels running through them. This research presents the first needles demonstrated with drug delivery channels running through the robust pyramidal needle shape.

In addition to the microchannel/microneedle fabrication procedure, microchannels were developed with inner structures as a method of creating hydrophobic surfaces on the inner walls of the channels. It was found that the channels developed had far too much variability in the diameter to accurately create a measurable reduction in flow; however, a loss coefficient was calculated showing increased flow rates in hydrophobically coated microchannels when hydrophobic structures are incorporated into the channel design.

It was also discovered that a hydrophobic coating, typically used to increase flow rates through a channel, can impede flow rate. There was no evidence found to suggest that hydrophobically coated microchannels of this size, with or without structures, will yield higher flow rates than non-coated microchannels.

ACKNOWLEDGEMENTS

Before all, I want to give the most heartfelt thanks and adoration to my wonderful wife, Mary Margaret. She has been a constant support and co-laborer through my undergraduate degree as well as both Master's degrees. Her love and companionship has given the journey purpose as well as made it bearable. I thank my two little children, Margaret and Joshua, for sending their daddy off happy to school and work each day with their smiles, laughs, and innocence.

I thank my parents for their example and encouragement of getting a good education. I'm grateful to my father, Stephen, for his insatiable (and hereditary) curiosity and example of hard work. I thank my mother, Cindy, for her love and caring support as well as her gentle guidance to discover new possibilities in my education and future career opportunities.

I thank my wife's parents, Lynn and Ann Summerhays for their acceptance of me as another son. Their interest and support in my work had been heartwarming. I also thank them for their incredible example of philanthropy and unquestioning aid. Through them, I have received the break I needed to be able to fulfill my dreams in grad school.

I thank my three committee members. Dr. Brian Jensen has been a trusted advisor and friend as I have clumsily ploughed my way through my research. I'm grateful for his

undeviating support, encouragement, and guidance in my work. I thank Dr. Robert Todd for his example to me and so many other students of high moral and religious principles intermixed with secular studies and occupations. Dr. Maynes has been a light at the end of many tunnels as I try to un-confound myself out of the mysteries of fluid dynamics. It was in his 512 class that I read a paper on "Nanoengineered Surfaces" that lead me to the inspiration that began this research.

I'm grateful for the friendship of so many engineers in the CMR lab. A big thanks to Brady Woolford, Kevin Jeffs, and Reese Garret in the microfluidics lab for their friendship and camaraderie. Brady, especially, has been a big help in showing me the finer points of testing fluid flow as well as giving me my initial introduction into the clean room.

My clean room expertise and confidence only exist because of the patient and unrewarded training I received from Josh Beutler. Beside the experience gained from my many failures, he taught me most of what I know how to do in the clean room. His training was supplemented by others at times, in particular Toa Shang, Yusheng Qian, and Evan Lunt.

Dr. Aaron Hawkins of the department of Electrical Engineering gave some great advice and direction concerning KOH etching and masking materials early on in the research and Dr. Greg Nordin of the department of Electrical Engineering has been a champion helping me understand the ICP process. I cannot thank him enough for allowing me to experiment with the equipment as I learned how to etch the microchannels. Dr. John Gardner of the department of Integrative Biology along with Mike Standing has been

invaluable in teaching me the use of the scanning electron microscope and giving encouragement along the way.

Thanks to Nate Rasmussen, a fellow Product Development student, for teaching me how to use LaTeX, Lisa Nelson with BYU printing services, for her help with high resolution transparencies. Thanks to Nancy Latta with the Stanford Nanofabrication Facility at Stanford University for her technical help concerning the DRIE process. Thanks to Joe Bussio of the BYU clean room for his technical support.

Thanks to Renea Beckstrand in the college of Nursing and representative of the IRB board for her advice and recommendations regarding possible human testing with the needles. Thanks to Burt Knudson for the Technology Transfer Office for his time and support regarding patenting in this research. Thanks to Kevin Cole in the department of mechanical engineering for all his time helping to wire the test stand and create a robust Labview program. Thanks to Sterling Anderson in the CMR lab for his skill in building the reservoirs used in the test stand.

Thanks to Kevin Mar and Victor Miller of IC Photomask for their help above and beyond the call of duty in ensuring that the lithography masks were manufactured correctly.

Thanks to Steve Brewer and Kellen Moulton for their patience and diligence while being trained in the many facets of this research, especially those things pertaining to the clean room. Best of luck to them in the future.

Lastly, I want to acknowledge the hand of God in my life and in this work. My faith has given meaning and joy to life and my prayers have been answered more times than I can count during the course of this research.

Table of Contents

Chapter 1 – Introduction 1
Chapter 2 – Literature Review 5
2.1 Microneedles 5
2.1.1 Microneedle Literature Review 5
2.1.2 Anisotropically Wet-Etched Microneedles 10
2.2 Hydrophobic Surfaces 13
2.2.1 Hydrophobic Surface Literature Review 13
2.2.2 Cylindrical Hydrophobic Microchannel Theory 18
2.3 Microchannel Flow 19
Chapter 3 – Design and Fabrication 23
3.1 Microneedle Parameters 23
3.2 Hydrophobic Lumen Parameters 26
3.3 Design Analysis 29
3.3.1 Microchannel Analysis 29
3.3.2 Microchannel Analysis 30
3.3.3 Microneedle KOH Mask Analysis 32
Simulation #1 33
Simulation #2 35
Simulation #3 36
Simulation #4 38
3.4 Fabrication Design Considerations 40
LPCVD Nitride 43
Photoresist 44
Mask 45
Lithography 45
RIE 47
KOH 47
HF 49
ICP Etch 49
Nanostrip 53
SEM 53
Chapter 4 – Microfabrication Results 55
4.1 Microneedles 55
4.1.1 Microneedle Fabrication 55
4.1.2 Microneedle Fabrication Analysis 64
4.1.3 Microneedle Modeling 69
4.2 Microchannels 77
4.2.1 Microchannel Fabrication 77
4.2.2 Microchannel Fabrication Analysis 78

4.2.3 Microchannels Fabrication Results ... 84
4.3 Combining Microchannels and Microneedles ... 87
4.3.1 Microneedle/Microchannel Fabrication ... 87
4.3.2 Microneedle/Microchannel Fabrication Results ... 89
Chapter 5 - Experimental Flow Results ... 93
5.1 Test Stand ... 93
5.2 Testing Procedure ... 103
5.3 Flow Results ... 105
Chapter 6 – Conclusion ... 123
6.1 Conclusion of Results ... 123
6.2 Recommendations for Future Research ... 124
6.2.1 Protective Needle “Cap” Over Channels to Prevent Clogging ... 124
6.2.2 Testing of Transdermal Fluid Delivery Rates ... 126
6.2.3 Silicon Micro-milling ... 127
6.2.4 Improved Channel Testing ... 128
References ... 129
Appendix A - Fabrication Precautions and Details ... 133
Spin Coating ... 133
Mask ... 134
Lithography ... 135
ICP Etch ... 137
Appendix B - Microneedle Fabrication Details ... 141
Karl Suss AZ3330 Settings ... 142
Type: Hard Contact Resist: Positive ... 142
Appendix C - RIE Operation Instructions ... 145
Appendix D - KOH Etch Experimentation ... 147
Etch #2 ... 147
Etch #3 ... 148
Etch #4 ... 153
Etch #5 ... 156
Etch #7 ... 158
Etch #8 ... 159
Etch #9 ... 160
Appendix E - Microchannel Fabrication Details ... 165
Karl Suss SPR-220 Settings ... 166
Type: Hard Contact Resist: Positive ... 166
Appendix F - ICP Etch Experimentation ... 169
Etch #1 ... 169
Etch #2 ... 171
Etch #3 ... 172
Etch #4 ... 173
Etch #5 ... 175
Etch #6 ... 177
Etch #7 ... 178
Etch #8 ... 179
Etch #9 ... 180

Appendix G - ICP Operation Instructions 183
Steps for using the ICP RIE for the Bosch Process 183
Appendix H - Human Pain Testing Draft for IRB Committee Approval......................... 185

List of Figures

Figure1-1: A cross sectional view of the outer layers of the human skin. A microneedle injected only as deep as the epidermis would be painless because it would not disturb the pain sensitive nerve endings located in the dermal layer of skin. 2
Figure 1-2: A droplet of water rests on the surface of a lotus leaf. The hydrophobic properties of the leaf cause the droplet to bead up into a nearly spherical shape which undergoes very little drag as is travels across the surface of the leaf....................3
Figure 2-1: An example of two single in-plane microneedles next to a human hair [3]. 6
Figure 2-2: Microneedles developed from single crystal silicon reported in (a) [5], (b) [6], (c) [7] and NiFe electroplating (d) [8]....................7
Figure 2-3: Cross-sectional view of the human skin modified from [10], showing the epidermis with its topmost layer, the stratum corneum, and the dermis underneath....................9
Figure 2-4: The shape of a square mask with compensation beams to be used in a KOH etch 11
Figure 2-5: (a) shows a pyramid etched half way with the mask still resting on the surface (b) shows a completely etched pyramid, the roughness of non-{411} planes can be seen at the base [12]. 12
Figure 2-6: Determining hydrophobicity of a surface by measuring the contact angle of a fluid droplet on that surface. (a) has a high contact angle and is therefore hydrophobic while (b) has a low contact angle making it hydrophilic. 14
Figure 2-7: The smaller the contact angle hysteresis (advancing angle minus receding angle) the greater the hydrophobicity. (a) is more hydrophobic than (b) due to its low hysteresis....................15
Figure 2-8: A microengineered structured surface and a fluid resting on top. A meniscus is formed over the gap that exists between each rib structure 16
Figure 2-9: A microstructured solid surface design will vary with the structure height (h_s), structure width (w_s), and gap width (w_g)....................17
Figure 2-10: Cross-sectional view of the structured lumen concept design 19
Figure 3-1: Octagonal microneedle design concept with smooth walled microchannels. (a) and (c) are side views, (b) is an overhead view, (d) is an angled view from above, and (e) is an angled view from underneath. 24
Figure 3-2: Square microneedle design concept with smooth walled lumen. (a) and (c) are side views, (b) is an overhead view, (d) is an angled view from above, and (e) is an angled view from underneath....................24

Figure 3-3: An overhead schematic of the needle and channel. The channel is offset 40μm from the center of the needle to avoid interfering with the tip of the needle. 25
Figure 3-4: Cross-sectional view of the structured lumen concept design 27
Figure 3-5: Microneedle design concept with structured lumen. (a) and (c) are side views, (b) is an overhead view, (d) is an angled view from above, and (e) is an angled view from underneath. 28
Figure 3-6: Images showing (a) a conceptual array of octagonal microneedles protruding from the base of a silicon substrate and (b) a magnified version of the same array 29
Figure 3-7: Mask used in the KOH simulation in Figure 3-8. 33
Figure 3-8: Simulation frames showing the resulting structure from the mask in Figure 3-7. 34
Figure 3-9: Mask used in the KOH simulation in Figure 3-10. 35
Figure 3-10: Simulation frames showing the resulting structure from the mask in Figure 3-9. 36
Figure 3-11: Mask used in the KOH simulation in Figure 3-12. 36
Figure 3-12: Simulation frames showing the resulting structure from the mask in Figure 3-11. 37
Figure 3-13: Mask used in the KOH simulation in Figure 3-14. 38
Figure 3-14: Simulation frames showing the resulting structure from the mask in Figure 3-13. 40
Figure 3-15: The essential steps in the microneedle fabrication process (a)-(i) and in the combined microchannel and microneedle fabrication process (j)-(t). 42
Figure 3-16: The concept of alignment strips on the mask allows near perfect orientation with the [100] plane of the wafer. 46
Figure 3-17: The basic design of a mask containing 9 separate quadrants each with an array of 64 individual needle masks. The alignment strips are shown on the bottom of the mask. 48
Figure 3-18: The isotropic etching produced by simply etching in an ICP process are shown in (a) while the anisotropic etching that results with alternative etching and passivation is shown in (b). 51
Figure 3-19: Over time the anisotropy of the Bosch process becomes apparent as the aspect ratio of a feature becomes greater. 52
Figure 4-1: Picture of the Teflon chuck and screws with a wafer clamped into it and ready for etching. 57
Figure 4-2: A schematic representation of the chuck resting in the dish filled with KOH which is in turn resting inside the heated tank full of water. 58
Figure 4-3: Time progression of a wafer after being immersed in KOH at about 78°C. As can be seen, bubbles begin to rise to the surface on the right hand side of the wafer and slowly spread throughout the entire wafer. Within two minutes of initial bubbling the wafer cannot even be seen because of the thick cloud of bubbles rising to the surface. 59
Figure 4-4: A clean room chart showing the etch rate of KOH as a function of temperature. At a temperature of about 79°C the etch rate should be just above 50μm/hour. 60

Figure 4-5: A wafer just after a KOH etching is seen on the left and the same wafer just after an etch in HF is seen on the right. The arrays of microneedles sectioned off from each other can be seen on the wafers in each picture. The white stripe in the middle is a reflection from an overhead light on the ceiling....62
Figure 4-6: A single silicon chip containing an 8X8 array of microneedles. 62
Figure 4-7: SEM images of fully etched microneedles. A side view of an octagonal needle is seen in (a) with angled views in (b) and (c) and an overhead view in (d). Side views of square needles are seen in (e) and (g), with and angled view in (f) and an overhead view in (h). 64
Figure 4-8: A general curve of needle structure height as a function of time showing the change in relative shape and size at particular points on the curve. 66
Figure 4-9: The maximum height of the needle and the etch time necessary to etch it will change according to the size of the mask used. The slopes will still remain constant. 67
Figure 4-10: (a)-(e) show SEM images of different size structures that have not reached the point of becoming needles yet. The cap on top of the structure is the same general height regardless of its width. A close up view is seen in (f) and an overhead view in (g). (h) shows that even square shaped needles will have this cap. 68
Figure 4-11: An individual array of needle masks. Each mask is $1050 \mu m^2$ and spaced 50μm from each other. This array is located in the center of the wafer as seen in Figure 4-12....70
Figure 4-12: Nine different arrays, each with the size of the square mask annotated in the top right hand corner of the cell, will yield nine different heights of needles at the end of an etch. 70
Figure 4-13: The depth etch rate, R_D, is the slope of the trend line formed from the time and depth of each etch. The point (0,0) is included as a data point as well....73
Figure 4-14: An overhead view of the mask and needle base outline. 74
Figure 4-15: Calculated values of ΔN and ΔT for experimental runs 9, 10, 12, 13, 14, and 16. Connecting lines are added for visual clarity. 75
Figure 4-16: Surface model showing the height of a microneedle as a function of the mask length and etch time....76
Figure 4-17: Microneedle etched with new 1115 μm length square mask. 77
Figure 4-18: The six different structured channels and control channel masks originally attempted are shown. Each quadrant contains a visual representation of the channel shape that existed in each array of that respective quadrant. All three control channels are the same size....79
Figure 4-19: Test structures designed to study selectivity of photoresist. In the top row all structures are 12μm high and vary in width from 10-30μm increasing incrementally by 2μm for each set of three. The second and third row have the same width structures as the first row only the height increases to 16 then 20μm in the second and third rows respectively. 80
Figure 4-20: A view of the original selectivity mask overlaid on an SEM image of the results features etched with the mask. This and other data were used to

determine the etching characteristics of the features. The shapes below the structures are reference marks. 81
Figure 4-21: Each channel design is shown in the quadrant where an array of the corresponding channel is located. The control channels were designed to increase in diameter and thereby have an equal diameter to that of the effective inside diameter of the structured channels. 83
Figure 4-22: Each quadrant of the mask shows the design number (ie: 7-12 in the top left quadrant, representing 7 structures each 12µm wide) and a picture taken through an optical microscope of the surface of one of the channels. 84
Figure 4-23: An optical microscope view of a typical 7-12 channel on the top surface (left) and on the bottom surface (right) of the wafer. These two pictures were taken at identical magnification. 85
Figure 4-24: A cross-sectional SEM view of a microchannel (a) 660 µm deep shows blowout at the bottom. A close-up view in (b) shows the blowout again. 86
Figure 4-25: Proportional SEM images of the front (a) and back side (b) of a channel in quadrant 5 of the wafer. The rough, high contrast, surface in (b) is an overhead view of the blowout that occurs in etching. Also noted is the fact that the structures will lose some of their definition by the end of the channel. 86
Figure 4-26: Representative SEM images of channel profiles in each quadrant space as shown in Figure 4-22 showing the general definition of the structures in each 660 µm long channel...87
Figure 4-27: Multiple views of a microneedles combined with microchannels. The channel is about 95µm in diameter and the needle base, measuring from opposing corners, is about 295µm. 89
Figure 4-28: The needle and channels masks were not accurately aligned in this sample. This revealing SEM image (of sample that did not undergo an HF rinse to strip the nitride) shows long thin nitride cylinders where microchannels once were. This sample was etched in KOH to a depth of about 435µm. 91
Figure 5-1: The complete test stand used to test the flow rates through the microchannels 94
Figure 5-2: The picture on the left shows the reservoirs, pressure transducer behind them, and solenoid valve behind and to the left of the pressure transducer. The picture on the right is a close up view of the small reservoirs. The black strip in the middle of the two reservoirs is the two rubber inserts with an array of microchannels in between them. 95
Figure 5-3: A side view of the two small reservoirs with an array of microchannels in between. The water flows into the top on the left side, through the channel in the middle of the system, and back out on the right hand top side....................96
Figure 5-4: Views of mating surfaces of the (1) reservoir, (2) rubber sealer, and (3) microchannel array can be seen above, while the exploded assembly view of these components can be seen below. 96
Figure 5-5: The reservoir assembly is sectioned out (above) views A-E and the cross-sectional cutaways are show (below). (A) Shows the “in-flow” reservoir, a rubber seal is in place in (B), the microchannel array is added in (C), in

(D) the other rubber seal sandwiches the array, and in (E) the "out-flow" reservoir is put into position. 97
Figure 5-6: A schematic of the small reservoirs and all interacting equipment. 99
Figure 5-7: A physical wiring schematic of all equipment used in the test stand. 100
Figure 5-8: A photograph of the wiring necessary to run and monitor the equipment used in the test stand. 101
Figure 5-9: A view of the operating window used for experimental test runs. 102
Figure 5-10: The schematic diagram of the Labview program used to operate and record data from the test stand. 103
Figure 5-11: An exaggerated depiction of the channel entry region on the left and the exit on the right. The top channel measures inside diameter for a hydrophobic channel. Because the channel walls taper this diameter is smallest at the exit. The bottom channel measures the outer limits of the cross-section for calculating hydraulic diameter. Again, an inaccurate calculation due to the tapering of the walls. 106
Figure 5-12: The large diameter entrance to the channel is shown in (a), while (b) shows the small diameter entrance to the channel. The arrows show the directionality of fluid flow through the channels. 108
Figure 5-13: This SEM image shows the front and back side of one of the channels in the sample #1 array. Note that the scale of the two images is not the same. 109
Figure 5-14: The steady state testing for sample #1 showing hydrophobically coated and non-coated test runs for flow entering both the large diameter opening and small diameter opening of the channels. 109
Figure 5-15: This SEM image shows the front and back side of one of the channels in the sample #3 array. Note that the scale of the two images is not the same. 110
Figure 5-16: The steady state testing for sample #3 showing hydrophobically coated and non-coated test runs for flow entering both the large diameter opening and small diameter opening of the channels. 110
Figure 5-17: This SEM image shows the front and back side of one of the channels in the sample #4 array. Note that the scale of the two images is not the same. 111
Figure 5-18: The steady state testing for sample #4 showing hydrophobically coated and non-coated test runs for flow entering both the large diameter opening and small diameter opening of the channels. 111
Figure 5-19: This SEM image shows the front and back side of one of the channels in the sample #5 array. Note that the scale of the two images is not the same. 112
Figure 5-20: The steady state testing for sample #5 showing hydrophobically coated and non-coated test runs for flow entering both the large diameter opening and small diameter opening of the channels. 112
Figure 5-21: This SEM image shows the front and back side of one of the channels in the sample #6 array. Note that the scale of the two images is not the same. 113
Figure 5-22: The steady state testing for sample #6 showing hydrophobically coated and non-coated test runs for flow entering both the large diameter opening and small diameter opening of the channels. 113
Figure 5-23: Three channel profiles show an empty channel cross section on the left, a hydrophobically coated channel with water running through in the middle, and a non-coated channel with water running through on the right. 117

Figure 5-24: This SEM image shows the front and back side of one of the channels in the sample #9 array. Note that the scale of the two images is not the same. 114
Figure 5-25: The steady state testing for sample #9 showing hydrophobically coated and non-coated test runs for flow entering both the large diameter opening and small diameter opening of the channels. 115
Figure 5-26: The steady state results of the hydrophobically coated control channels. The first and third runs were done through the small diameter entry and the second run was done through a large diameter entry. This test run was unique in that the channels were not dried out between runs of different flow directions. 118
Figure 5-27: Plot showing the steady state K_L results for all test samples including control channels. 120
Figure 5-28: Plot showing the steady state K_L results, on a log scale, for all test samples except the control channels. This plot without the control channels allows for a more detailed view of the structured channel K_L results. 121
Figure 6-1: Microneedle concept with a lumen diameter of 48 µm opening up about half way up the structure. (a) and (b) are angled views from above, (c) is a view from directly overhead, (d) and (f) are side views, and (e) is an angled view from underneath..125
Figure 6-2: Microneedle design concept with structured lumen. (a) and (b) are angled views from above, (c) is a view from directly above, (d) is an angled view from underneath, and (e) is a side view 125
Figure 6-3: Images showing (a) a conceptual array of microneedle protruding from the base of a silicon substrate and (b) a magnified version of the same array 126

Figure A-1: The viewing range through a mask is shown with the outline of a typically oriented wafer inside the Karl Suss lithography machine. 130
Figure A-2: The viewing range through a mask is shown with the outline of a re-oriented wafer modified for alignment with the mask inside the Karl Suss lithography machine..137
Figure D-1: The slender pinwheel shaped mask in (a) created nubs like the one seen in (b)...147
Figure D-2: The mask in (a) created the structure in (b) 148
Figure D-3: The mask in (a) created the structures in (b), an angled view and (c), an overhead view of the same structure...149
Figure D-4: The mask in (a) created the structures in (b), an angled view and (c), an overhead view of the same structure...150
Figure D-5: The mask in (a) created the structures in (b), an angled view and (c), an overhead view of the same structure...151
Figure D-6: The mask in (a) created the structures in (b), an angled view and (c), an overhead view of the same structure...152
Figure D-7: The mask in (a) created the structures in (b), an angled view and (c), an overhead view of the same structure...153

Figure D-8: The mask in (a) created the structures in (b), an angled view and (c), an overhead view of the same structure. 154
Figure D-9: The mask in (a) created the structures in (b), an angled view, (c), an overhead view, and (d) a close up view of the same structure, ...155
Figure D-10: A mask with member widths greater than that of Figure D-8 and smaller than that of Figure D-9 was used to create the structures seen in (a) and (b). 155
Figure D-11: The mask in (a) was used to create the needle seen in (b). An array of these same needles can be seen in (c). 156
Figure D-12: The mask in (a) was used to create the structure in (b). An array of these structures can be seen in (c). 157
Figure D-13: The various sizes of the mask in (a) were used to create various needles (b) or “unfinished” needles (c). 158
Figure D-14: The structure in (a) was formed with a mask similar like that in Figure D-13. The needle in (b) was etched to the point that it almost disappeared altogether. An array of needles is shown in (c) and a mis-formed needle due to a mask with a poor pattern transfer from a blemish in the photoresist is shown in (d). 159
Figure D-15: The square mask in (a) was used to create the unfinished needles seen in (b) and (c). 160
Figure D-16: The 1100µm square mask in (a) created the needles in (b) – (e) shown from various angles. 161
Figure D-17: The mask in (a), with 20µm square pinwheel members, created square needles like those seen in (b), (c), and (d). The height of the needles varied depending on whether the body of the mask was a 900, 945, or 990µm square. 162
Figure D-18: The mask in (a), with 40µm square pinwheel members, created structures like those seen in (b), (c), and (d). The width of the structures varied depending on whether the body of the mask was a 900, 945, or 990µm square, but all heights of these structures were the same. 163
Figure F-1: This channel is 110µm deep and shows the ridges of the channel just as they appear on the mask. A polymer residue has been left on the surface of the wafer. 170
Figure F-2: When the photoresist for the second etch was spun on, it flowed around existing hole like water around a rock. Three levels can be seen here. The top level is the egg shaped hole that etched from the top surface during the second etch period. The second level is the last remnants of hole from the first etch period. This is estimated to be about 10µm thick. The hydrophobic structures can still be seen along the perimeter. The third level is the rough walled circle in the middle. This is about 100µm deeper than the initial etch so it reaches about 210µm into the wafer substrate. It was etched during the second etch period. 170
Figure F-3: The three images here show sequentially zoomed-in portions of the same hole. Small ridges can be seen clearly when zoomed in sufficiently indicating the distance that is etched during each etch/passivation cycle of the ICP process. 171

Figure F-4: Here, a close-up view of a single channel that has undergone the double etch process shows the effects that take place after long periods of etching. In the image on the right, the small ridges that indicate a good sidewall are being etched away and large sidewall striations are left in their place. 171
Figure F-5: A top and side view shows where bubbles formed in the photoresist and created large holes in the substrate. The left image shows a small hole intentionally created from the mask just above the two accidental holes. 172
Figure F-6: Top and side views of a hole that was etched around the perimeter but had too much unexposed (and therefore undeveloped) photoresist blocking the etch. This physical phenomenon is known as “grass” and is a result of micromasking which can occur from photoresist or from heavy passivation...173
Figure F-7: A series of images shows the same double hole progressing from a side to a top view. As can be determined from the stalagmite looking structures at the base of this hole, there was slight micromasking during the etch.................175
Figure F-8: A series of angles reveals the quality of the etch recipe on a single channel. The channel tapers at the bottom and heavy striations on the side wall are revealed. 177
Figure F-9: These two images were taken at the same magnification and show the difference in diameter of the same size hole between the top and the bottom side of a wafer. The image on the right shows the “blowout” that occurs at the bottom of the wafer due to the nitride mask on the backside of the wafer. 177
Figure F-10: This image shows an intentional hole (on the right) next to a “burnt” hole (on the left). The accidental hole has a different sidewall profile from that in etch #2 and is most likely due to a poor application of photoresist. 178
Figure F-11: The image of this channel reveals how a poor recipe can give disappointing results. It is interesting to note that the top surface of the wafer rises a little at the mouth of the hole. This is the way the photoresist settles on top of the wafer but as the photoresist is burned through, as happened on this etch, it elevation differences are magnified onto the substrate. 179
Figure F-12: A fairly anisotropic channel going all the way through the wafer is shown. 180
Figure F-13: Although a perfect cross-section of this channel hasn’t been made yet, surveying this channel gives good indications of decent anisotropy. The image on the right shows a close-up view of the blowout that has occurred.......181
Figure H-1: Images of microneedles from other research groups (Gardeniers 2003, Stoeber 2005, Griss 2003, McAllister 1999) 186
Figure H-2: CAD images of the BYU microneedle designs with and with out channel structures. (Diehl 2005) 187
Figure H-3: Computer rendering of a silicon chip of an array of microneedles without channels. This would be used for the testing of pain associated with needle insertion...188

Figure H-4: Computer renderings of a silicon chip of an array of microneedles with channels. This would be used for the testing of needle structure integrity associated with insertion. 189

List of Tables

Table 2-1: Tabulated thickness for the human epidermis and the stratum corneum at various body locations [11]..........9
Table 3-1: The design parameters and significant values for the four lumen designs..........27
Table 4-1: The lateral etch rate values for each mask in each run. Each value is equal to d_2 divided by T. Some of the values are left blank because they correspond to underdeveloped needles..........74
Table 4-2: The left column shows the design identification, labeled just as those in Figure 4-21, along with the predicted or desired identification number that should correspond to the fully etched channel..........83
Table 4-3: The design I.D. of each array is shown with the quadrant number in which it is located and the calculated cavity fraction, F_c, based on the measurement of cross-section of the channel at the top of the wafer surface..........87
Table 5-1: Hydraulic diameter, D_h, for five different cavity fractions including three standard deviations accuracy. These measurements were taken from the "sample 12" arrays, "sample 13" are about 90% this size..........105
Table 5-2: A comparison of steady state flow rates. For each sample the channel characteristic is identified that has the highest flow rate. ie: the coated and non-coated sample #1 curves were compared against each other; for the two large opening curves, the coated date set had the higher steady state flow rate. The symbol, "--" means that both curves have matching steady state flow rates..........116

Table A-1: The units used in each parameter setting of an ICP process for both the etch and passivation cylces..........137
Table A-2: The desired outcome of several etching attributes is shown next to the necessary adjustment that need to be made to several parameters of the ICP machine..........139
Table E-1: The most up-to-date recipe used in the ICP process for etching microchannels..........167
Table F-1: Recipe used in etch #1..........169
Table F-2: Recipe used in etch #2..........172
Table F-3: Recipe used in etch #3..........173
Table F-4: Recipe used in etch #4..........173
Table F-5: Recipe used in etch #5..........175
Table F-6: Recipe used in etch #6..........178
Table F-7: Recipe used in etch #7..........179
Table F-8: Recipe used in etch #8..........180
Table F-9: Recipe used in etch #9..........181

Chapter 1 – Introduction

We live in an age of rapidly advancing medical techniques where we, as patients, demand less painful and less invasive procedures in our medical treatments. One medical treatment that we are all familiar with is receiving injections for vaccines and medication. This is a painful experience and many patients will postpone or ignore their necessary medical attention in order to avoid an unpleasant visit to the doctor's office. Many of us have an aversion to medical treatments that has originated from traumatic experiences nearly in our infancy.

The American Academy of Pediatrics recently reported:

> Acute pain is one of the most common adverse stimuli experienced by children, occurring as a result of injury, illness, and necessary medical procedures. It is associated with increased anxiety, avoidance, somatic symptoms, and increased parent distress. Despite the magnitude of effects that acute pain can have on a child, it is often inadequately assessed and treated. … Pediatricians are responsible for eliminating or assuaging pain and suffering in children when possible [1].

A simple injection at a young age can have far reaching psychological effects causing us to view medical treatments in a negative light. Although most patients expect to receive injections only on an infrequent basis, this is not always the case. One group of people who experience pain due to frequent injections are those, such as diabetics, who must take injections regularly. Aside from the pain associated with needle injections there are

other concerns as well. Medical assistants work with the threat of contaminating themselves with blood-born pathogens through accidental needle pricks. Injections can also be difficult to administer in a non-clinical environment and often require trained personnel. Due to the great amount of discomfort and inconvenience suffered throughout the world from current methods of injection it is anticipated that a painless form of transdermal drug delivery would be well received.

Within the past few years a number of researchers have begun testing and refining transdermal drug delivery through the use of microfabricated needles. These microneedles are so small that they are capable of delivering medication in the top layer of skin, or epidermis (see Figure1-1), but will not penetrate deep enough to disturb the nerve endings, thus eliminating the pain associated with the injection.

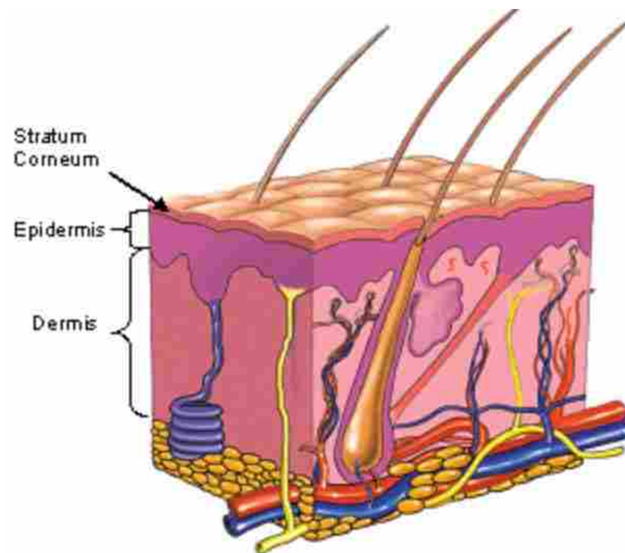

Figure1-1: A cross sectional view of the outer layers of the human skin. A microneedle injected only as deep as the epidermis would be painless because it would not disturb the pain sensitive nerve endings located in the dermal layer of skin.

One of the obstacles that seems to dominate the effectiveness of microneedles is the very low fluid flow rate that can be achieved through the microchannel, or lumen, of the needle when using reasonable pumping pressure. One step that has been taken to improve this problem is to increase the number of microneedles used at the area of insertion. A dense array of microneedles will have a higher overall fluid delivery rate than will a single microneedle. However, more improvements can be made. Another method that is used to increase flow rate is by making the walls of the channels water repellent, or hydrophobic.

Hydrophobic surfaces have been observed in nature for quite some time and one common example is the lotus leaf which repels water to help keep the surface of the leaf free of contaminants (see Figure 1-2). So popular is this example of hydrophobicity that the term “lotus effect” has been adapted for surfaces that display hydrophobic properties [2]. The lotus effect can be mimicked within microneedles by increasing the surface roughness of the channel walls at the micro level.

Figure 1-2: A droplet of water rests on the surface of a lotus leaf. The hydrophobic properties of the leaf cause the droplet to bead up into a nearly spherical shape which undergoes very little drag as is travels across the surface of the leaf.

The primary purpose of this research is to demonstrate the fabrication process necessary to create an array of microneedles containing microchannels. The secondary purpose of this research is to show that microchannels with a micro level surface roughness will cause greater hydrophobicity and therefore an increased flow rate for a given pumping pressure.

It is anticipated that this work, accompanied with other existing research, will lead to the general improvement of medical procedures involving injections. With a system available for painless hypodermic injections patients can expect a more pleasant experience at the doctor’s office and the negative connotations associated with medical practices will begin to subside.

Chapter 2 – Literature Review

2.1 Microneedles

2.1.1 Microneedle Literature Review

Our world has seen amazing enhancements to everyday life due to the ever-advancing technologies in microfabrication. The medical community, in particular, has great potential for improvement with the use of microfabricated products. One microfabricated product that shows great promise for medical procedures around the world is the microneedle. These devices are designed with two purposes: drug delivery to the patient and blood extraction from the patient for biosampling.

The fabrication processes for micro-sized products are still relatively new and great creativity is often necessary to fabricate a micro-sized product that would be otherwise simple to create at a macro level. Fluid flow at the micro level is also more difficult to achieve than at the macro level. This is due to the fact that the pressure needed to give identical flow rates as those in a typical macro sized hypodermic needle are much greater in smaller microneedles. The complexities due to limitations in microfabrication and the unique considerations of microfluidic flow necessitate creative approaches in order to produce a microneedle design that can compete with currently-used needles in the medical field.

The research of microneedles originally began with an "in-plane" microneedle design [3, 4]. These were fabricated from single crystal silicon as a single long slender needle in which the needle and fluid channel (lumen) ran *parallel* to the substrate of the silicon wafer. However, due to the size of the lumen, these needles did not allow for very large flow rates (see Figure 2-1). Attempts have been made to fabricate several in-plane microneedles as a single unit because increasing the number of needles will increase the flow rate. Unfortunately, these are time consuming and complicated to produce and awkward to use anyway due to the possibility of the ends breaking off while under the surface of the skin. Many research groups have now begun to fabricate "out-of-plane" microneedles [5-8]. These are microneedles where the lumen is fabricated *perpendicular* to the substrate. Compared to complex in-plane microneedles, out-of-plane microneedles are very easy to fabricate in arrays of needles which helps increase the fluid flow rate possible from a single injection.

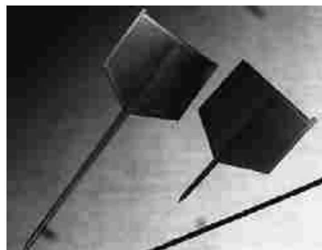

Figure 2-1: An example of two single in-plane microneedles next to a human hair [3].

Microneedles take on a variety of shapes, sizes, and fabrication processes. Often one shape will necessitate certain fabrication techniques that another will not. The images in Figure 2-2 show several different microneedle designs that have been fabricated throughout the world. Most out-of-plane microneedles are made of single crystal silicon,

silicon dioxide (SiO_2), or some type of metal which is electroplated onto a removable mold.

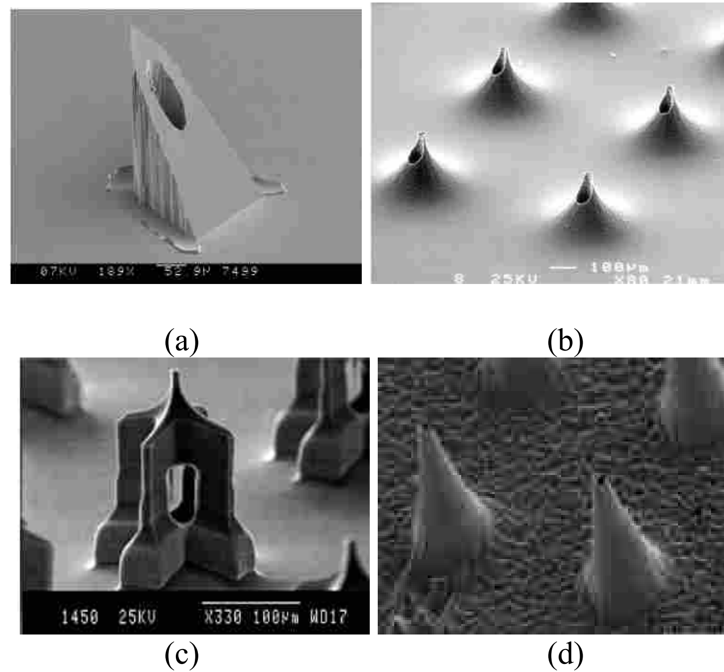

Figure 2-2: Microneedles developed from single crystal silicon reported in (a) [5], (b) [6], (c) [7] and NiFe electroplating (d) [8].

The shape of a microneedle must not be determined by fabrication techniques alone but also by considerations of interaction with the skin. A microneedle must be designed with the ability to puncture the skin easily. This includes having a relatively sharp tip and a needle with a fairly high aspect ratio (the ratio of height to base length) as well as a lumen positioned correctly so that it doesn't plug up during skin penetration. Understanding the different layers of the skin will enable a better design of microneedle for more efficient skin penetration.

The human skin is composed of three primary layers; the topmost layer is the epidermis, the layer underneath that is the dermis, and the deepest layer is the hypodermis. The two major layers of concern in the epidermis are the stratum corneum and the stratum spinosum. The topmost layer of the skin, which is what is exposed to the outside environment of the body, is the stratum corneum. The stratum corneum is composed of thick, dry, compacted skin cells. This layer is denser than other layers of the skin and thus acts as a protective layer against contamination and harsh contact with other objects. The stratum corneum is followed by two very thin layers called the stratum lucidum and the stratum granulosum. These layers are followed by the relatively thick stratum spinosum, the other primary layer of the epidermis. Between this layer and the dermis, which is the secondary layer of the skin after the epidermis, lies a thin separating layer called the stratum basale. The thickness of these layers will vary depending on where they are in the body but generally the stratum corneum is less than 40 μm thick and the epidermis is between 0.2 and 0.3 mm thick. However, the epidermal layer of skin has been reported to be as much as 1.5 mm thick [9]. A simple cross section of the human skin can be seen in Figure 2-3.

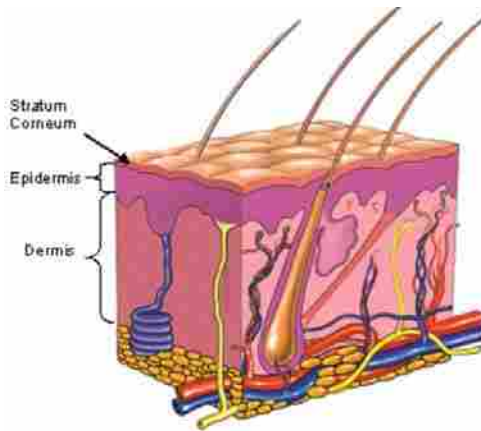

Figure 2-3: Cross-sectional view of the human skin modified from [10], showing the epidermis with its topmost layer, the stratum corneum, and the dermis underneath

Some typical approximate thicknesses of the stratum corneum and the entire epidermis at different regions of an adult body are tabulated in Table 2-1.

Table 2-1: Tabulated thickness for the human epidermis and the stratum corneum at various body locations [11].

Body Location	Full Epidermal Thickness (μm)	Stratum Corneum Thickness (μm)
Elbow	325	70
Knee	210	35
Leg	195	35
Chest	205	25
Palm	210	45

In general, a microneedle must be able to penetrate at least 40 μm into the surface of the skin, through the stratum corneum, in order to be used effectively for transdermal drug delivery. A microneedle designed solely for transdermal drug delivery, however, should not penetrate much deeper than the epidermal layer of the skin. This layer is capable of absorption of fluids [9] and the delivery of medication will be painless. The second layer of the skin is the dermis. This layer is typically much thicker than the epidermis. At the

top-most part of this layer nerve endings and blood vessels begin to appear. A microneedle that is designed for blood extraction should be long enough to penetrate into the dermis. This is because it is necessary to reach the blood vessels in the dermis in order to extract blood for sampling. Unfortunately, a microneedle will not encounter blood vessels without also encountering the nerve endings in the skin. Thus, blood extraction with a microneedle may sometimes be accompanied with at least a small degree of pain; however, if the microneedles are slender enough and don't penetrate the dermis too deeply then contact with the nerves will be kept to a minimum and the pain associated with blood extraction will be minimal as well. For instance, Moon and Lee have performed painless blood extraction from the dermal layer of skin [9].

2.1.2 Anisotropically Wet-Etched Microneedles

The microneedle that will be fabricated for this research is a pyramidal shaped needle with either an octagonal or square shaped cross section. Examples of these needles have been made by Offereins and Dizon [12, 13]. The needle is created by applying a mask to the surface of the (100) silicon substrate and submersing it in a KOH-water solution to give a wet anisotropic etch. It has been found that a KOH-water solution will underetch a mask at different rates on the different crystallographic planes of the silicon. For a (100)-oriented silicon substrate the fast etching plane is the {411} plane, meaning that this is the plane that is exposed in a KOH etch because material is etched along the surface of this plane faster than in any other direction [12-16]. Theoretically, by placing a square mask oriented along the $\langle 110 \rangle$ direction of a wafer, a uniform three-dimensional trapezoid can be formed having four {411} oriented walls. This results from the

underetching of the four convex corners on the square mask. In reality, experimental result from this research (discussed in chapter 4) show a four sided needle is not produced but rather an eight sided needle.

The etching of a four sided truncated pillar with {411} oriented sides is not possible using a square mask. This shape of mask will not allow etching at only four planes at the same time. To compensate for this problem compensation beams are added to the ends of the square mask, as shown in Figure 2-4. The compensation beams allow four alternating {411} planes to be etched while the other four are left unexposed in the etching process. The resulting four {411} planes of the truncated pyramid are smooth and well defined even at considerable depths from the surface of the mask [12] although a significant amount of surface roughness exists at the base of the needles.

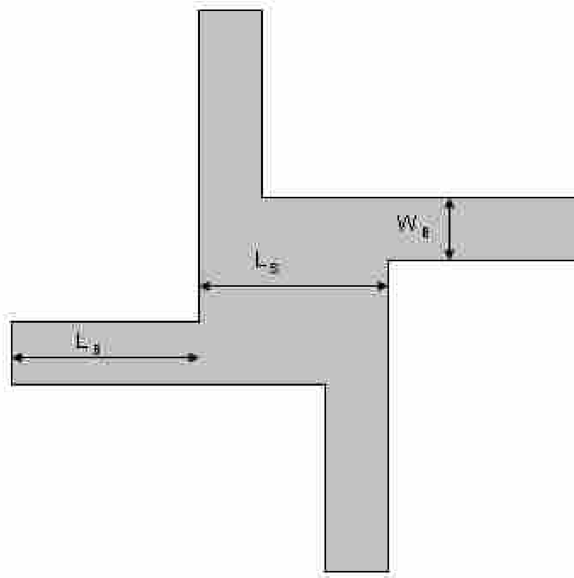

Figure 2-4: The shape of a square mask with compensation beams to be used in a KOH etch

The depth of the etch is controlled by the amount of time that the substrate is left in the aqueous KOH-water solution. The depth to which the pyramid can be etched before the four {411} walls meet can be increased by extending the length of the compensation beams on the etch mask. It is anticipated that with the proper dimensions of the mask and a proper exposure time in the solution a four sided pyramid will be produced that looks similar to the pyramid in Figure 2-5.

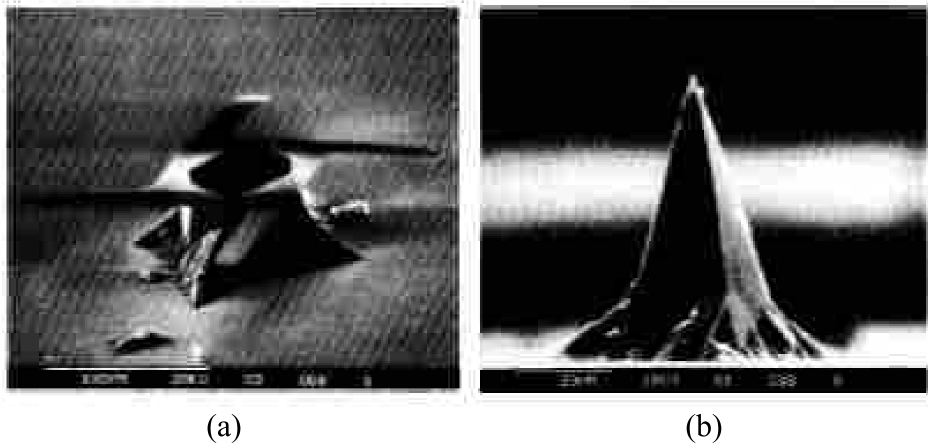

(a) (b)

Figure 2-5: (a) shows a pyramid etched half way with the mask still resting on the surface (b) shows a completely etched pyramid, the roughness of non-{411} planes can be seen at the base [12].

In the design phase of this research, this microneedle design will be repeated over the substrate surface so as to form an array of microneedles on the silicon substrate. This array will consist of 50 to 100 microneedles, depending on the spatial constraints of the microneedle masks. It should be remembered that if the needles are placed too closely together a “bed of nails” effect may occur which would prevent the needles from properly penetrating the stratum corneum layer of the skin.

Current research has only progressed to the point of making these needles solid with no existing channel for drug delivery. They are currently capable of being dipped in medication and punctured into the skin with the hope that the medication coating the needles will be transferred to the epidermis and absorbed by it. One of the purposes of this research will be to find a way to create these needles with microchannels running through them so that they can facilitate a more effective drug delivery.

2.2 Hydrophobic Surfaces

2.2.1 Hydrophobic Surface Literature Review

As mentioned earlier, high fluid flow rates at the micro-level are difficult to attain at low pumping pressure. In addressing the issue of low fluid flow rate in microneedles, results from other studies in the field of microchannel flow are valuable. One way that has been found to improve microfluidic flow is through the use of hydrophobic and superhydrophobic channels. A hydrophobic surface is one that repels water and other similarly viscous fluids. The easiest way to identify a hydrophobic surface is to view a droplet of fluid on that surface. As the droplet rests on the surface it forms an angle between the fluid and the solid. This angle is referred to as the contact angle. The contact angle is determined by observing the angle made between the solid surface and the droplet as shown in Figure 2-6. A fluid-solid interface that forms a contact angle any greater than 90° is considered a hydrophobic surface while anything below 90° is a hydrophilic surface. The higher the contact angle, the more hydrophobic the surface is. If the contact angle is exactly 90° then the surface is considered neither hydrophobic nor hydrophilic.

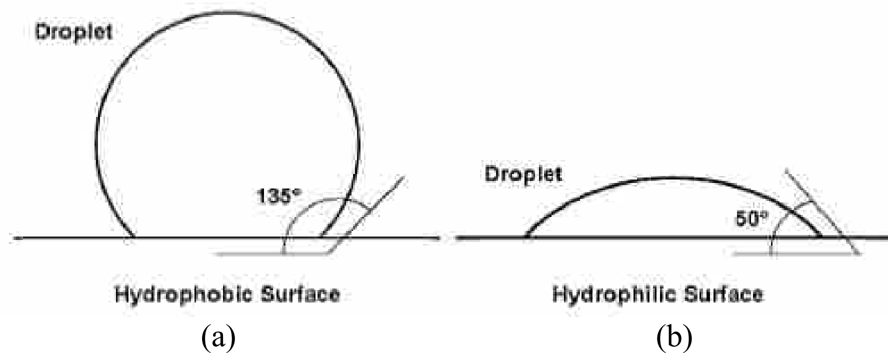

(a) (b)

Figure 2-6: Determining hydrophobicity of a surface by measuring the contact angle of a fluid droplet on that surface. (a) has a high contact angle and is therefore hydrophobic while (b) has a low contact angle making it hydrophilic.

A second test of hydrophobicity is to measure the contact angle "hysteresis" of the droplet. The angle hysteresis is determined by measuring the difference between the advancing and the receding angles of a droplet as it moves across the surface of a solid (see Figure 2-7). The smaller the angle hysteresis is, the more hydrophobic the solid surface is. The angle hysteresis is important because it is a good way to determine the flow resistance of a fluid on a solid surface. Regardless of whether the contact angle of a solitary stationary droplet is high or low, if the droplet moves across the surface only with great difficulty then the surface can hardly be considered hydrophobic in any practical sense [17]. Likewise, regardless of whether the contact angle of a solitary stationary droplet is high or low, if the droplet glides across the surface with great ease then the surface can be considered hydrophobic for many applications requiring low flow resistance. However, in general a droplet must have both a high contact angle and low angle hysteresis to be considered hydrophobic.

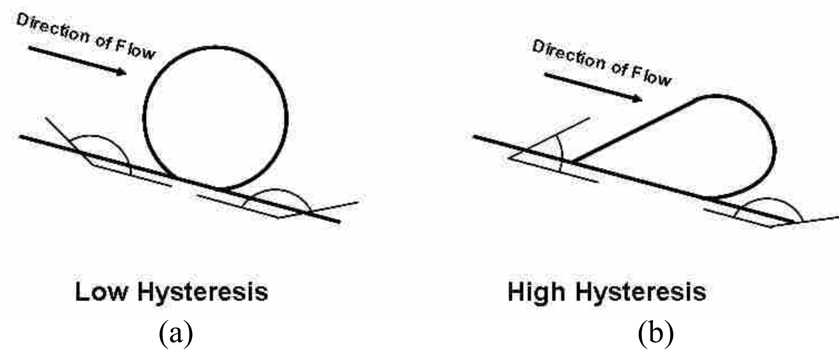

(a) (b)

Figure 2-7: The smaller the contact angle hysteresis (advancing angle minus receding angle) the greater the hydrophobicity. (a) is more hydrophobic than (b) due to its low hysteresis

Hydrophobicity of a surface is caused in two ways. The first cause of hydrophobicity is the surface structure of a solid. Different materials have different amounts of surface energy and the less surface energy a material has the more hydrophobic that material will be. The surface energy of a solid is not only affected by its material composition but also by the microstructure of that surface. Reduced contact between a surface and a fluid at the fluid-solid interface causes the solid to be more hydrophobic. This occurs frequently in nature. The surfaces of many plant leaves, like the lotus leaf, are quite rough at the microscopic level. Observation of water on a lotus leaf shows that the droplets bead up on the surface and will roll off the leaf quite easily. This effect takes place on many substances and is fairly common in nature. Due to the familiarity of this phenomenon associated with the lotus leaf it is often referred to as the "lotus effect" [2].

A better conceptual understanding of this phenomenon comes when considering a surface that is evenly covered with microstructures, with a fluid layer on top, as seen in Figure 2-8. The gap between the structures can be made small enough that the fluid will form a meniscus over it, preventing the gap from wetting. The maximum size of this gap is determined by the surface tension of the fluid, the pressure gradient imposed on the fluid,

and the hydrophobicity of the fluid-solid interface (which can be measured by the contact angle of the droplet). As a fluid flows over this surface, the reduced surface contact on the fluid for a given area will show reduced drag on the fluid over that area and thus give an increase in fluid velocity. This leads to an increase in the flow rate of that fluid for a given pressure drop.

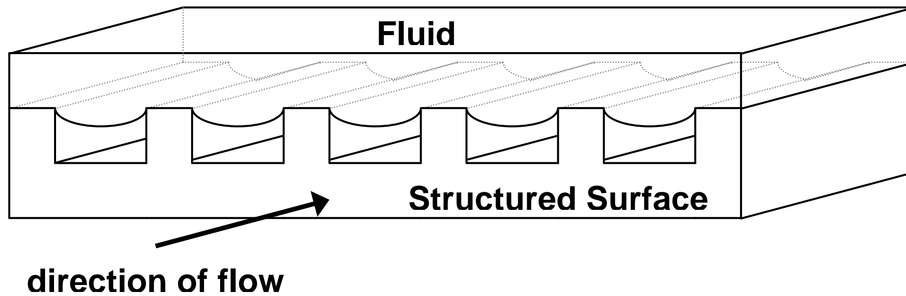

Figure 2-8: A microengineered structured surface and a fluid resting on top. A meniscus is formed over the gap that exists between each rib structure

An important parameter for this type of homogeneously structured surface is referred to as the cavity fraction, F_c (see Equation 2-1). The cavity fraction is simply the fraction of the width of a single gap between structures divided by the sum of the width of a gap and the width of a structure (see Figure 2-9). It has been shown that for increasing F_c the flow rate for a given pressure drop through a microchannel increases [18].

$$F_c = \frac{w_g}{w_s + w_g} \quad \textbf{(2-1)}$$

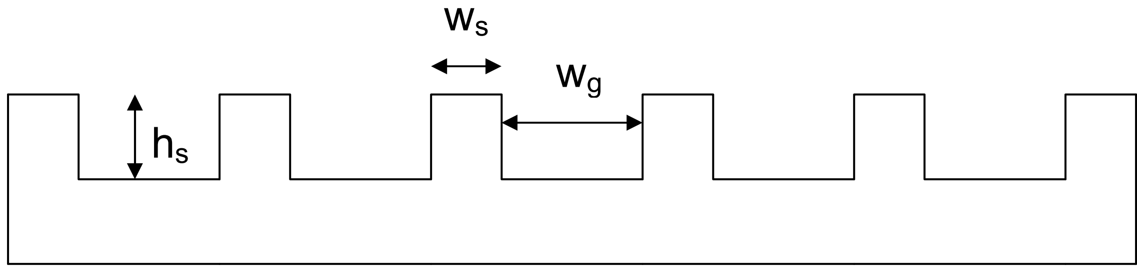

Figure 2-9: A microstructured solid surface design will vary with the structure height (h_s), structure width (w_s), and gap width (w_g).

The second cause of hydrophobicity on a surface is its surface chemistry. Some coatings repel water very well. Coatings can replace the surface energy effects that would otherwise be present due to the composition of the solid surface material, however, coatings on surfaces can only yield contact angles as great as 120° [17-21]. To achieve higher contact angles a surface structuring must also be present. The right combination of surface structuring and chemical application can produce significant hydrophobicity. Once the contact angle of a fluid-solid interface has exceeded about 150° the surface is considered to be superhydrophobic or ultrahydrophobic [2, 21, 22].

Some of the coatings that have been used in conjunction with microstructured surfaces to create ultrahydrophobic surfaces include three different organosilanes: dimethyldichlorosilane (DMDCS) [17], *n*-octyldimethylchlorosilane (ODMCS) [17], heptadecafluoro-1,1,2,2- tetrahydrodecyldimethylchlorosilane (FDDCS) [17, 19]. Teflon [20] and other specially manufactured chemicals [18], [21] have also been used. The effect of an ultrahydrophobic surface on fluid flow is desirable for many microfluidic applications including the improvement of fluid delivery time in microneedles.

Results from several studies [2, 17, 20-24], show the effects of microstructures on the contact angle and angle hysteresis of fluid droplets. Other investigators, [18-20, 25], have also shown reduced pressures and increased flow rates in microchannels approximating two parallel plates. [26, 27], have demonstrated improved flow through long circular hydrophobic channels. At this point no known literature exists for hydrophobic fluid flow over evenly engineered microstructures inside a short circular channel.

2.2.2 Cylindrical Hydrophobic Microchannel Theory

Just as the flat surfaces with micro structures will improve flow in parallel plate channels the concept can be extended to cylindrical channels as well. The lumen of the microneedle can be designed to be hydrophobic by creating a surface roughness on the walls of the channel. Microstructures can be fabricated around the side of the channel as seen in Figure 2-10. The structures are of identical widths and are evenly spaced all the way around the channel. By varying the number of structures and the spacing of the structures, the gap between each structure can be widened or shortened. Thus, the cavity fraction F_c can be altered to enhance hydrophobicity as discussed earlier.

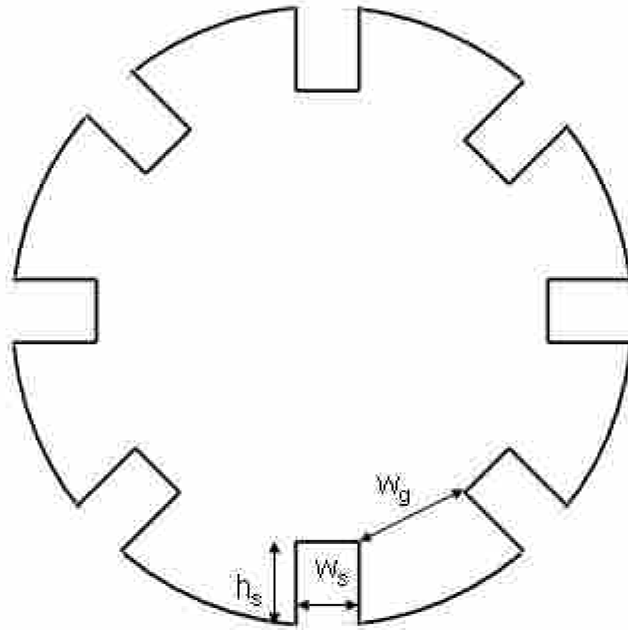

Figure 2-10: Cross-sectional view of the structured lumen concept design

The cavity fraction (see Equation 2-1) is applied to the circular channel just as it is the flat channel. The ratio of the total gap spacing to the overall inside circumference of the channel, or similarly the ratio of a single gap spacing to the sum of the gap and structure width, will give the percentage of cavity fraction in the microchannel. By varying the number of structures, their widths, heights, and spacing the cavity fraction can theoretically be altered to any desired amount.

2.3 Microchannel Flow

To better understand the effects that hydrophobic channel walls can have on fluid flow it is first necessary to understand flow in a basic smooth walled channel. The pressure drop

Δp required to drive a fluid through a smooth walled circular microchannel may be expressed as Equation 2-2 from the mechanical energy equation

$$\Delta p = \mu \frac{f\,\mathrm{Re}}{\pi} \frac{QL}{D^4} + \rho \frac{8}{\pi^2} \frac{Q^2}{D^4} (K_1 + K_2) \qquad \textbf{(2-2)}$$

where $f = \frac{64}{\mathrm{Re}}$ and $\mathrm{Re} = \frac{4\rho Q}{\pi \mu D}$ for a circular channel, μ and ρ are the dynamic viscosity and the density of the fluid respectively, Q is the flow rate, L is the length of the channel, and D is the diameter of the channel. K_1 and K_2 are parameters used to compensate for minor losses at the entrance and exit of the channel respectively. Here K_1=0.5 and K_2=1.0 and the values listed are approximations used in similar macro and microchannel flow studies [6, 28].

It is important to note that pressure drop for a given flow rate is inversely proportional to the diameter of the channel raised to the fourth power. This means that as the diameter of the channel decreases the pressure required to drive the fluid rises dramatically. It should also be noted that the second term in Equation 2-2 is significant for shorter channels but as L gets very large the second term becomes negligible; however, channels in very short channels, as Q increases, the second term will dominate the expression.

It is anticipated that a channel with a superhydrophobic surface will decrease the pressure drop required for a given flow rate by reducing the friction factor f in the first term of Equation 2-2. Or stated another way, while $f\mathrm{Re} = 64$ for a regular, smooth walled, circular channel, a structured hydrophobic channel will result in $f\mathrm{Re} < 64$. Since $f\mathrm{Re}$ is a measure of flow resistance in a channel it is also a measure of the hydrophobicity of a channel.

Based upon the literature review given, a study and development of hydrophobic short structured circular microchannels has never been performed. One purpose of this research will be to design and fabricate such microchannels and test them for improved microfluidic flow rates over similar sized smooth walled circular microchannels. These structured microchannels will not be incorporated with microneedles; however, similar sized smooth walled microchannels will be incorporated with microneedles. Specifically, the microchannels will be fabricated with KOH etched silicon microneedles, which, to this point have never been fabricated with microchannels. These microneedles, with microchannels, will not be tested for microfluidic flow conditions, nor will they be tested for transdermal drug injection, or for pain associated with injections.

Chapter 3 – Design and Fabrication

3.1 Microneedle Parameters

The microneedles discussed in chapter 2 will be designed in two different forms, one with an octagonal base and one with a square base. Figure 3-1 and Figure 3-2 shows the basic concept of the microneedle designs. These designs are similar to shapes reported by Offereins, Dizon, and Mukerjee [12, 13, 29]. The preferred design will be the octagonal needle due to the extra structural support surrounding the microchannel inside the needle as well as the simplicity of the KOH mask design. The design specifications call for dimensions that are only a rough estimate of what fabrication should yield. The design of a single needle has a height of 400 μm and a square base of about 230 μm across with a tip angle of about 37.5 degrees measured from the needle edges and 33.7 degrees measured from the needle flats. The channel is 48 μm in diameter and is placed in the needle so that the center of the channel is offset 40 μm from the center of the needle as seen in Figure 3-3.

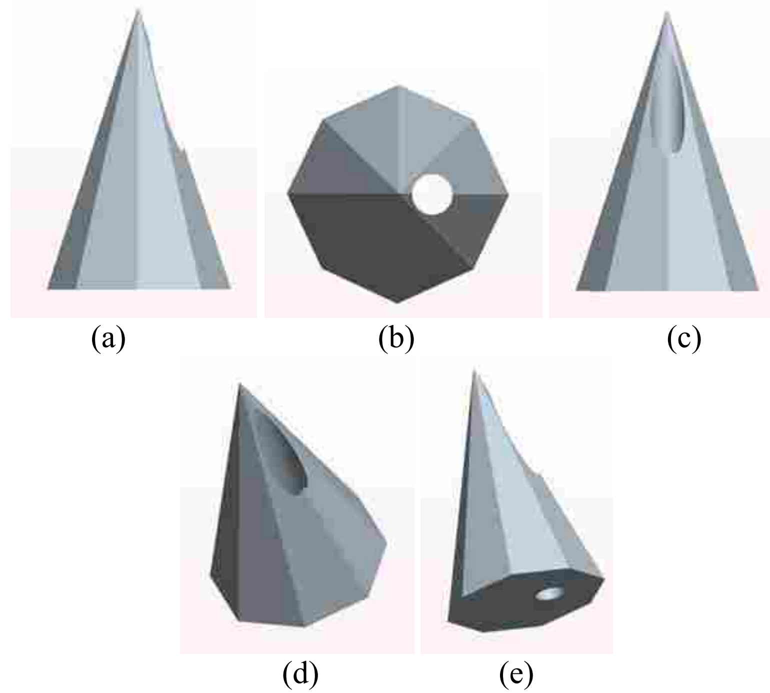

Figure 3-1: Octagonal microneedle design concept with smooth walled microchannels. (a) and (c) are side views, (b) is an overhead view, (d) is an angled view from above, and (e) is an angled view from underneath.

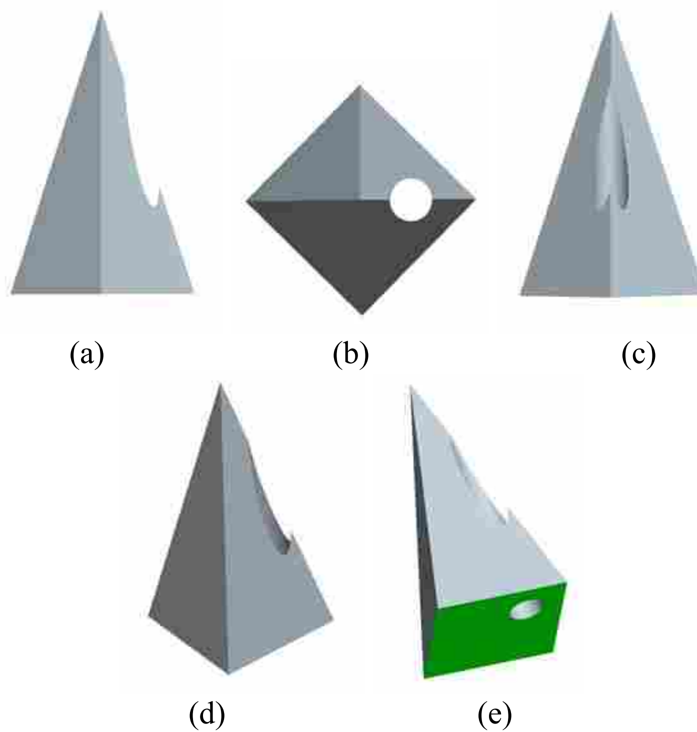

Figure 3-2: Square microneedle design concept with smooth walled lumen. (a) and (c) are side views, (b) is an overhead view, (d) is an angled view from above, and (e) is an angled view from underneath.

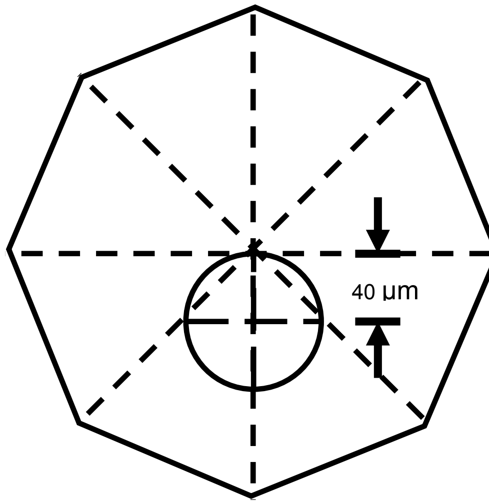

Figure 3-3: An overhead schematic of the needle and channel. The channel is offset 40µm from the center of the needle to avoid interfering with the tip of the needle.

It is important to have a microchannel with as large a diameter as possible in the microneedle; however, the greater the diameter of the channels, the lower the elevation where the channel will first penetrate the side of the needle. A larger channel diameter is desired because it will allow for a greater flow rate; however, a smaller diameter is also desired because it will ensure that the entire exit region of the channel is high enough on the needle to be entirely submersed into the essential layers of skin. Thus, these two requirements in design necessitate a compromise in diameter versus height of the microchannel opening in the microneedle. The current microchannel design is perceived as the ideal one for this needle due to the diameter chosen for the channel as well as the height on the needle surface at which the channel opens up. The dimensions for this channel are subjective and were chosen based on designer preference.

It is noted to the reader that the fabrication techniques used to create the pyramid shaped needle require that the ratio of height to base remain constant. An increase in the dimensions of the base would give an increase in the height. An increase in this overall size would allow a greater lumen diameter. However, two factors limit the width and height of the needle structure itself. First, the epidermal layer has a limited thickness and a microneedle that is too long will penetrate all the way through the epidermis and too far into the pain-sensitive dermal layer of the skin. Second, the silicon substrates from which the needles will be fabricated are only 660 μm thick. The fabrication process used to create the pyramid shaped needles is performed by etching away all of the surrounding substrate material. If the needle stands too high, the silicon under the base will have been etched away and there will be nothing underneath the needle base to support it.

3.2 Hydrophobic Lumen Parameters

As discussed in chapter 2 the lumen of the microneedle is designed to be hydrophobic by creating a surface roughness on the walls of the channel. Microstructures are fabricated around the side of the channel as seen in Figure 3-4. The structures are of identical widths and are evenly spaced all the way around the channel. By varying the number of structures and the spacing of the structures, the gap between each structure can be widened or shortened. Thus, the cavity fraction F_c can be altered to enhance hydrophobicity as discussed earlier.

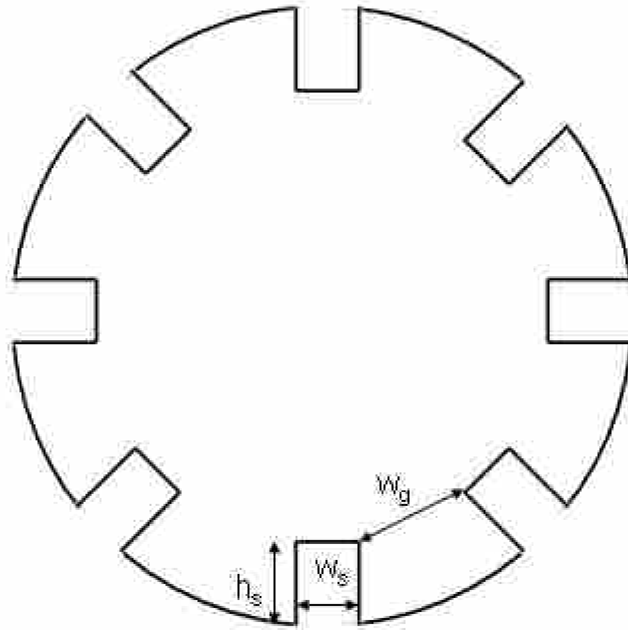

Figure 3-4: Cross-sectional view of the structured lumen concept design

The microstructures utilized here were designed to be 16 μm high and 5-8 μm wide. The spacing of the gaps varies with the number of structures in a given channel. Table 3-1 summarizes the dimensions for each needle design. The characteristic that distinguishes each channel design from the others is the cavity fraction.

Table 3-1: The design parameters and significant values for the four lumen designs

Structure Width w_s (μm)	# of Structures	Gap Width w_g (μm)	Cavity Fraction F_c (%)	Structure Height h_s (μm)
8	7	13.5	63	16
8	6	17.1	68	16
5	9	11.8	70	16
5	8	13.9	73	16
5	7	16.5	77	16
5	6	20.1	80	16

Due to enlargement of the channel during fabrication the design of the microchannel fabrication mask will have different dimensions than the actual channel. This is based upon experimental results that will be discussed in chapter 4.

By combining the design for the microneedles and the hydrophobic lumen the resulting concept shown in Figure 3-5 is produced.

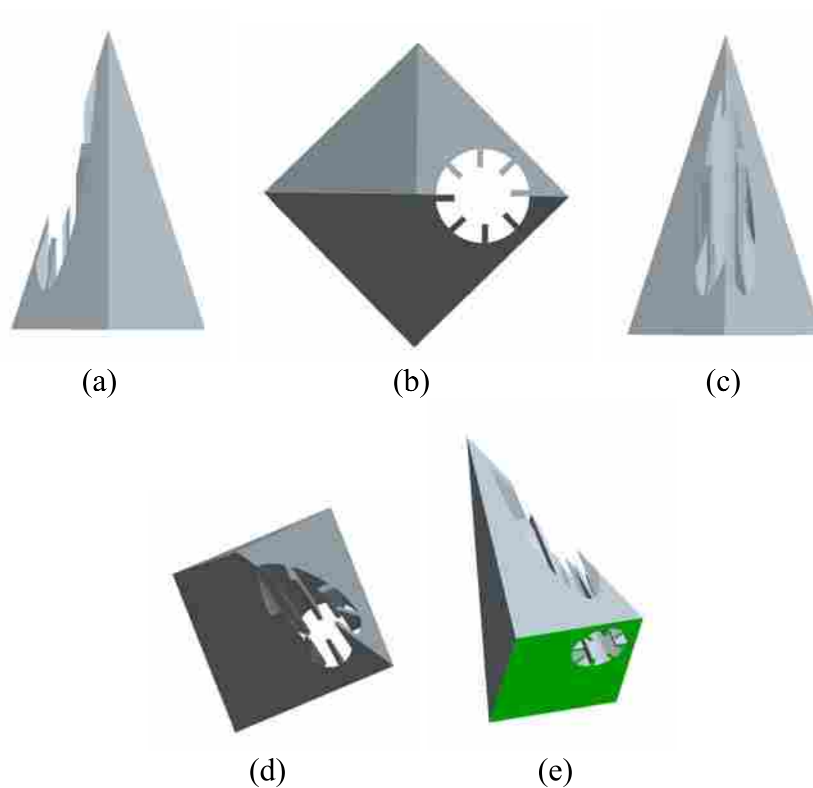

Figure 3-5: Microneedle design concept with structured lumen. (a) and (c) are side views, (b) is an overhead view, (d) is an angled view from above, and (e) is an angled view from underneath.

As stated previously, it is anticipated that the microneedle concept described will be incorporated into an array of needles, like that in Figure 3-6, that will prove to effectively demonstrate a reduced friction factor, *f*Re, and therefore a higher fluid delivery rate for a given pressure drop.

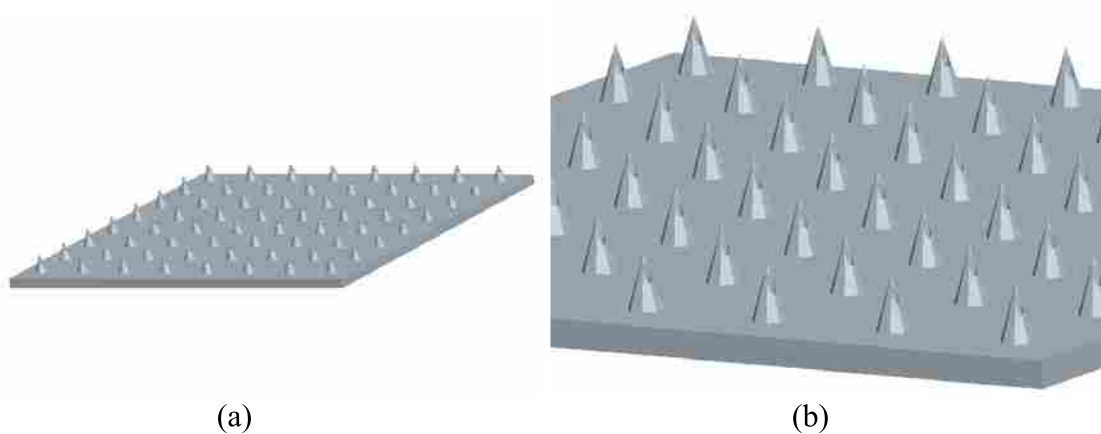

Figure 3-6: Images showing (a) a conceptual array of octagonal microneedles protruding from the base of a silicon substrate and (b) a magnified version of the same array

3.3 Design Analysis

A few aspects of the microneedle must be carefully analyzed before fabrication. First, an examination must be made of the maximum allowable gap width that can exist between structures on the side walls of the lumen before the fluid meniscus will completely wet the inside trough of the gaps. Second, the actual ability of the needle to penetrate the stratum corneum deep enough for proper transdermal fluid delivery is of concern. These issues will be addressed in this section.

3.3.1 Microchannel Analysis

The maximum gap spacing between structures of a solid surface is dependent on the surface tension of the fluid, the pressure imposed on the fluid, and the hydrophobicity of the fluid-solid interface (which can be determined by the contact angle a droplet would

form on the surface of the solid). A simple equation (see Equation 3-1) that is used to determine gap spacing w is derived from Young's Law [19] and simplified as

$$w = \frac{4\sigma}{\Delta p}\cos(\pi - \theta), \quad \textbf{(3-1)}$$

where σ is the surface tension of the fluid (this is a function of temperature and also varies with what type of substance the fluid is contacting at its interface [28]), Δp is the pressure drop between the fluid and the air gap below the meniscus, and θ is the contact angle that a droplet of the fluid would form on the surface of the solid. A typical value for σ is expected to be about 0.00728 N/m and the expected range of Δp, based on other studies [6, 7, 18] and desired values for maximum gap spacing, cannot exceed about 5 kPa. The contact angle is unknown but a rough estimate can be made based on previous studies to give a minimum expected droplet contact angle of about 120° [19]. Based on the minimum contact angle estimate and a maximum pressure drop of 5 kPa the gap spacing should be no bigger than 20 µm wide. This is a conservative estimate and in all likelihood the maximum gap width can be even bigger. The chosen maximum gap width for these channel designs is 20.1 µm which means that wetting of the gap may be possible for the most extreme cavity fraction channel but generally is not expected to occur.

3.3.2 Microchannel Analysis

Another concern in the needle design is the needle's ability to actually puncture the stratum corneum deep enough to completely submerse the exit of the lumen in the epidermal layer. Some of the factors that determine this are the needle's aspect ratio (that

is the ratio of its height to its base length) and the position of the lumen openings relative to the needle.

Several effective microneedle designs have been reviewed and one of the measurements used to characterize a microneedle is the aspect ratio. The aspect ratio is calculated simply as the height of the needle divided by the length of the base. Depending on the shape of the needle this can be a fairly accurate or quite a rough calculation. It has been found that most microneedle aspect ratios from the research range from 0.47 - 10 [6]. The aspect ratio of microneedle designs most similar to the one in this research, made from single crystal silicon, are no greater than 4.0 [5-7, 9, 30]. The microneedle in this research has an aspect ratio of 2.8 and based on penetration tests of other microneedles this one is expected to easily penetrate the stratum corneum.

Despite the ease of penetration, skin distortion and resistance to penetration will increase at greater depths of needle penetration. For this reason it is important for the lumen openings to be as close to the tip of the microneedle as possible since it is not expected that the needle will penetrate the skin a full 400 μm to the microneedle base. As mentioned in section 3.1, due to the necessity of the lumen to open near the tip of the needle, the diameter of the channel is constrained. The microchannels have been designed with a 55 μm diameter which means the lowest point of exit surface on the needle is about 235 μm below the tip. It is anticipated that the height of this lumen opening will be high enough on the microneedle to be completely submersed under the stratum corneum layer into the epidermis for proper fluid delivery.

The microneedle must also be able to withstand the forces associated with puncturing the skin. It is important that a portion or the entire needle does not break off while entering or while submersed within the skin. Several puncture tests have been performed on various needle designs to determine the robustness of microneedles. Surfaces that have been tested include saran-wrap [31], aluminum foil [7], fresh skinless chicken breast [6], porterhouse steak (New York Style) [3], rats [5], and human skin [5, 9, 30]. In all cases, the microneedles were found to be very robust and capable of repetitious punctures into the same material. Similar results are expected with the microneedle created for this project.

3.3.3 Microneedle KOH Mask Analysis

Analysis of the microneedle mask was performed after many different mask designs had already been attempted. The analysis was done to determine the ideal mask design that would lead to square cross-sectioned needles. Using an etch simulation program called ACES, many mask designs were reviewed to find an ideal shape.

Due to limitations in the program, parameters could not be set to exactly match those desired; however, a general concept of the right mask design was created. The parameters in the simulation were set as follows.

Orientation	Face: [110], Edge: [100]
Process	Silicon Wet Etching
Etchant	KOH 30% (1.4µm/min)

The process was stepped every 5, 10 or 20 minutes depending on the simulation. The structure etched in the silicon substrate along with the accompanying mask outline are both shown in each simulation frame in Figure 3-7 – Figure 3-14.

This "slender pinwheel" mask was used to first simulate early experimentation done with this type of mask. The total length from top to bottom and side to side was 300 µm with a member width of 14 µm. Each frame represents 20 minute increments of the simulation.

One may notice that in the frame labeled "180 min" a miniscule needle with sides in the [411] crystallographic orientation is barely exposed above the [111] sided pyramid.

Simulation #1

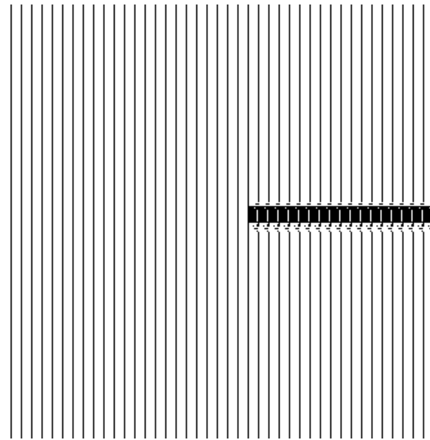

Figure 3-7: Mask used in the KOH simulation in Figure 3-8.

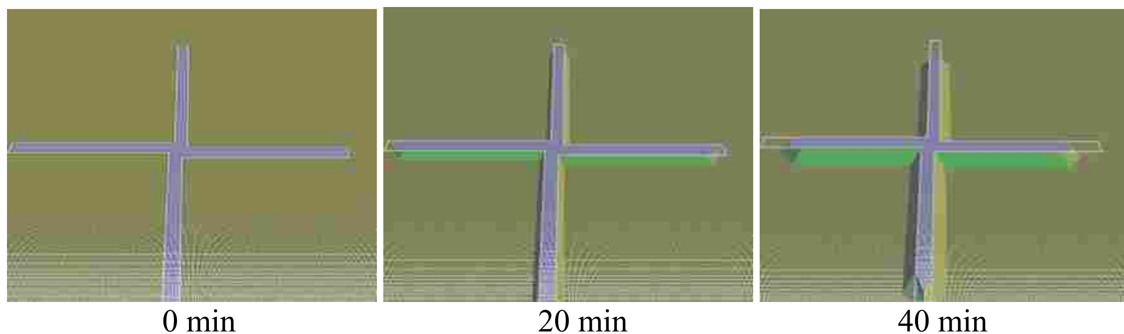

0 min 20 min 40 min

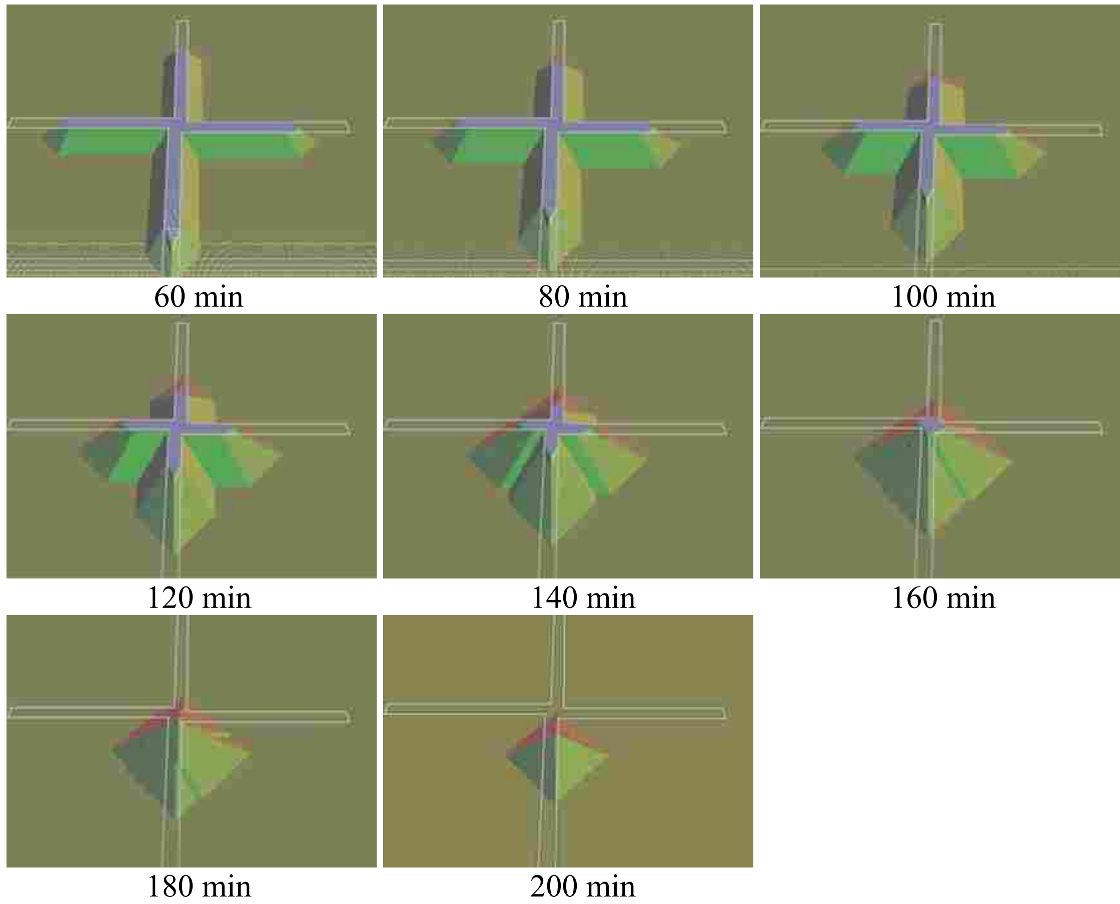

Figure 3-8: Simulation frames showing the resulting structure from the mask in Figure 3-7.

The next etch simulation was done using a square mask like the one that was used in real experimentation prior to running the simulation. The mask is 100 μm square and the frames are shown in 10 minute increments.

This mask produces an eight sided pyramid, all [411] planes, as predicted. As can be seen, starting in the frame labeled “160 min”, once detached from the surface of the mask the needle retains its shape but gradually etches away.

Simulation #2

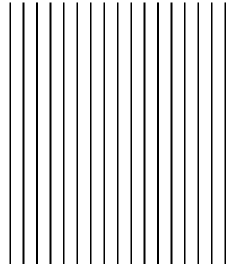

Figure 3-9: Mask used in the KOH simulation in Figure 3-10.

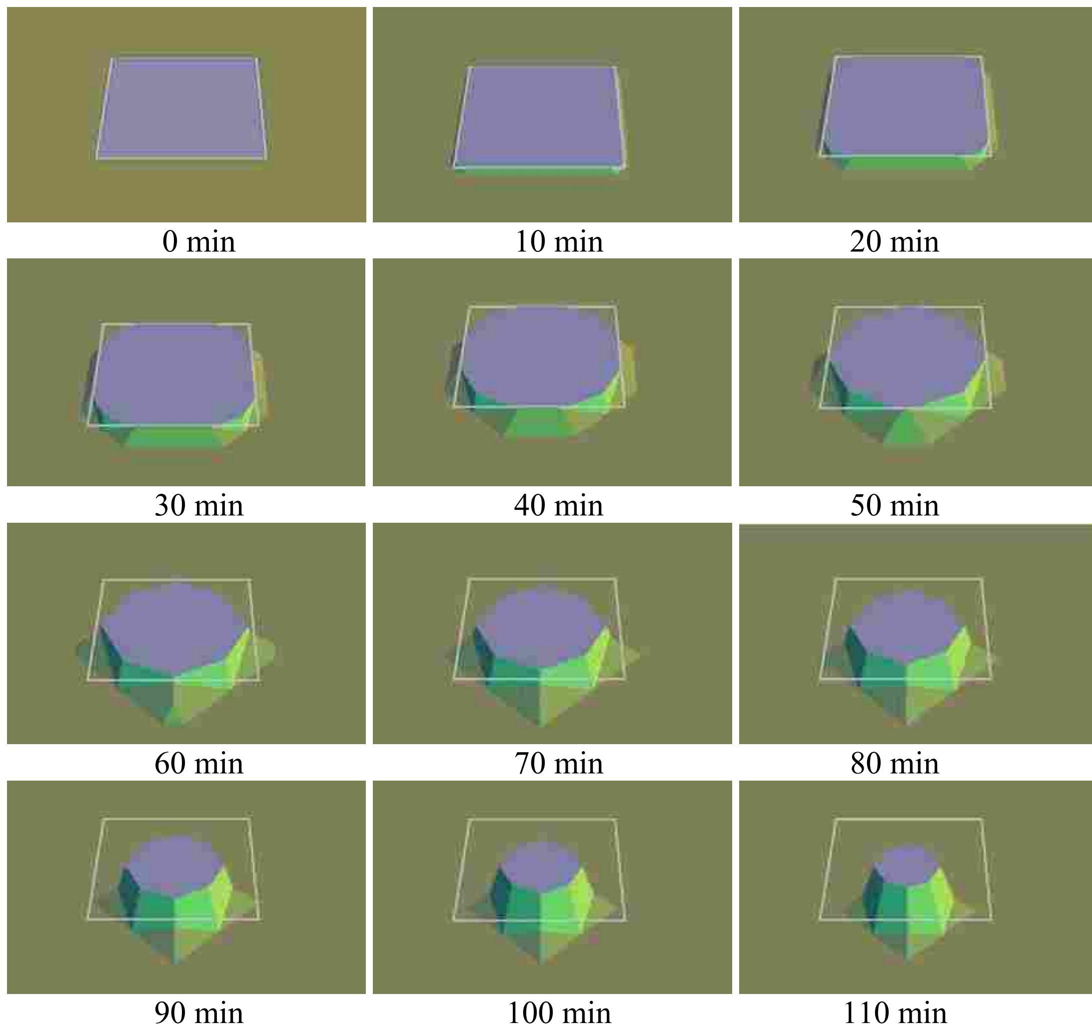

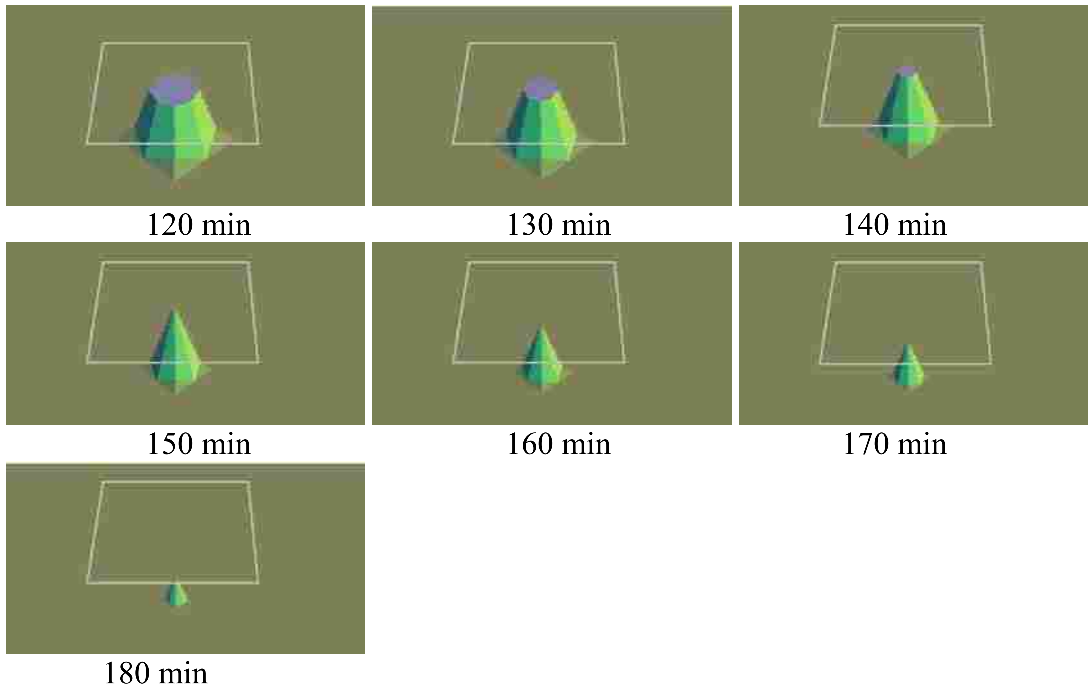

Figure 3-10: Simulation frames showing the resulting structure from the mask in Figure 3-9.

The next etch uses a pinwheel with short members. Much iteration was necessary to get a mask that would yield the desired results of a four sided needle. The four sided needle has significantly more surface roughness at the base than does the eight sided needle. The frames are shown in 20 minute iterations.

Simulation #3

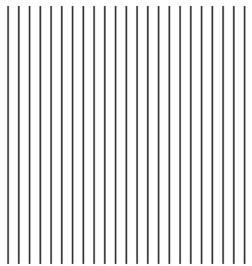

Figure 3-11: Mask used in the KOH simulation in Figure 3-12.

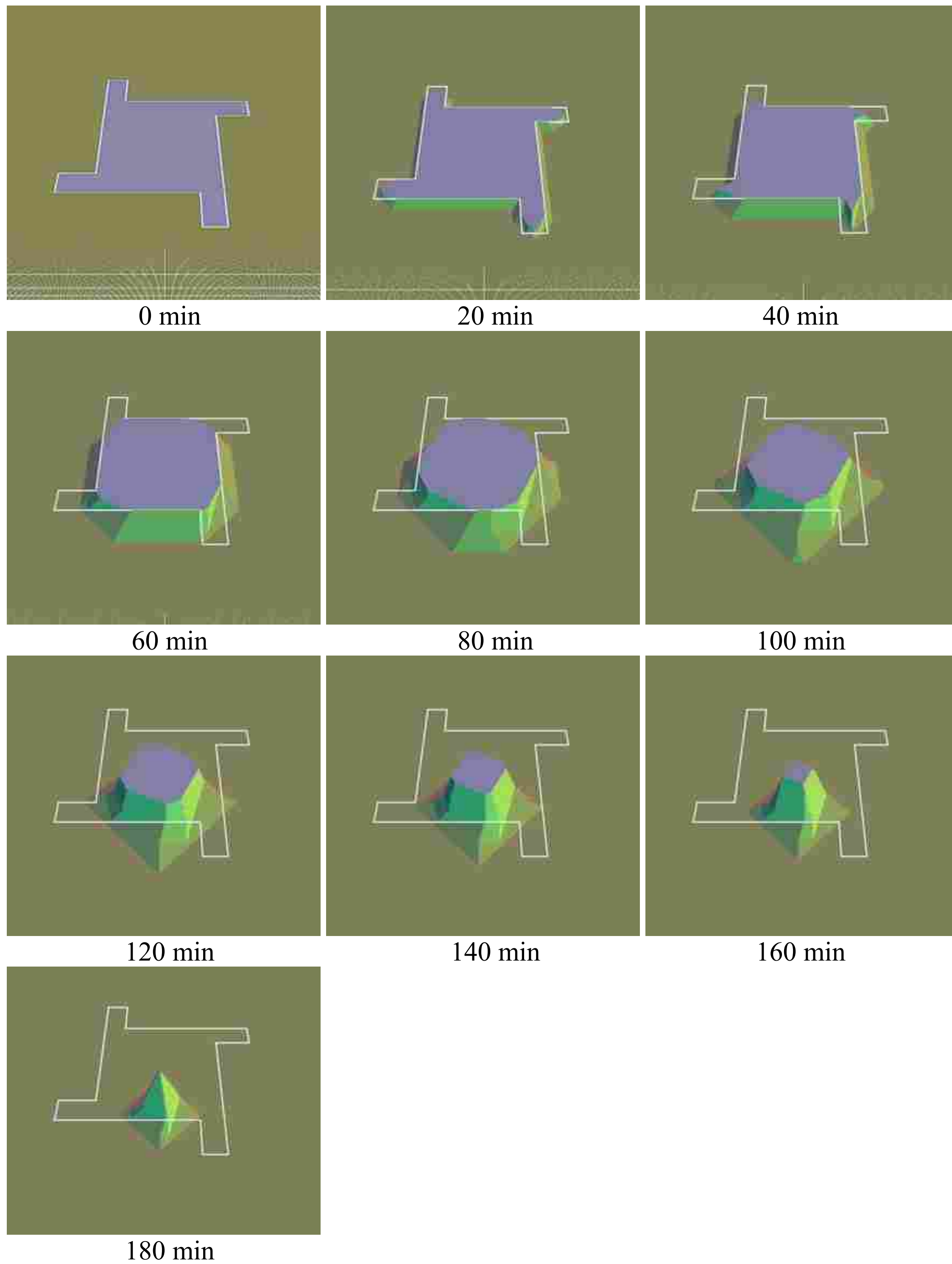

Figure 3-12: Simulation frames showing the resulting structure from the mask in Figure 3-11.

The final etch mask contained one square and three similar pinwheel shapes. The pinwheels are all slightly different from each other and had dimensions that were varying

proportions to the square mask. The intent was to determine a mask that would yield a four sided needle at approximately the same time that an eight sided needle was fully developed. From these results a pinwheel mask would be designed in similar proportions to the mask as were found in the simulation. Each frame in this simulation shows 20 minute iterations in the initial stages of etching and 5 minute iterations in the final etching stages of the simulation.

Simulation #4

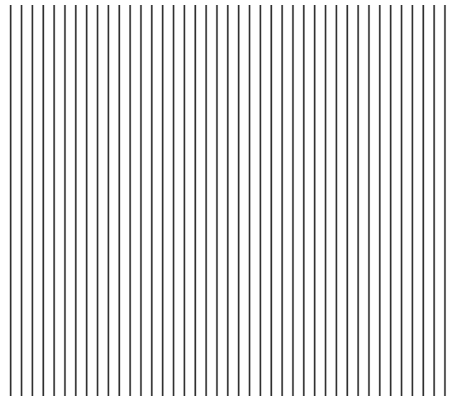

Figure 3-13: Mask used in the KOH simulation in Figure 3-14.

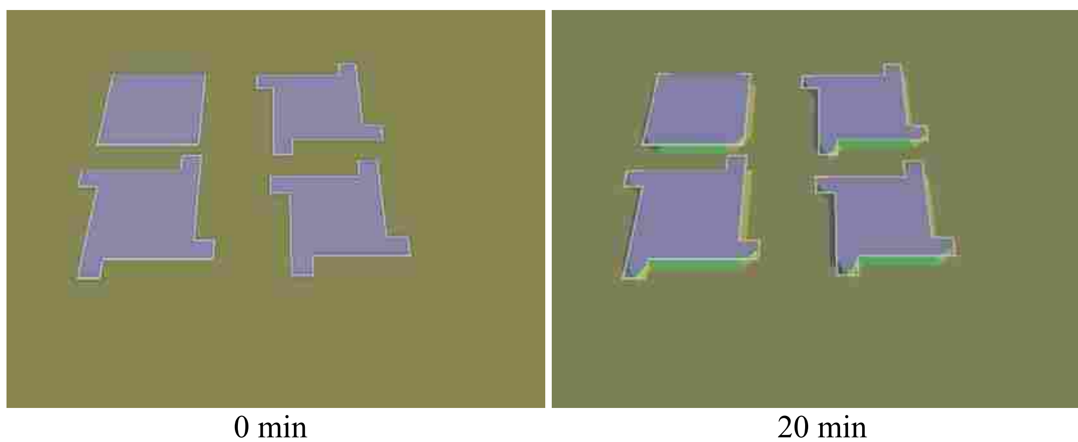

0 min 20 min

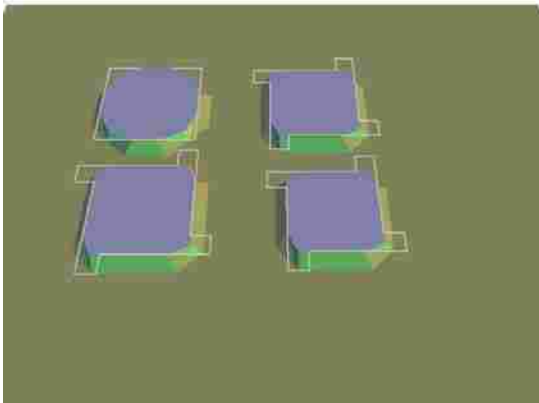
40 min

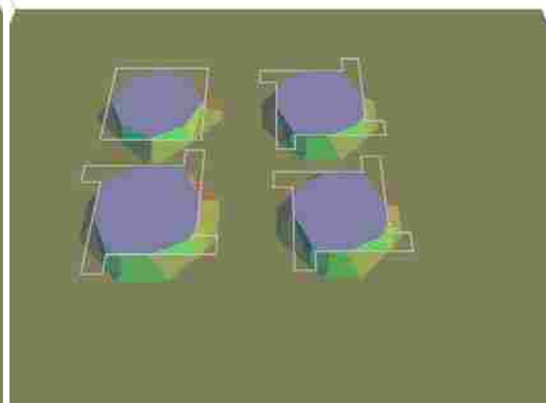
60 min

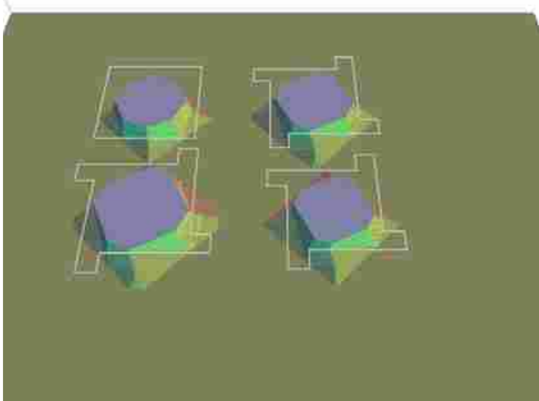
80 min

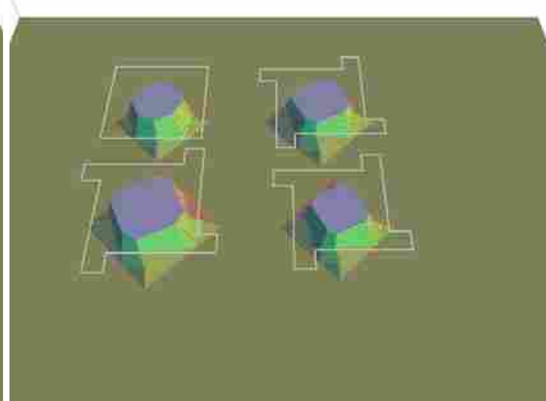
100 min

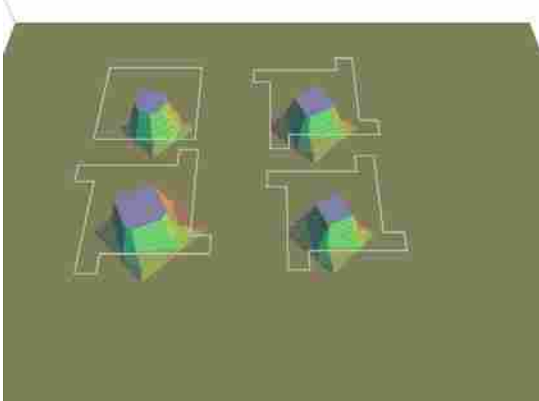
120 min

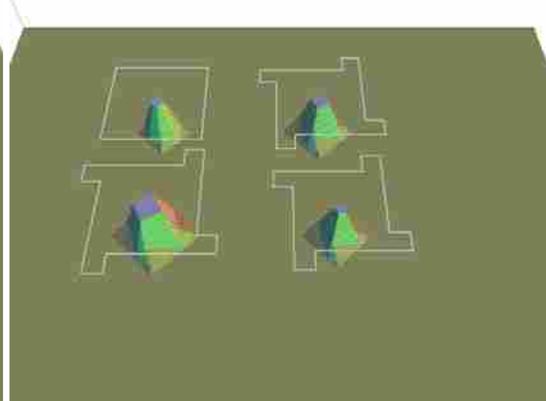
140 min

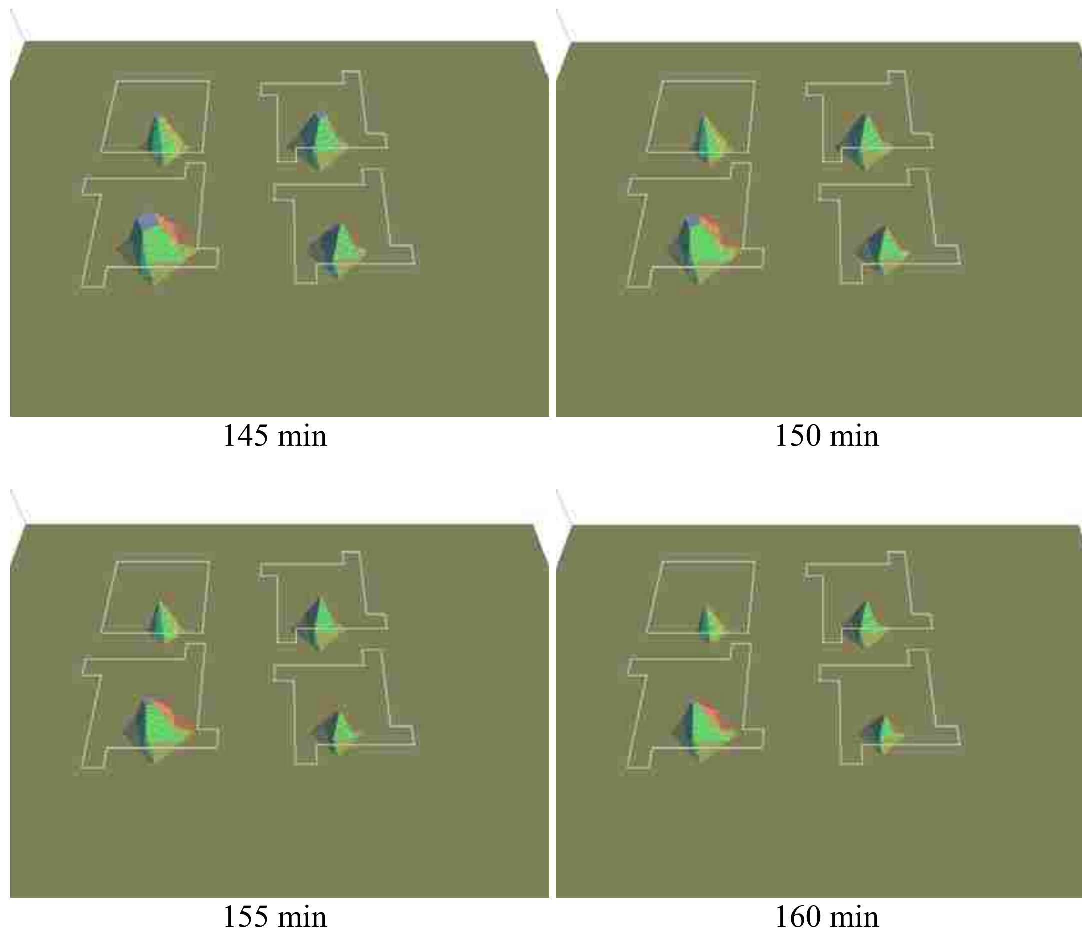

Figure 3-14: Simulation frames showing the resulting structure from the mask in Figure 3-13.

Based upon the analysis of the masks used in the simulation, a real mask could be made to produce four sided microneedles in a KOH etch. Until this designing phase the experimental research for this project had failed to produce four sided needles as will be discussed in chapter 4.

3.4 Fabrication Design Considerations

The microneedle design depends on several different microfabrication processes and materials. These processes and materials vary in complexity and some or more essential than others to the specific design. This chapter will describe the physical mechanisms of

each of these processes and materials and how they pertain to the fabrication of the microneedle and microchannel design while the following chapter will describe specific recipes and data necessary to the reproduction of each process or proper application of the material.

The fabrication of the microneedles and microchannels require several steps as diagramed in Figure 3-15. Most steps require some amount of pre or post preparation as well, so the fabrication process quickly becomes complex as any number of processing steps can have a far reaching influence on the outcome.

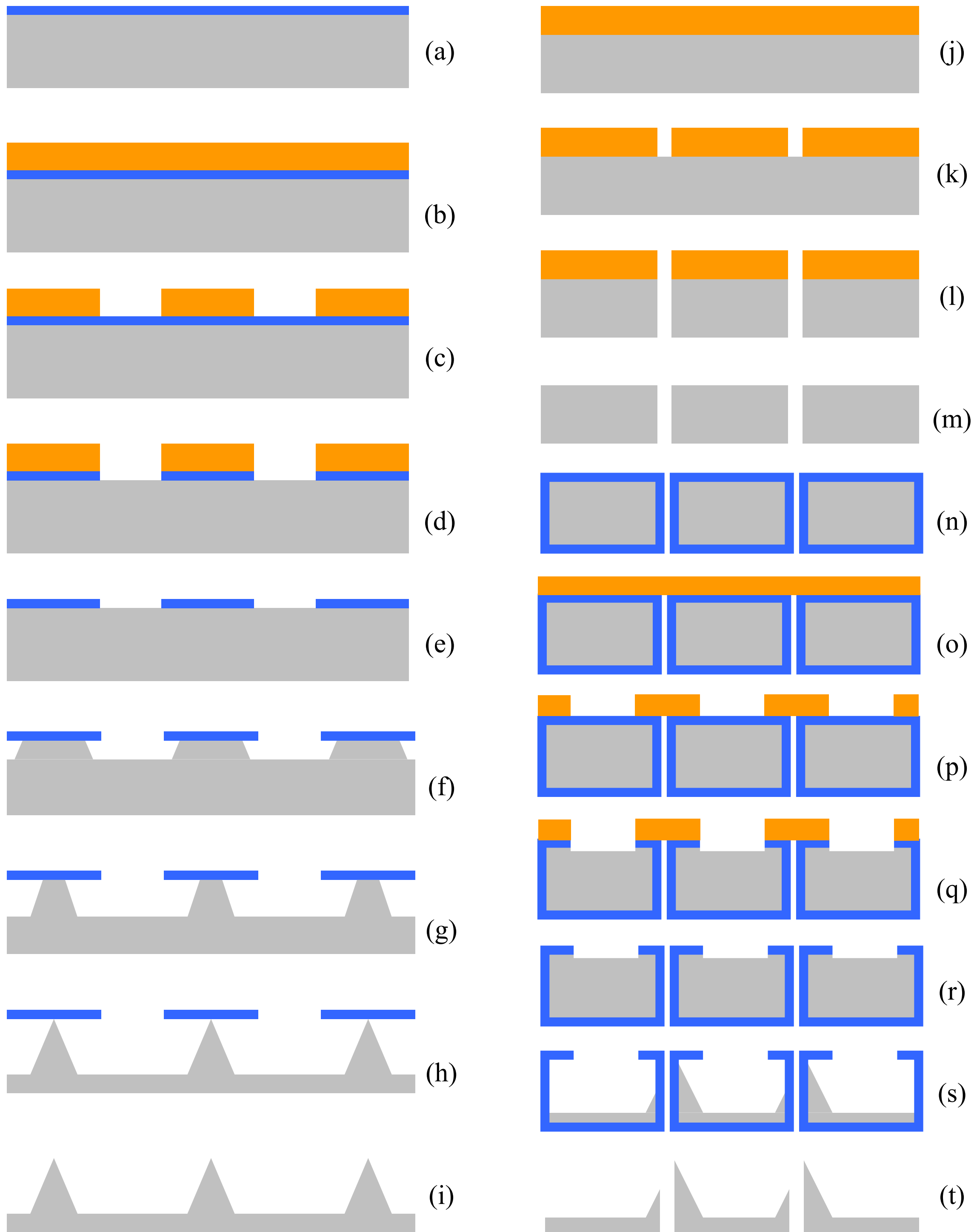

Figure 3-15: The essential steps in the microneedle fabrication process (a)-(i) and in the combined microchannel and microneedle fabrication process (j)-(t).

To fabricate microneedles, a layer of nitride is applied to the silicon substrate (Figure 3-15 a) and then a layer of photoresist (Figure 3-15 b). The photoresist is patterned (Figure 3-15 c) after which the pattern is transferred to the nitride (Figure 3-15 d). The photoresist is removed (Figure 3-15 e) and the silicon is etched in a bath of KOH where over time needles are formed (Figure 3-15 f-h) and the nitride is removed (Figure 3-15 i). The microchannels are made by applying a layer of photoresist (Figure 3-15 j) and putting a pattern into it (Figure 3-15 k). This pattern is used to create channels running through the wafer (Figure 3-15 l). Once the channels are etched the photoresist is removed (Figure 3-15 m). At this point it is possible to continue processing if one desires to create microneedles to accompany the microchannels. The wafer with the microchannels is deposited with nitride (Figure 3-15 n) and the steps used to create microneedles are thereafter followed (Figure 3-15 o-t). The nitride on the wafer is coated everywhere and protects the channels from etching with the KOH from the inside out.

There are many design considerations that are determined primarily by the processes and equipment used in fabrication. As it is important to understand each of the processing steps and the equipment used to perform them, all processes will be described in this section. Where necessary some additional detail will be given in Appendix A.

LPCVD Nitride

To deposit nitride onto the surface of the wafer a process called Low Pressure Chemical Vapor Deposition (LPCVD) is used. The wafer is placed in a long furnace where gases are introduced at high temperatures (around 600 °C) and deposited onto the wafer. The length of time in the furnace determines how thick the layer of nitride will be. Once the

nitride layer has been deposited onto the wafer it will be very durable and usually only comes off with special processing that will be discussed later. The nitride will provide the hard mask needed for KOH etching. LPCVD nitride deposition is one of the few processes that is outsourced in this research.

Photoresist

Photoresist, a light sensitive polymer, is used to transfer patterns from a pre-fabricated mask onto the substrate of the wafer. Positive photoresist is applied by spin coating the material onto the wafer. A positive photoresist is one in which the portions of the resist that have been exposed to light will rinse away when put in a photoresist “developer” solution. Conversely, a negative photoresist is one in which the portions not exposed to light will rinse away when developed.

Photoresist is used to create a mask for both the RIE etching and the ICP etching processes necessary for the fabrication of the microneedles. Two types of photoresist are used. AZ3330, a positive photoresist, is used as a masking material for the RIE process. A relatively thin layer is spun onto the wafer and the photoresist mask is used in the RIE etch to transfer a pattern onto the nitride layer that has already been deposited onto the wafer. SPR-220 (7.0), the other positive photoresist, is used as a mask in the ICP etch. This photoresist must be spun on relatively thickly due to the prolonged amount of time it will be exposed to the ICP etch. Both the RIE and ICP etches will be discussed later in this chapter. Procedural tips for proper application of photoresist through spin coating are given in Appendix A.

Mask

The lithography mask is first designed by computer. Many different programs are available for mask layout but for this research a program called L-Edit was used. Once the design for the mask is created it is converted into a GDS II format and sent to a mask making facility. Depending upon the complexity of the mask, two mask making methods are possible. One method is done through pattern generation and the other with e-beam lithography. Typically a 5 inch wide square soda-lime glass with chrome masking is used to make the mask unless the user requires other, more expensive, materials. The mask making process will be explained in greater detail in Appendix A to ensure clarity on the subject.

Lithography

Lithography is used to transfer a pattern from a mask to a surface material on the wafer substrate. The pattern transferred into the photoresist is then used for further processing. After a photoresist is spin coated onto a wafer it is heated to a temperature and time specific to the material and its thickness on the wafer. This heating step is called a soft bake.

After the soft bake the photoresist is ready for lithographic exposure to light. After exposure the wafer will usually be exposed to heat again. This step is called a hard bake. At this point the wafer is ready for other processes. A thorough discussion of the process used for exposure through the mask is found in Appendix A.

As discussed previously, the nitride mask used to form the microneedles in KOH must be aligned at 45° relative to the [100] orientation of the wafer. To ensure that this happens, the mask patterns are also aligned 45° relative to a set of alignment strips located close to the near side of the mask. These alignment strips are then aligned with the major flat of the wafer when in the Karl Suss lithography machine (see Figure 3-16). As a result the individual hard mask for the microneedles will be aligned satisfactorily relative to the [100] wafer.

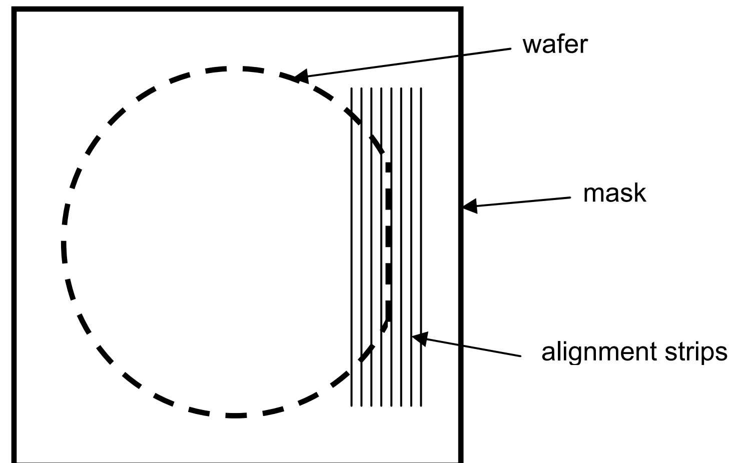

Figure 3-16: The concept of alignment strips on the mask allows near perfect orientation with the [100] plane of the wafer.

Sometimes it will be necessary to align the microneedle mask to a wafer that has already undergone significant processing. This will be the case when the microneedles are etched over the microchannels. To ensure that the needles and the channels align properly there will be alignment marks on each of the masks. The channels mask will have alignment marks that etch into the wafer that will then align to identical alignment marks on the needle mask. Using these alignment marks as a reference the needles will be positioned

approximately (within a few micron) where they are needed to create microneedles with microchannels running through them. The design of the needles and the channels is such that mask misalignments up to 10 μm are acceptable.

RIE

For some of the processing needed, it is necessary to transfer a pattern onto a thin layer of silicon nitride covering the wafer substrate. A pattern in the nitride is referred to as a hard mask. To create this hard mask a few steps are necessary. First the nitride must be deposited onto the surface of the wafer. Then a photoresist pattern, or soft mask, needs to be created, as has been discussed above. Once a soft mask is made the pattern can be transferred to the nitride layer using Reactive Ion Etching (RIE).

The RIE machine holds the wafer in a pressure controlled chamber where a plasma of CF_4 gas is induced. This plasma has high etch selectivity to the nitride compared to the photoresist. The exposed nitride underneath the photoresist soft mask is etched away by the CF_4 plasma transferring the pattern from the photoresist onto the nitride. The photoresist is then rinsed off and the nitride pattern over bare silicon is ready for further wafer processing.

KOH

The microneedles are created with a wet anisotropic etch in 45% weight potassium hydroxide (KOH). KOH will etch some crystallographic planes in a silicon wafer faster than others as discussed in the previous chapter. The microneedles will be about 400 μm high and will need to have a substantial base to support them. This base will need to be at

least 200 μm thick so the wafers used to create microneedles will need to more than 600 μm thick.

In order to make the microneedles as functional as possible they are designed to be closely spaced together and centered in the middle of a “chip” which can be used for post-fabrication testing. The chip is designed to be about 2 cm square. This should be big enough for a person to handle the chip and attach it to any testing equipment necessary for future work. A typical 4 inch wafer can hold 9 full chips of this size. A concept of this mask is shown in Figure 3-17.

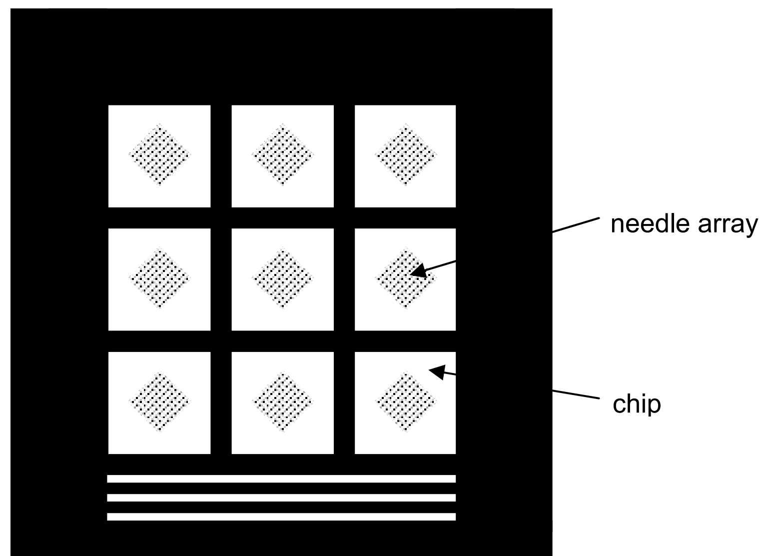

Figure 3-17: The basic design of a mask containing 9 separate quadrants each with an array of 64 individual needle masks. The alignment strips are shown on the bottom of the mask.

The mask contains 64 microneedles per chip laid out in an 8 X 8 array, centered on the chip. The microneedles are spaced as closely together as possible but are constrained by the necessarily large size of the square mask for each individual needle. Therefore the

needles are spaced 1,150 μm apart from each other. This needle spacing results in an array of about 9 mm square.

The 9 chips that will have microneedles etched onto them represent a significant portion of the surface area of the wafer which means that a high percentage of the wafer will have a greatly reduced thickness and thus structural rigidity. To help the wafer maintain structural integrity through all of the fabrication procedures the 9 chips are separated by narrow bands which are designed in the mask. These bands on the mask will result in unetched strips running the length of the etched wafer and will provide sufficient structure to keep the substrate from breaking in undesired locations.

HF

Hydrofluoric acid (HF) is used to remove nitride from the wafer. It is typically used after the KOH etch is complete. Usually a bath of 49% weight un-buffered HF will remove the 450 nm thick nitride and oxide layer in 10-20 minutes. This time needs to be increased to 3 hours for a 500 nm layer of LPCVD nitride. HF is the most dangerous chemical used in the clean room due to it toxicity both in liquid and vapor forms. It is important that all safety precautions prescribed by the clean room training sessions as well as those of the office of risk and safety management be observed.

ICP Etch

The channels are etched through a dry anisotropic etch process called inductively coupled plasma etching (ICP). The ICP etch is just one of several possible methods for deep reactive ion etching (DRIE). DRIE is a process of creating a plasma within a sealed chamber and etching exposed portions of a wafer through ion bombardment originating

from the chamber. For adequate etch rates and a uniform etch all the way through a wafer, the Bosch process is used. This is a process where alternating plasmas are induced to etch then passivate the sample in a cyclical fashion. The etch gas will typically be SF_6 or another fluorine based gas while the passivation gas will be C_4F_8 or a similar organic gas. The etch cycle etches silicon in two ways. First, the SF_6 reacts chemically with the silicon to wear it away. Second, the physical bombardment of ions from the plasma erodes the silicon. The pure etching cycle is isotropic, etching away the side walls of the silicon as well as the base. For this reason a passivation cycle is needed. In passivation the C_4F_8 ions are uniformly coated onto the surface of the silicon. This creates a fluorocarbon bi-product that forms a chemically protective layer against SF_6 interaction with the side walls of the silicon [32, 33]. The passivation cycle is used to protect the side walls of a feature and keeps the etch generally anisotropic. Figure 3-18 shows a conceptual comparison of two etching cycles, one without a passivation cycle and one with a passivation cycle.

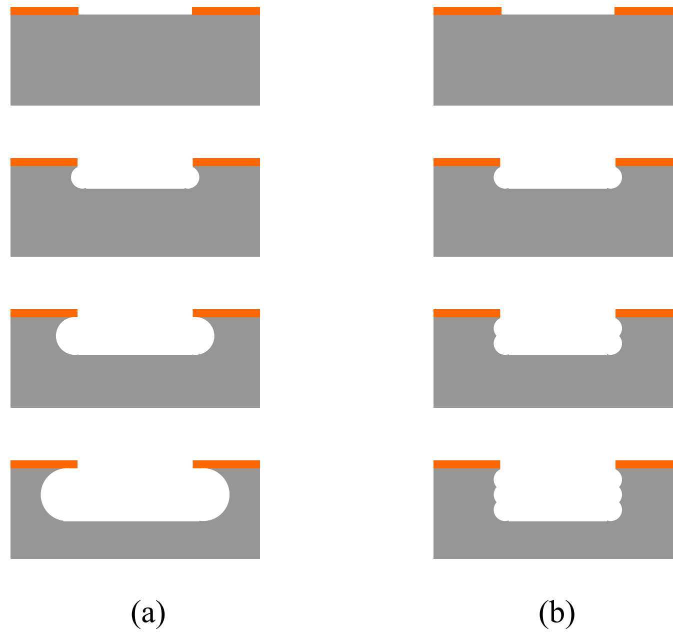

Figure 3-18: The isotropic etching produced by simply etching in an ICP process are shown in (a) while the anisotropic etching that results with alternative etching and passivation is shown in (b).

A feature that has only undergone a few etching cycles would not be considered totally anisotropic. However, as the etched feature increases in aspect ratio, the anisotropy is readily apparent as seen in Figure 3-19.

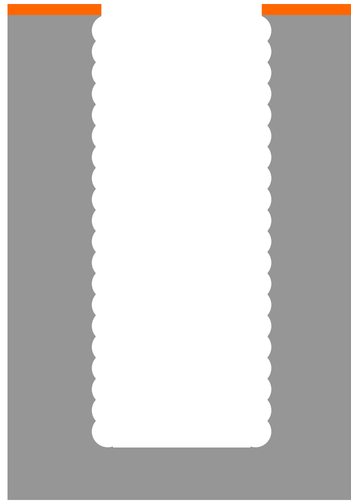

Figure 3-19: Over time the anisotropy of the Bosch process becomes apparent as the aspect ratio of a feature becomes greater.

The scalloping that is created in the ICP process gives side walls a slightly rugged surface but the ridges are only about 0.6-0.7 μm apart so the non-anisotropic effect is negligible for large anisotropic features. For the channels being etched, the ratio of the depth of the etch versus the gap between scalloped ridges is about 100/1.

The channels to be etched are positioned on the mask with exactly the same spacing as the microneedles on the wafer. Thus, nine separate quadrants with 8 X 8 arrays of microchannels in each one can be overlaid with corresponding arrays of microneedles. To make alignment of the needles and channels possible, a set of alignment strips is included on the channel mask and unique alignment marks are found on each mask to help align one set of features to the other.

ICP etching has been used in a few microneedle designs including those found in [5-7]. Although each application tends to be unique the method of ICP etching for the microneedles in this research has been sufficiently proven in other work.

Nanostrip

When a sample is etched with the ICP process it must be adhered to a full 4 inch base wafer. The base wafer is necessary to protect the equipment underneath the etched wafer as well as provide a heat sink to draw energy out of the wafer being etched. The etching wafer and the base wafer can be "glued" together with photoresist, preferably something easy to work with like AZ-3330. Once the wafer has been etched it needs to be separated from the base wafer. The best way to do this is to soak it in Nanostrip. This is a chemical that will breakup anything organic, including photoresist. Once the wafers are separated the etched wafer is ready for further processing.

SEM

After all fabrication has taken place the samples are reviewed to determine appropriate changes for future fabrication improvements. This is done in a Scanning Electron Microscope (SEM). The details of how an SEM is used will not be discussed in this paper. It is simply noted that most SEM images will be taken on JEOL JSM840a SEM machine. They are taken with an aperture setting of 3 or 4, at a working distance of 48 mm, and 20.0 kV.

Chapter 4 – Microfabrication Results

4.1 Microneedles

4.1.1 Microneedle Fabrication

Microneedles were successfully developed using the procedure described in chapters 2 and 3. To ensure that the entire process can be reproduced, a complete list of specifications and recipes is provided.

The wafers used for this research were purchased from Montco Silicon Technologies, Inc.[1] They were 100 mm (4 inch) diameter test grade wafers. The wafers were n-type phosphorus doped with a resistivity of 1-30 ohms/square. They had a <100> crystal orientation and were reported to be 600 μm thick $\pm$ 25 μm. Both single sided polished and double sided polished wafers were used.

The wafers were to receive a layer of LPCVD nitride which was outsourced to Process Specialties, Inc.[2] They suggested using a thermal oxide layer under the LPCVD nitride to

---

[1] Montco Silicon Technologies, Inc.
500 S. Main Street, Spring City, PA 19475
Tel: (610) 948-6880
Web: www.silicon-wafers.com

[2] Process Specialties, Inc.
1660 W Linne Rd Bldg A, Tracy, CA 95377
Tel: (800) 533-8820
Web: www.processspecialties.com

balance out residual stresses. Per their suggestion all wafers received 300 nm of thermal oxide topped by 150 nm of LPCVD nitride.

Once the wafers were delivered nearly all process steps could be completed in Brigham Young University's clean room facilities. The wafer is coated with photoresist and a mask pattern is applied through lithography. The pattern is then transferred to the nitride layer using the RIE process. Detailed process steps are outlined in Appendix B and follow the process outlined in Chapter 3 and Appendix A. Once the nitride mask is created microneedles can be etched in the wafer with KOH.

KOH will etch nitride as well as silicon, albeit at a much slower rate. Any pinholes or scratches in the nitride can allow the KOH to penetrate the nitride at that point and etch the silicon wafer in undesirable ways. For this reason the backside and sides of the wafer should be protected as much as possible from the KOH. The clean room staff has created a "chuck" made especially for KOH etching. The chuck is made of a Teflon back panel and a Teflon ring which sandwich the wafer and leave only the top surface of the wafer exposed. The two Teflon panels seal in the wafer with O-rings and are screwed together with twenty concentrically placed Teflon screws. Teflon is used as the chuck material because it is inert to KOH. This chuck, with a wafer inside, is shown in Figure 4-1.

When tightening the screws around the chuck they should first be screwed in finger tight and then tightened just a little more with a screwdriver. In order to avoid cracking the wafer the screws should not be too tight. They should also be screwed in an alternating fashion on opposite sides of the chuck just like tightening lug nuts when changing a tire. This will keep stresses from building on any one location of the wafer.

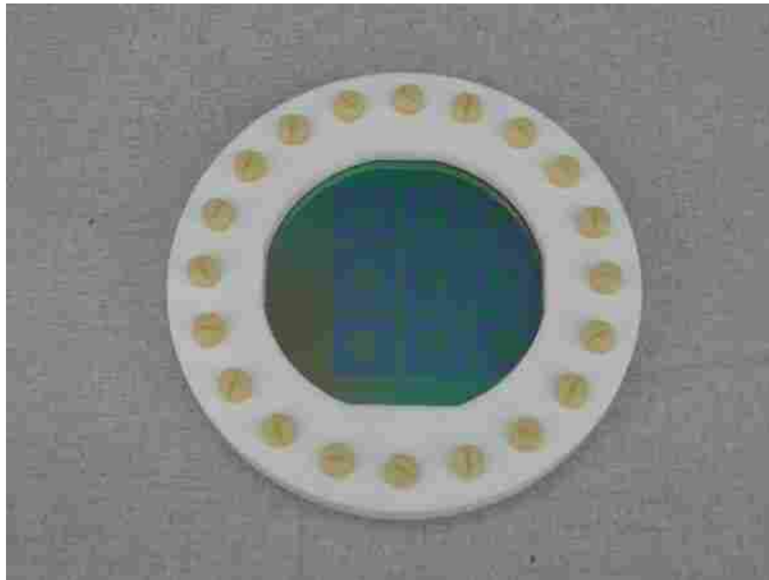

Figure 4-1: Picture of the Teflon chuck and screws with a wafer clamped into it and ready for etching.

To prepare for the KOH etch a dish with a 6.5 inch diameter should be filled 1/2 to 2/3 full with 45% weight KOH solution. The dish should rest on a base inside the wet etch tank and the tank should then be filled with water. A lid is placed over the dish to prevent water and water vapor from entering and diluting the KOH solution. The water in the tank is then brought up to a level just below the top of the KOH dish. The water and thus the KOH are heated at a temperature setting of 79 °C. This will take at least a half hour to get the tank to reach a stable temperature. The temperature usually does not stabilize at 79 °C but between 78.0 and 78.5 °C.

When the wet etch tank has reached a stable temperature the chuck with the wafer is ready to be placed in the KOH bath. The chuck is simply lowered into the KOH bath and the lid is placed over the dish. A schematic representation of this is shown in Figure 4-2.

The reaction does not take place immediately. Although KOH does react immediately with silicon the wafer will have a chemical residue on it from the RIE process. There is a thin fluorocarbon layer on the surface of the silicon that the KOH will penetrate in 3-4 minutes at which time the etching of the silicon will take place. This can be observed because small bubbles will begin to form and rise to the surface of the KOH. Within a minute or so the surface of the wafer can no longer be seen due to the clouds of bubbles rising from the surface (see Figure 4-3).

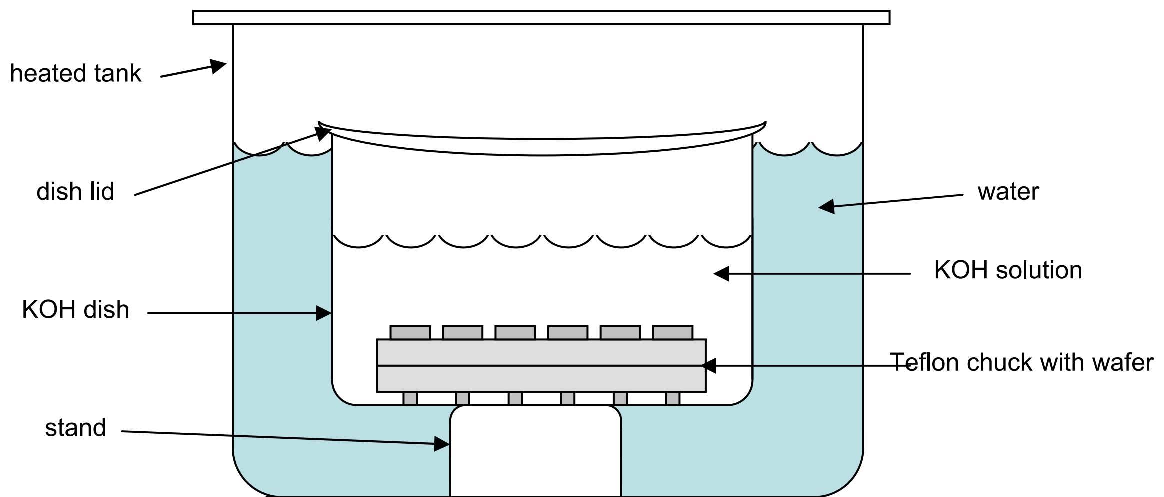

Figure 4-2: A schematic representation of the chuck resting in the dish filled with KOH which is in turn resting inside the heated tank full of water.

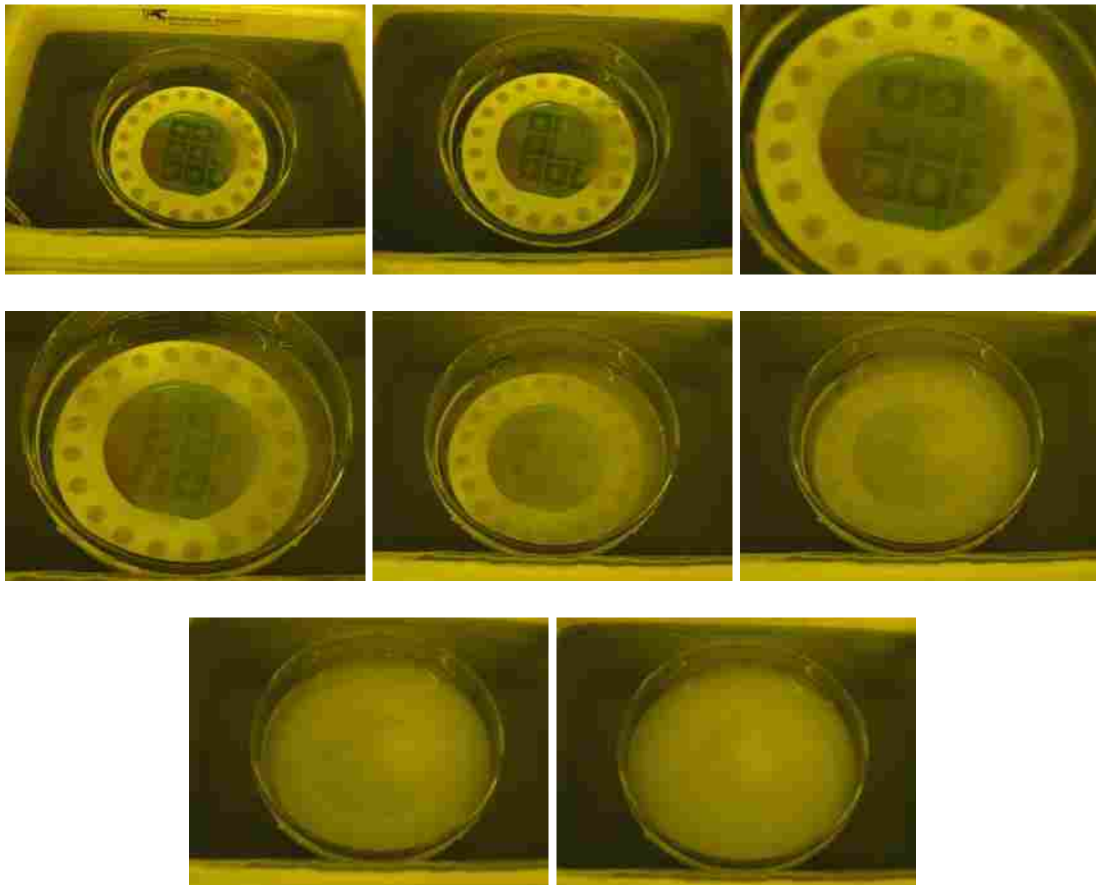

Figure 4-3: Time progression of a wafer after being immersed in KOH at about 78°C. As can be seen, bubbles begin to rise to the surface on the right hand side of the wafer and slowly spread throughout the entire wafer. Within two minutes of initial bubbling the wafer cannot even be seen because of the thick cloud of bubbles rising to the surface.

The depth of the etch, and therefore the height of the needles or other structures, is determined by the temperature and duration of the etch. Etch rates have been approximated by the clean room staff and the etch rate chart for the etching of [100] silicon in 45 % KOH solution is shown in Figure 4-4. According to the trend line shown, a temperature of 78-79 °C will result in an etch rate of just more than 50 μm/hour. Accordingly, the wafer will be etched for around 8 hours to produce microneedles that are 400 μm high. The exact etch time is found experimentally and will be discussed later in this chapter.

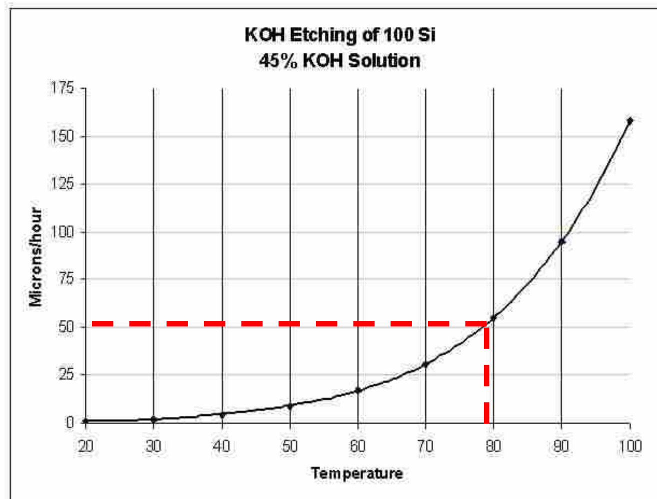

Figure 4-4: A clean room chart showing the etch rate of KOH as a function of temperature. At a temperature of about 79°C the etch rate should be just above 50µm/hour.

Due to the length of the KOH etch, all etching was done in two sessions where the first etch lasted 4 hours $\pm$ 1 hour and the second etch, done on a later day, was etched the remaining portion of time.

Over the course of the etch, the water in the tank will slowly evaporate. The tank will usually be checked at least once to refill the water back to a level just below the top of the KOH dish. When the etch period is over the KOH dish is removed from the heated tank and the chuck is removed from the dish. The height of the microneedles can be diminished quickly in hot KOH so the process is controlled to reduce the variation in the results from one etch to the next. First the chuck is allowed to air cool (upside down for proper KOH drainage) for 30 seconds then is cooled by spraying deionized water on the backside of the chuck for another 30 seconds. Then the chuck is thoroughly rinsed on the top side for several minutes to remove all of the KOH solution. This cooling process is used to prevent the wafer from cracking under severe quenching.

If only the first period of etching has been completed then the wafer remains in the chuck and is stored for the next session of etching. Over time a very thin silicon dioxide layer will develop on the surface of the silicon and the nitride. No noticeable alterations in the end results have been observed from this natural growth. It is quickly dissolved once it enters the KOH so nothing has been done to prevent this growth.

If the etch is completely finished, the wafer is removed from the chuck. It must be handled carefully because many portions of the wafer are significantly thinner and can break easily. The chuck is cleaned and stored. The KOH is still reusable and can be left in the dish for another etch or two. No batch of KOH was ever used to etch more than three sets of microneedles.

After the wafer is etched it needs to have the remaining nitride mask stripped off the surface of the silicon. This is done by immersing it in 49 % unbuffered hydrofluoric acid (HF). The wafer remains in the HF for 10-20 minutes depending on the dilution of the HF. When handling HF extreme caution must be exercised. Just a little bit of HF spilled directly on the skin can be lethal. After the HF nitride strip, the wafer is submersed in a special tank of water for at least five minutes. When turned on, the tank will produce nitrogen bubbles to agitate the surface of the wafer and help rinse off all residual HF. A wafer before and after the HF etch can be seen in Figure 4-5.

At this point the wafer is ready for cleaving. The mask has been designed so that perfect cleaving lines are created surrounding the arrays of needles. When these lines are cleaved chips should be formed that contain an 8 X 8 array of needles in the center, as seen in

Figure 4-6. Cleaving, although made easier by design, should still be done with caution as the wafer substrate is only about 200 µm thick and can break and puncture easily.

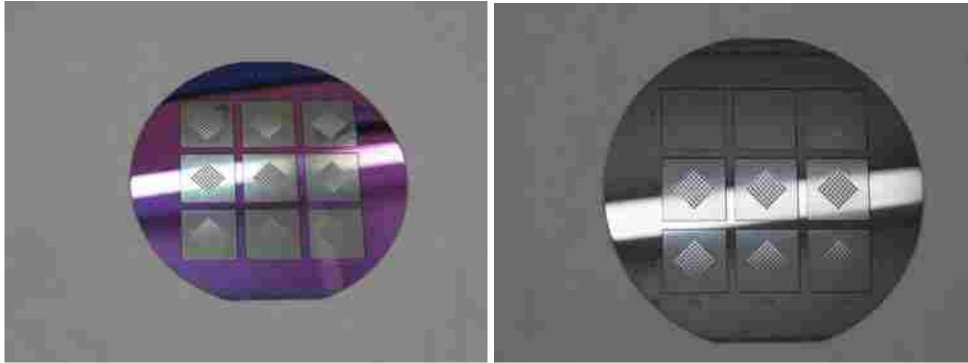

Figure 4-5: A wafer just after a KOH etching is seen on the left and the same wafer just after an etch in HF is seen on the right. The arrays of microneedles sectioned off from each other can be seen on the wafers in each picture. The white stripe in the middle is a reflection from an overhead light on the ceiling.

Figure 4-6: A single silicon chip containing an 8X8 array of microneedles.

Each chip is labeled with an ID number. This allows the user to know which etch made these needles and which quadrant they came from, and is done in this fashion (etch # - quadrant #). A microneedle chip that was made in the 5th etch and came from the bottom left hand corner of the wafer will be labeled 5-7 according to the ID labeling system.

Quadrants are labeled from left to right and from top to bottom so that the upper left is quadrant #1 and the lower left is quadrant #9.

Images of the completed needles can be seen in the SEM images in Figure 4-7. Both octagonal and square cross-sectioned microneedles are shown. Ultimately, it was decided that octagonal cross-sectioned needles would be selected over square cross-sectioned needles. The octagonal needles will penetrate the skin deeper. They also have slightly greater cross-sectional area at any given height at the higher points on the needle where the channel will open up on the surface. This will add stability to the structure of the needle.

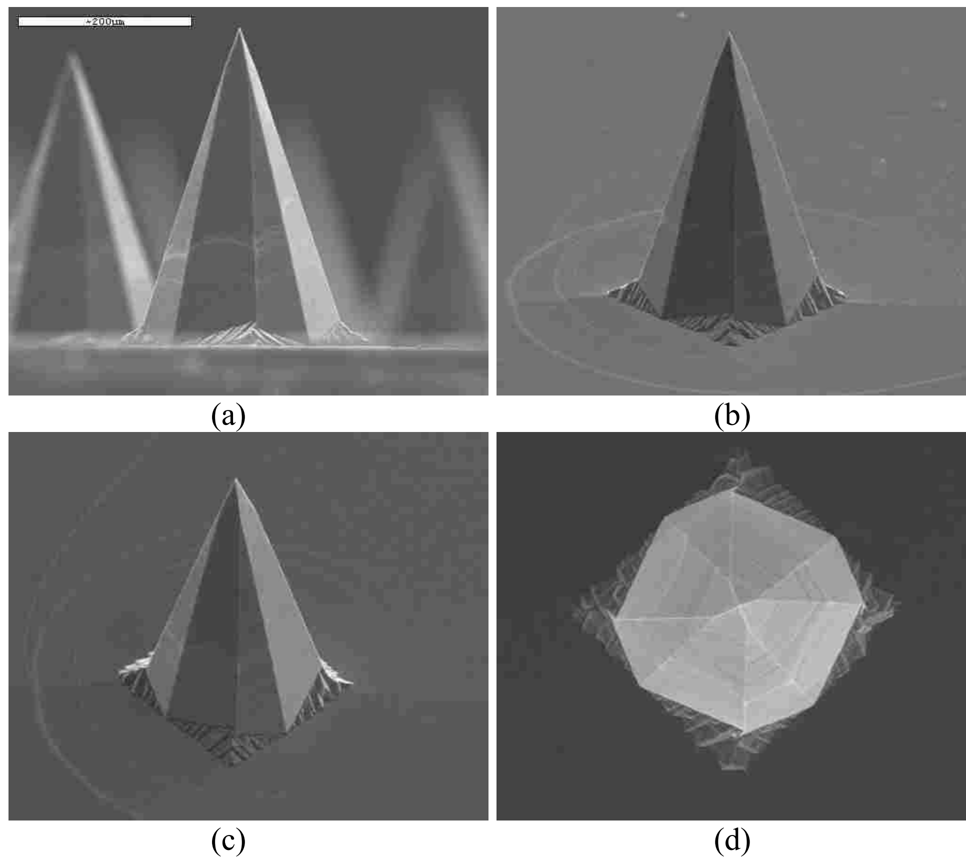

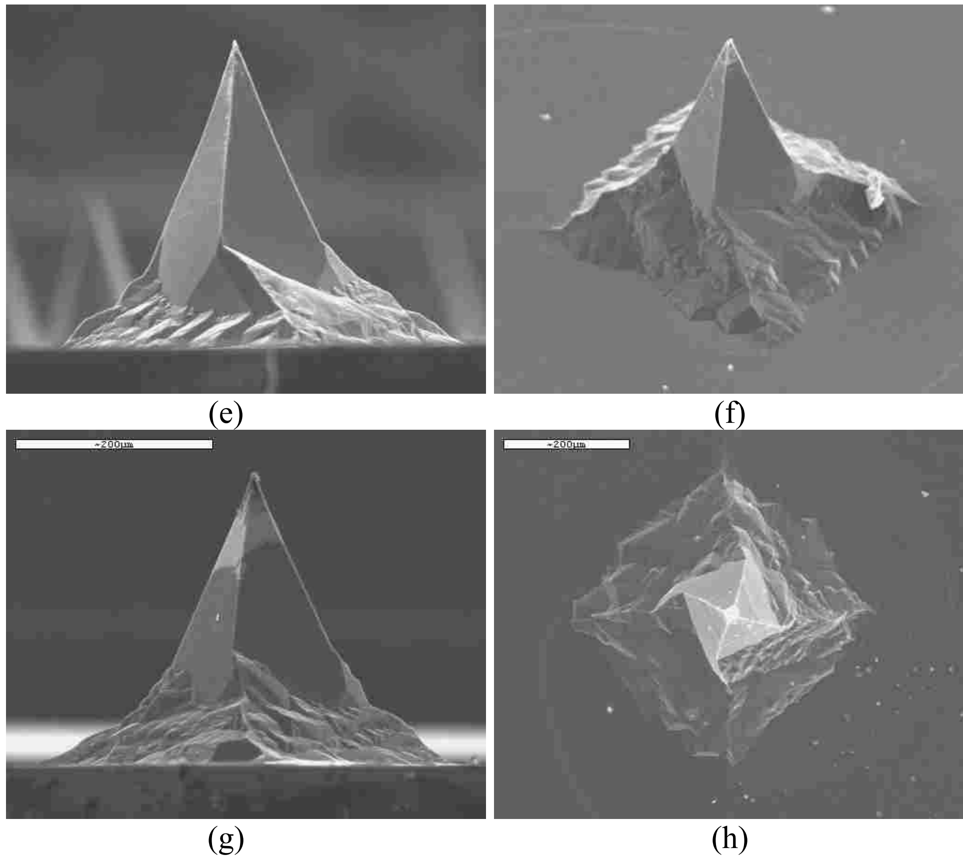

Figure 4-7: SEM images of fully etched microneedles. A side view of an octagonal needle is seen in (a) with angled views in (b) and (c) and an overhead view in (d). Side views of square needles are seen in (e) and (g), with and angled view in (f) and an overhead view in (h).

4.1.2 Microneedle Fabrication Analysis

Once the fabrication method was refined experimental results could be used to create a needle height model. The height of the microneedles is dependant on many factors, including temperature of the etch, dilution of the KOH, size of the original mask, and duration of the etch. Therefore, a model must exist to effectively create needle of a desired height. A few of the factors mentioned were held constant to reduce the cost and time associated with experimentation. The KOH was always 45 % by weight because that is the standard weight used by the BYU clean room facility. The temperature was also

held constant, set to 79 °C in the etch bath. Thus the only two significant dependant variables affecting the experiment were the mask size and the etch duration.

The mask design was held semi-constant. A mask can be expensive to make so just one was used. The mask had nine different arrays of needle masks and each array had 64 identically sized masks in it. However, each array had a different set of mask sizes in it. The squares forming the masks were of varied sizes of length 1000, 1015, 1030, 1040, 1050, 1060, 1070, 1085, 1100 μm. The redundancy of the arrays ensured that a good sampling of needles could be attained for each size in every experimental run. The square masks would yield octagonal cross-sectioned needles. Experiments were done with these needles because, as mentioned in Appendix C, the square cross-sectioned needles had a more difficult mask design that was not discovered until much of the experimentation had been done.

The duration of each etch was iterated and readjusted with each run to the appropriate time needed to create a needle at its maximum height. Once a needle reached its maximum height it quickly reduced in size. The ideal run is one where the etch is stopped just as the needle comes to a point but before it has had any time to etch away any further. The general concept of the needle with the maximum height can be seen in Figure 4-8.

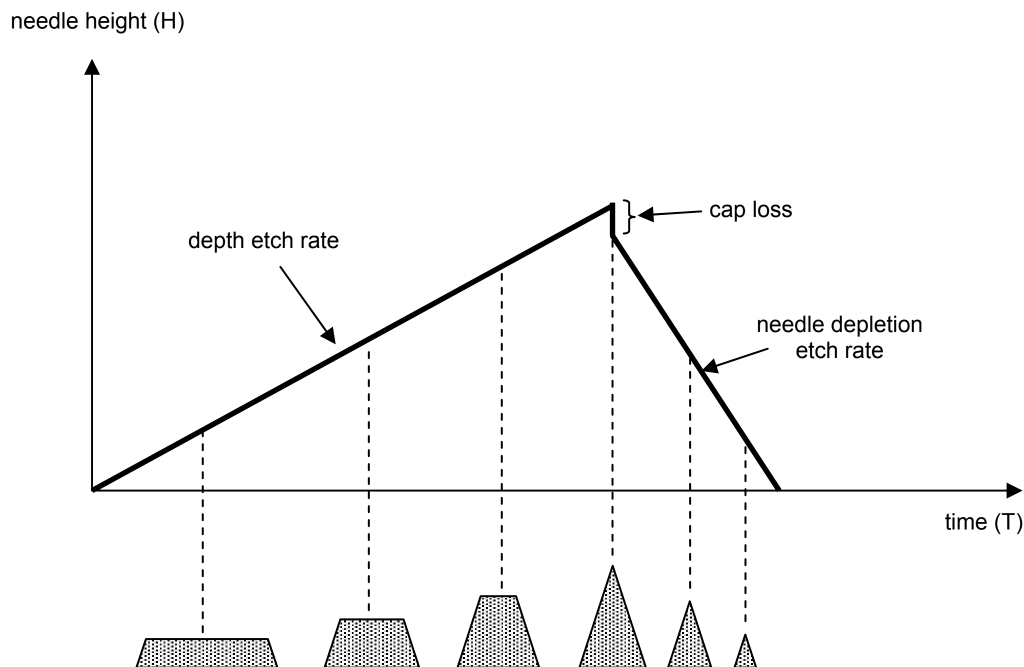

Figure 4-8: A general curve of needle structure height as a function of time showing the change in relative shape and size at particular points on the curve.

The needle will reach a different height depending on the size of the mask used to create the needle. As can be seen in Figure 4-9 each mask has a similar etch profile but the larger the mask to begin with, the longer it takes for the needle to be etched to its full height. A needle that takes a longer time to reach it maximum height will also be a taller needle.

Figure 4-8 and Figure 4-9 show a depth etch rate on the positive slope of the curve, which is the rate of silicon etch with respect to time, and the needle depletion rate on the negative slope of the curve, which is the rate that the needle shrinks once it is fully formed. Both figures also show what is called the “cap loss”. This refers to a small layer of silicon that caps the needle in formation until all sides of the needle come to a point at the top and the cap falls off. SEM images of such caps can be seen in Figure 4-10 below.

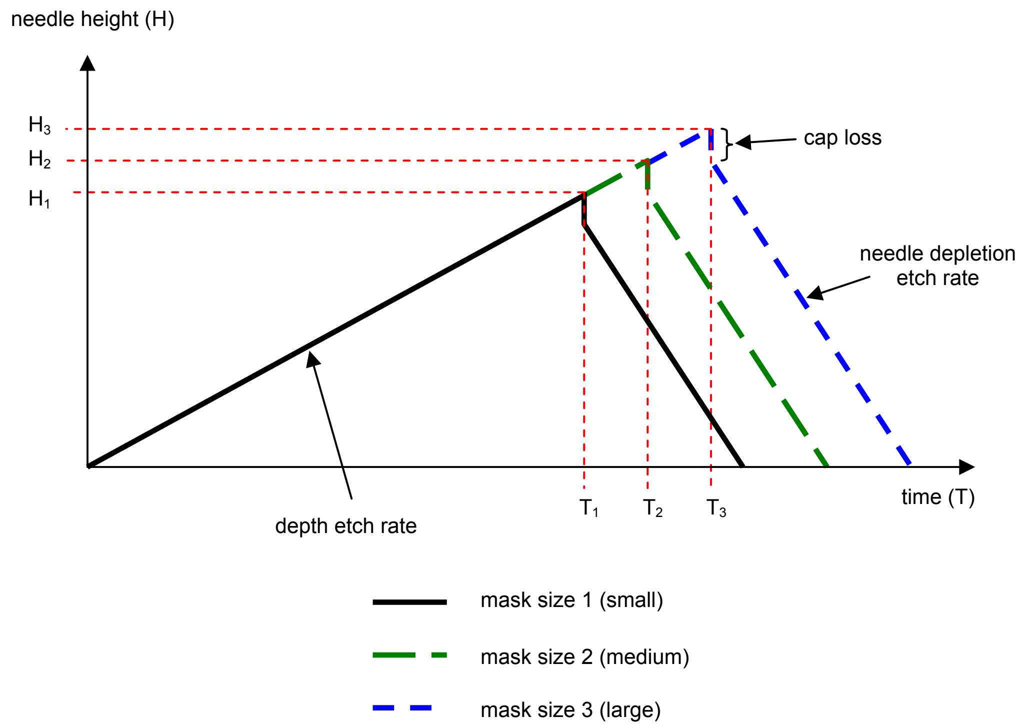

Figure 4-9: The maximum height of the needle and the etch time necessary to etch it will change according to the size of the mask used. The slopes will still remain constant.

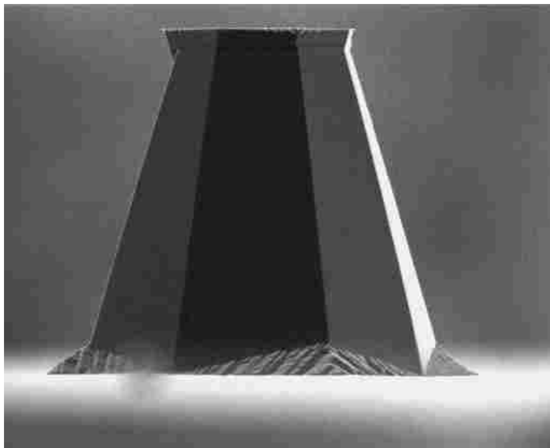
(a)

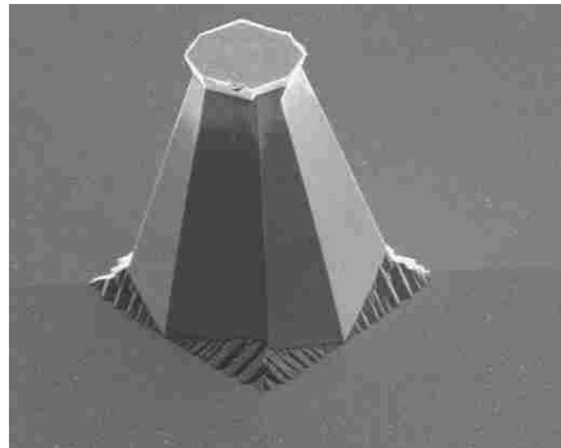
(b)

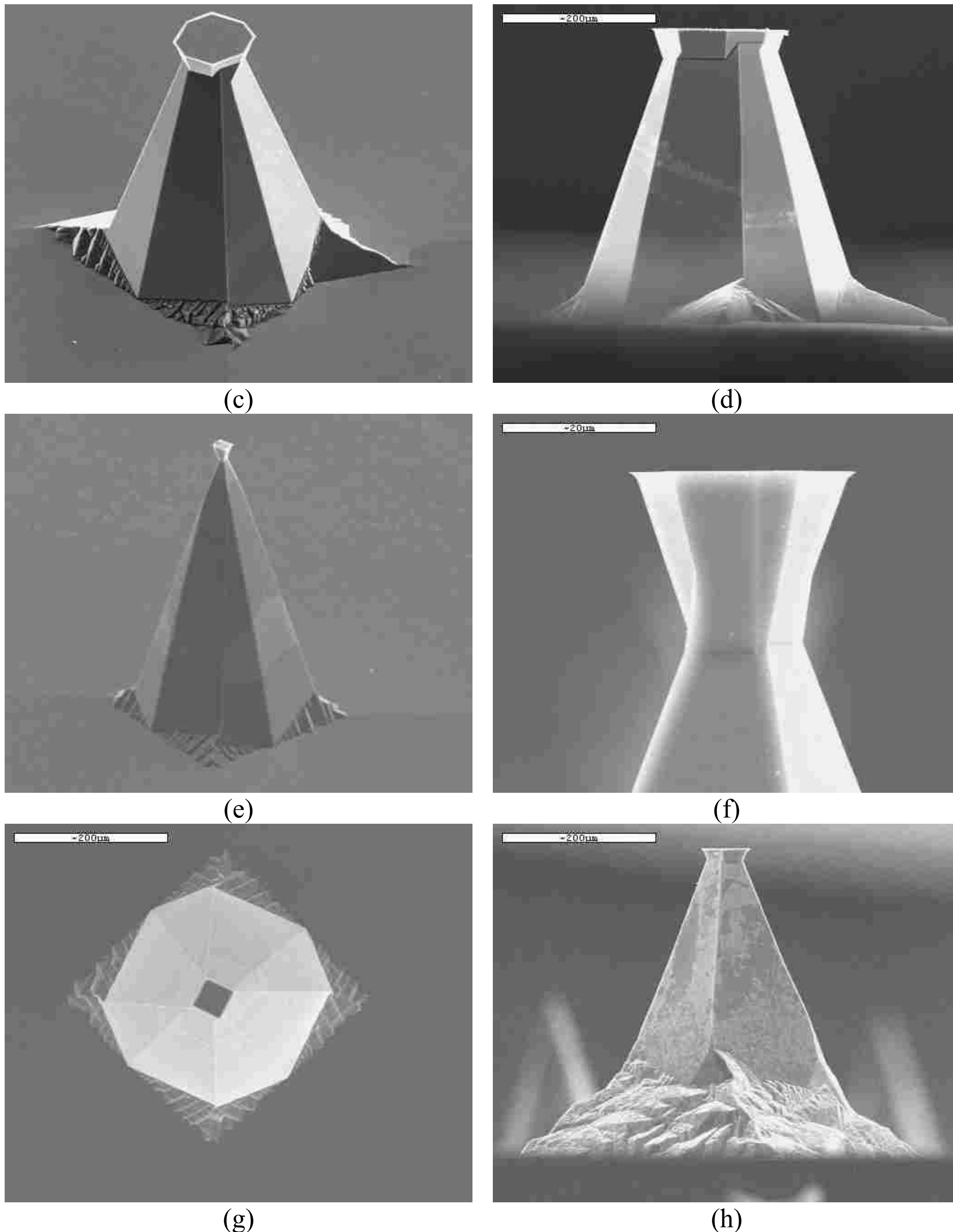

Figure 4-10: (a)-(e) show SEM images of different size structures that have not reached the point of becoming needles yet. The cap on top of the structure is the same general height regardless of its width. A close up view is seen in (f) and an overhead view in (g). (h) shows that even square shaped needles will have this cap.

As can be seen the cap is comprised of [411] planes just as the needle and mirrors the [411] planes of the needle. The cap has been measured anywhere from 12-35 μm high but the average height of the cap (measured from the small part of the neck where the cap and needle meet) is about 17 μm.

4.1.3 Microneedle Modeling

Based on experimental data a model has been created to predict the height of the needle based on the inputs of time and the size of the square mask used in etching. Some nomenclature used to create this model is given and defined below.

Needle Height (μm)	N_i
Predicted Needle Height (μm)	N
Time (min)	T
Depth Etch Rate (μm/min)	R_D
Lateral Etch Rate (μm/min)	R_L
Time of Max Needle Height (min)	T_x
Max Needle Height (μm)	N_x
Cap Height (μm)	C
Needle Depletion Rate (μm/min)	R_N
Square Mask Length (μm)	L
Needle Angle (deg)	θ
Delta Needle Height (μm)	$\Delta N = N_x - N_i$
Delta Etch Time (min)	$\Delta T = T_x - T$
Needle Base Line (μm)	d_1
Mask Base Line (μm)	d_2

The needle height, N_i, is the height of a needle measured at the end of an etch. As discussed previously, each etch produces nine different arrays of needles where each array's needle height varies from all other eight arrays on the wafer because different sized masks were used for each different array. Figure 4-11 and Figure 4-12 show an individual array of needle masks and the location of each array on the actual mask.

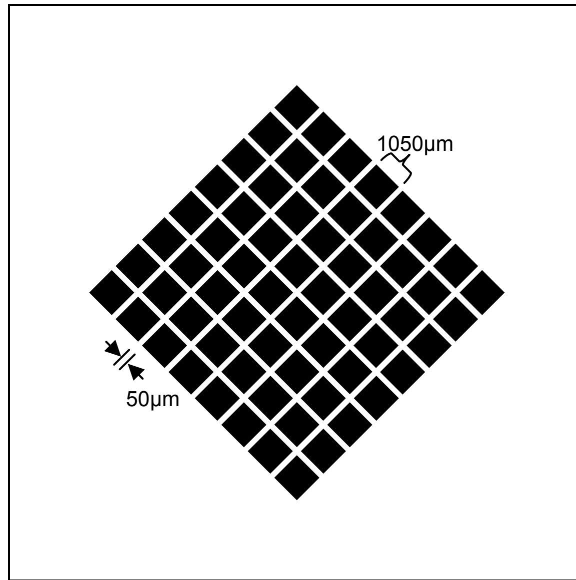

Figure 4-11: An individual array of needle masks. Each mask is 1050μm^2 and spaced 50μm from each other. This array is located in the center of the wafer as seen in Figure 4-12.

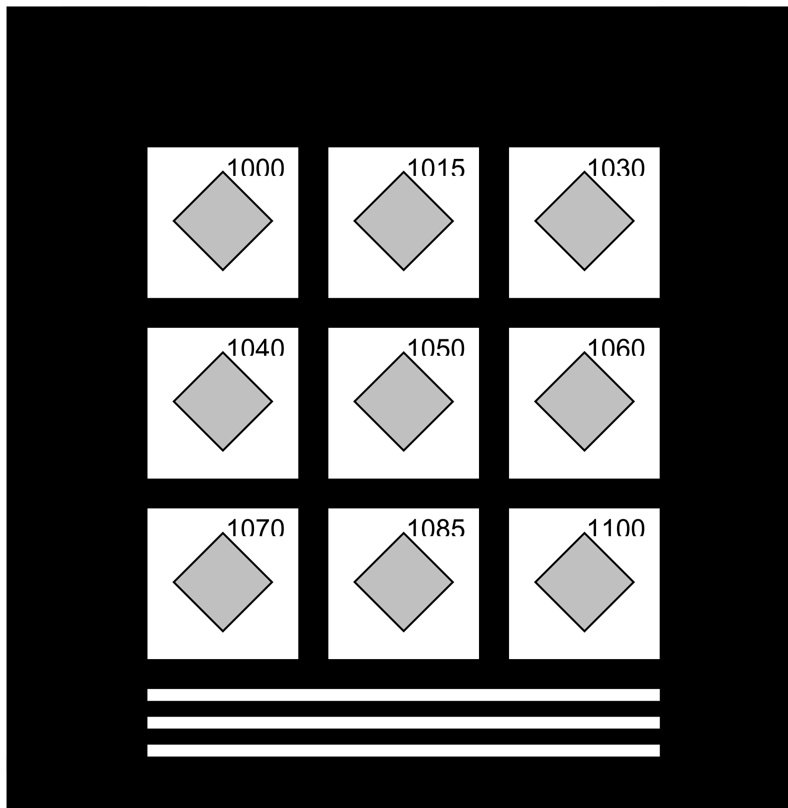

Figure 4-12: Nine different arrays, each with the size of the square mask annotated in the top right hand corner of the cell, will yield nine different heights of needles at the end of an etch.

The predicted needle height, N, is the calculated height of a needle based on the mask size and the duration of the etch. The time, T, is the duration of an individual etch. Etch times ranged from 450 to 482 minutes. The depth etch rate, R_D, is the rate at which the KOH etches down into the silicon substrate. The lateral etch rate, R_L, is the rate at which the needle structures are etched parallel to the surface of the substrate. The max needle height, N_x, is the maximum height needle that can be created by the square mask being used. This value is constant for a particular size mask. The time of max needle height, T_x, is the etch duration necessary to create the maximum height needle. The cap height, C, is the height of the cap at the top of the underdeveloped needle. The average value of C is 17μm. The needle depletion rate, R_N, is the rate at which the needle height decreases once the needle is fully formed and the mask is no longer protecting it from direct KOH etching. The square mask length, L, is the length of a given side of the mask used to create the needle. The needle angle, θ, is the angle between the base parallel to the substrate and the edge of the needle. The value of θ is approximately 72°. ΔN, is measured for each run and each mask size and is equal to the difference between the maximum needle height of a given square and the actual needle height in a particular run of the same given square. ΔT, is similar to ΔN except it is the difference between the maximum needle height time of a given mask and the actual etch time for a particular run. Needle base line, d_1, is the distance from one side of the base to the other measured from opposing corners and mask base line, d_2, is the distance from the edge of the needle base to the point where the outer edge of the mask had been prior to etching (see Figure 4-14).

The values N_i, T, L, and d_1 are measured from each experimental run. The values C, and θ are constant. The values N_x (see Equation 4-1), T_x (see Equation 4-2), N (see Equation 4-3 and Equation 4-4), d_2 (see Equation 4-5), R_D, R_L, and R_N, are calculated from the measured and constant values. These calculations are shown or explained below.

for (*T=Tx*) $$N_x = \left(R_D \cdot T_x\right) - C \tag{4-1}$$

$$T_x = \frac{\frac{\sqrt{2}}{2} \cdot L}{\frac{R_D}{\tan\theta} + R_L} \tag{4-2}$$

for ($T<T_x$) $$N = R_D \cdot T \tag{4-3}$$

for ($T>T_x$) $$N = \left(R_D \cdot T\right) - C + R_N\left(T - T_x\right) \tag{4-4}$$

$$d_2 = \left(\frac{\sqrt{2}}{2} \cdot L\right) - \frac{d_1}{2} \tag{4-5}$$

The three rates R_D, R_L, R_N, are not shown in equation form as easily as the others so will be explained in detail. The depth etch rate, R_D, is found by acquiring the slope of the trend line formed by the etch time and etch depth data points for each experimental run. The trend line and experimental data for the depth etch rate can be seen in Figure 4-13. The slope, R_D, of the trend line was found to be 0.89µm/min.

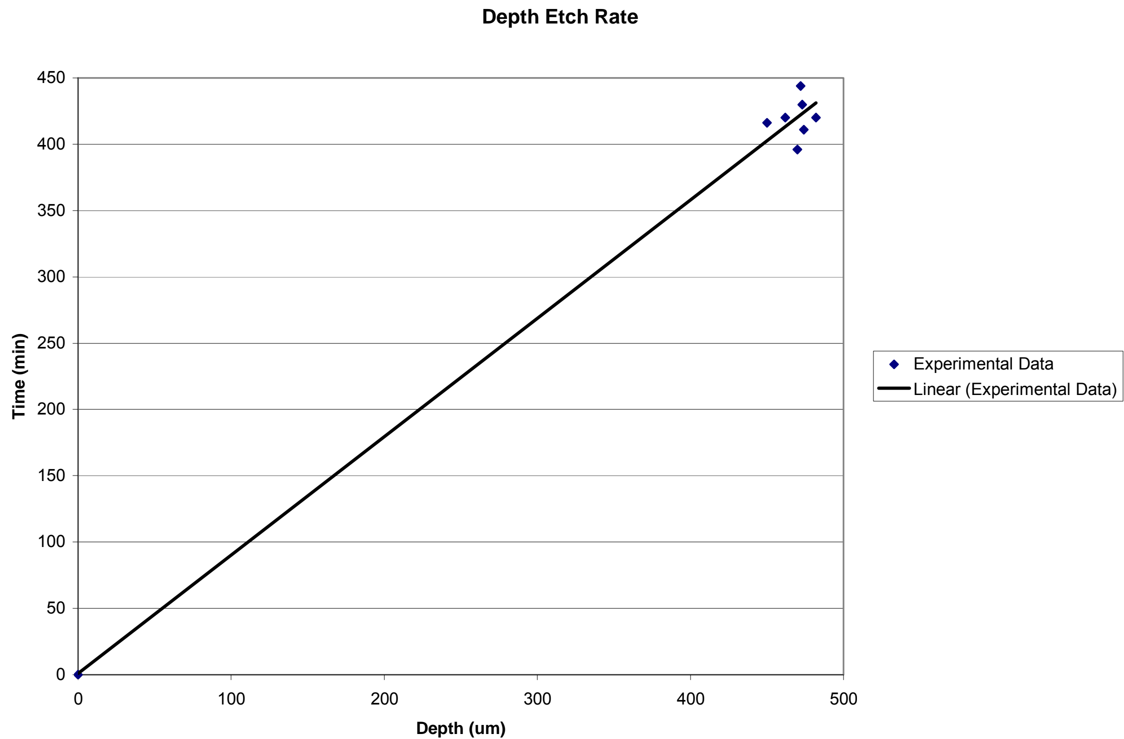

Figure 4-13: The depth etch rate, R_D, is the slope of the trend line formed from the time and depth of each etch. The point (0,0) is included as a data point as well.

The lateral etch rate was found by averaging the lateral etch rates of each experimental run. At the time of the creation of this model there were 7 experimental runs and the lateral etch rate, *L*, was found to be 1.38 µm/min with a standard deviation of 0.06 µm/min. The lateral etch rate of each run was found by averaging the lateral etch rate of each square mask size. Thus nine lateral etch rates per experimental run were found. Standard deviations for each run were usually 0-0.01 µm/min (see Table 4-1).

Table 4-1: The lateral etch rate values for each mask in each run. Each value is equal to d_2 divided by T. Some of the values are left blank because they correspond to underdeveloped needles.

	Run #						
Mask	**9**	**10**	**11**	**12**	**13**	**14**	**16**
1000	1.37	1.35	1.26	1.39	1.45	1.42	1.43
1015	1.37	1.35		1.39	1.44	1.41	1.43
1030	1.38	1.35		1.39	1.44	1.41	1.44
1040	1.37	1.35		1.39	1.45	1.41	1.44
1050	1.37	1.34		1.39	1.44	1.41	1.43
1060	1.36	1.35		1.39	1.44	1.41	1.43
1070	1.38	1.35		1.38	1.45	1.41	1.43
1085	1.37	1.34		1.39	1.45	1.42	1.43
1100	1.36			1.34	1.44	1.41	1.43
average	1.37	1.35	1.26	1.38	1.45	1.41	1.43
R_L	**1.38**						

The values for d_1 and d_2 are found from the geometries of the needle base and the mask for that needle. An overhead view of these geometries used can be seen in Figure 4-14.

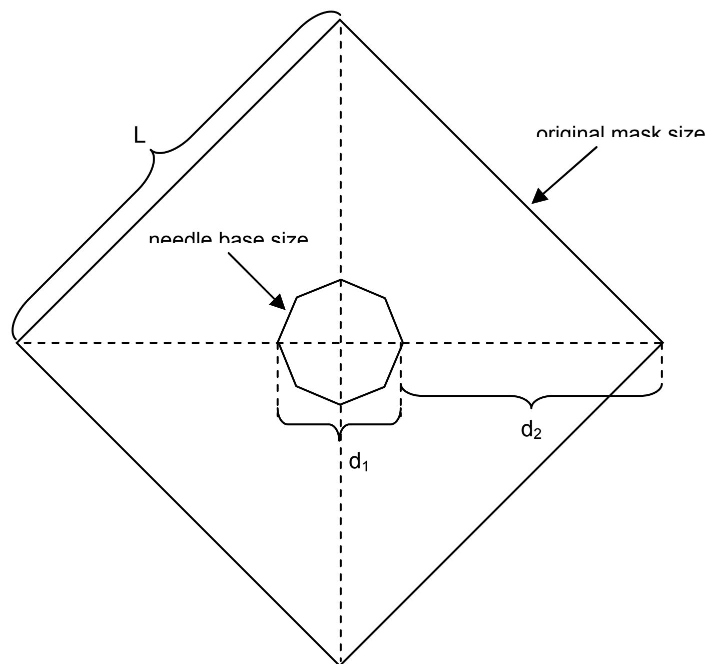

Figure 4-14: An overhead view of the mask and needle base outline.

The needle depletion etch rate, R_N, was the rate at which a fully developed needle would decrease in height as it underwent continuous KOH etching. This rate was found to be about 4.14 μm/min with a standard deviation of about 0.16 μm. This rate is the average of six different slopes found from the trend lines of ΔN plotted against ΔT for six different experimental runs (see Figure 4-15). There are nine different values of ΔN and ΔT for each run derived from the nine different values of N_x, N_i, and T_x from each run.

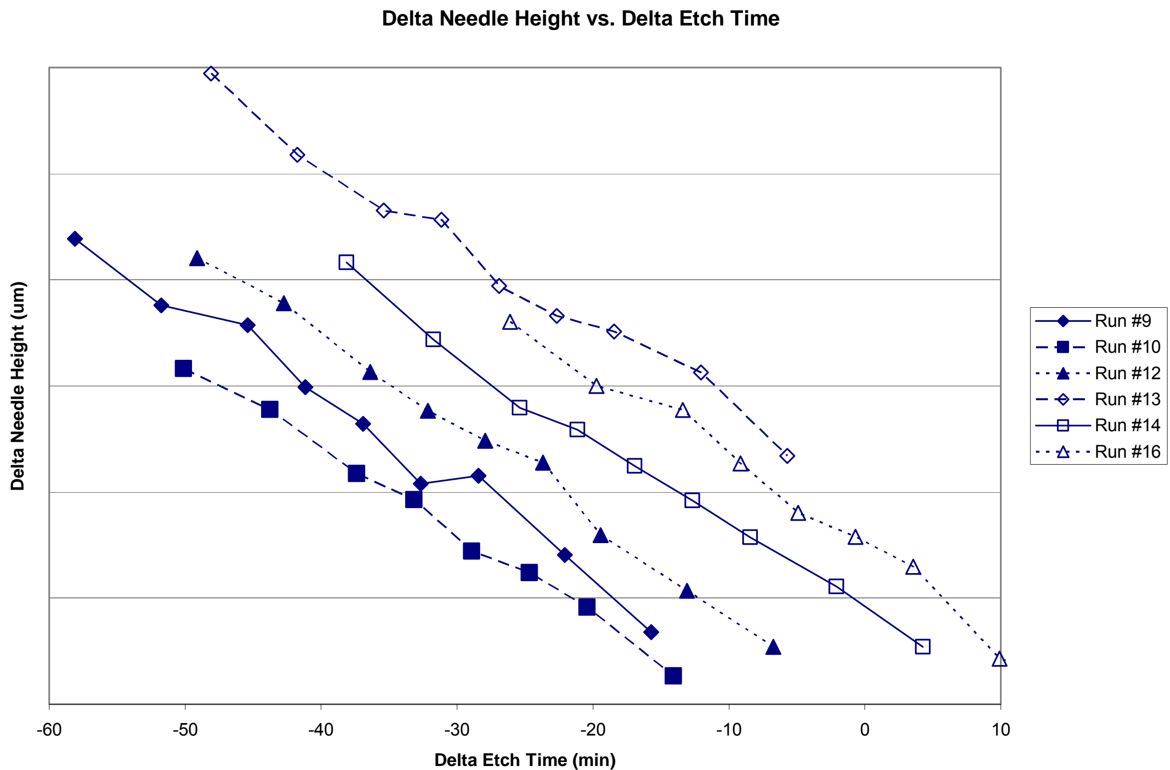

Figure 4-15: Calculated values of ΔN and ΔT for experimental runs 9, 10, 12, 13, 14, and 16. Connecting lines are added for visual clarity.

Based upon calculations, the height of a microneedle can be predicted based upon the size of the square mask (referenced by its length, L) the duration of the etch, T. A surface

model showing height as a function of square size and etch time is shown in Figure 4-16. The data for this plot is derived from Equation 4-3 – Equation 4-4.

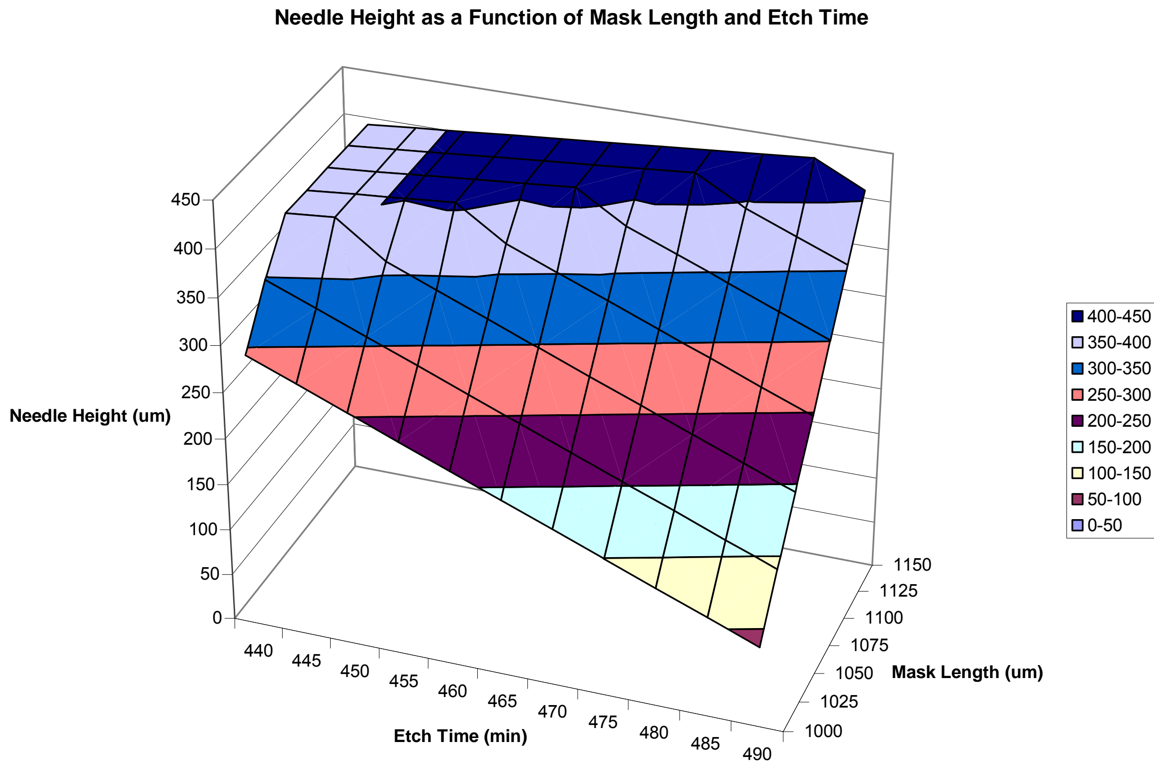

Figure 4-16: Surface model showing the height of a microneedle as a function of the mask length and etch time.

Based upon experimental results, a mask was created to make nine arrays of identically sized needles. The mask lengths are 1115 µm and the maximum needle height, N_x, expected from these masks is 404 µm high. The expected time, T_x, to etch these needles is about 472 minutes or 6 hours and 52 minutes. SEM images of the final needles etched from the 1115 µm mask size can be seen in Figure 4-17.

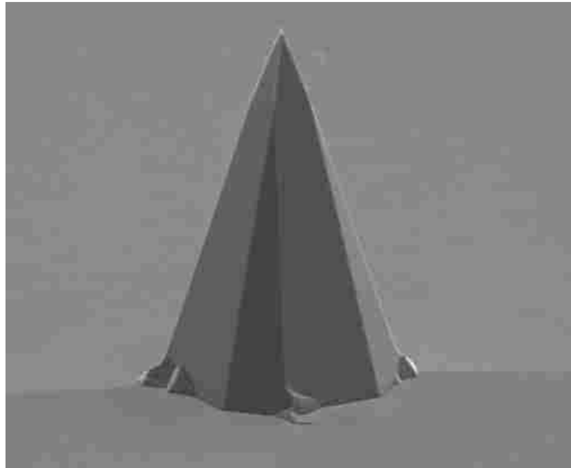

Figure 4-17: Microneedle etched with new 1115 µm length square mask.

4.2 Microchannels

4.2.1 Microchannel Fabrication

Microchannels were successfully developed using the procedures described in chapters 2 and 3. To ensure that the entire process can be repeated a detailed description of specifications and recipes is provided in Appendix E.

The nitride covered wafers described in section 4.1.1 were used to create the microchannels. There were also some thin wafers (325 $\pm$ 25 µm) used that were acquired from the Stanford Nanofabrication Facility at Stanford University.

The wafers were stripped of the LPCVD nitride, rinsed and dehydration baked so as to have a clean surface to start with. The thin wafers had no films deposited on them so they only required a dehydration bake for preprocessing.

When prepared, the wafer would then be coated with photoresist yielding a 10-12 µm thick coating on the surface of the wafer. The mask pattern would be exposed onto the

resist and the wafer is attached to a base wafer. At this point the wafer would be ready for the ICP etch. The recipe for this etch and the process by which is was discovered is found in Appendix F and ICP operating instructions are found in Appendix G.

After the etch is complete the sample wafer (still attached to the base wafer) is rinsed in acetone and isopropanol to remove the SPR-220 from the surface of the wafer. Then the two wafers are place in a dish containing "Nanostrip" which will attack the photoresist glue holding the two wafers together. The dish is placed on a hotplate set to 90 °C for at least 2 hours. Nanostrip will not attack the silicon wafers so there is no danger of leaving the wafers in longer than 2 hours. When separated, the wafers are removed from the Nanostrip and rinsed with fresh distilled water for at least 5 minutes in the same water tank that is generally used for rinsing after an HF stripping. At the completion of all these processes the wafer can be cleaved and labeled for channel flow testing.

4.2.2 Microchannel Fabrication Analysis

The original microchannel mask was made with channel structures both 3 and 5 μm wide. Although it was not known at the time, structures this small will not endure an ICP etch for 4 hours and 20 minutes. The resulting channels contained no structures because they had been etched away during the ICP process.

The photoresist, acting as a mask for the desired features, is not completely resistant to the ICP etching process and over time the masking material is etched away exposing the silicon underneath which is then etched as well, at a much faster rate than the photoresist.

The ratio of the etch rate of the silicon compared to that of the photoresist is called "selectivity".

The original design for the channels, which had to be discarded, can be seen in Figure 4-18. In this figure each quadrant shows a single channel profile with its design identification. The first number in the identification is the number of structures in the channel. The second number in the identification is the width of the structures in that channel. The control channels were designed to be the same diameter as the effective inside diameter of the rest of the channels.

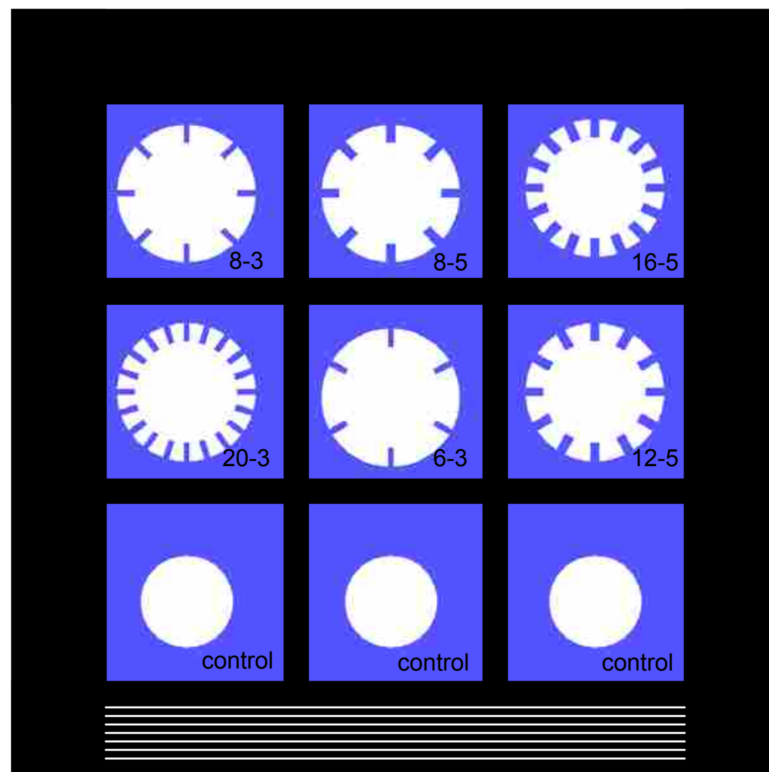

Figure 4-18: The six different structured channels and control channel masks originally attempted are shown. Each quadrant contains a visual representation of the channel shape that existed in each array of that respective quadrant. All three control channels are the same size.

Once the difficulties regarding selectivity were understood a test pattern was created and included with one of the masks to be able to determine the selectivity with structures like the ones hoped for in the microchannels. The test pattern had identical sets of structures in threesomes. Each set of structures was 12, 16, or 20 µm high and the sets range in structure width from 10 to 30 µm increasing incrementally in width by 2 µm from one set to the next. These test structures can be seen in Figure 4-19.

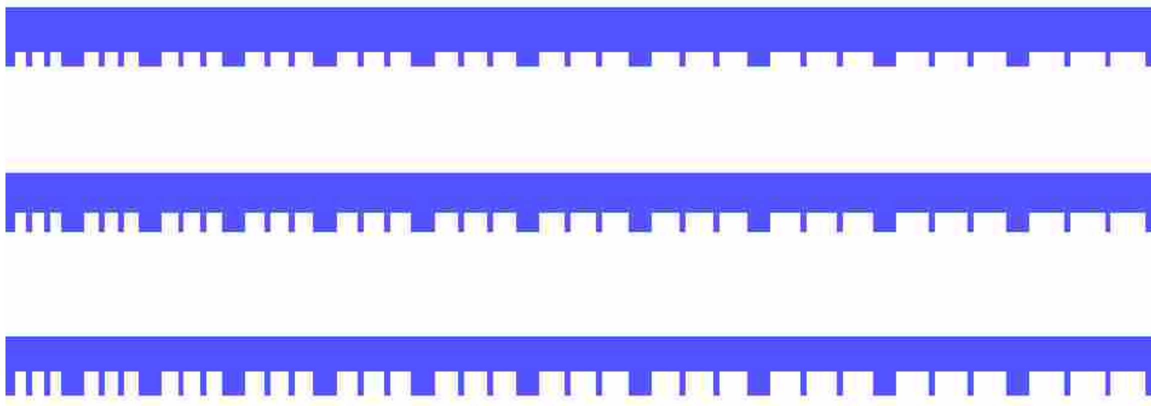

Figure 4-19: Test structures designed to study selectivity of photoresist. In the top row all structures are 12µm high and vary in width from 10-30µm increasing incrementally by 2µm for each set of three. The second and third row have the same width structures as the first row only the height increases to 16 then 20µm in the second and third rows respectively.

A second set of set test shapes were created to understand the expansion of the channels during the etch. It had been observed that the diameter of the channels was greater after being etched than were the original diameters of the masks. To understand the selectivity effects on channels, six sizes of smooth walled circular masks were designed to find the increase of a typical microchannel during an etch. The diameters of these circular masks were 50, 55, 60, 65, 70, and 75 µm.

The selectivity study was done using the same etch parameters intended for the final microchannel design. The results show the effects of the ICP etch on these particular features. The difference between the original test mask and the final etch results can be seen in Figure 4-20, where a portion of the original mask is overlaid on an SEM image of the etched silicon. Some of the effects, in particular, are a 9 μm increase in the diameter of any channel or the tendency for structures to etch away altogether if they are smaller than 16 μm high or about 18 μm wide. In sets of three the middle structure tends to keep its shape better than the outside ones and structures with other features near them, such as the reference marks that were included, will retain their shape better than those not near other etched features.

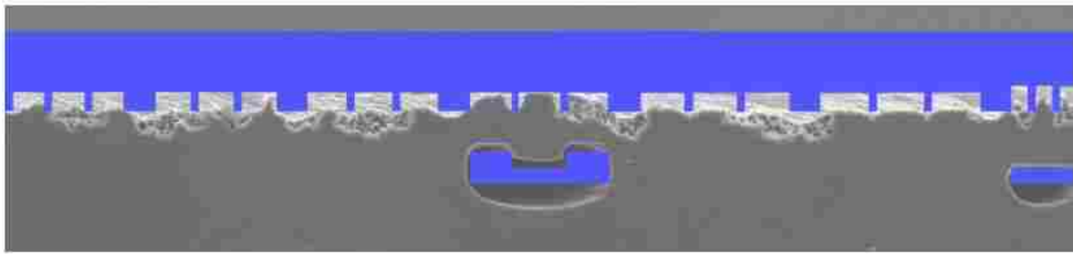

Figure 4-20: A view of the original selectivity mask overlaid on an SEM image of the results features etched with the mask. This and other data were used to determine the etching characteristics of the features. The shapes below the structures are reference marks.

The new mask design was designed to compensate for the increase in diameter of the channels and the reduction in size of the channel structures. The following parameters and constraints are important to consider in the design of the new mask.

- $w_{s0} = w_{s1}+7$ μm (based on experimental results)
- $w_{s1} \geq 5$ μm (designer preference, any thinner and the structures may disappear altogether by the end of the etch)

- $w_{s1} \leq w_{g1}$ (designer preference to get at least F_s of 50%[3])
- $w_{g0} \sim w_{g1}$-7 µm (based on experimental results)
- $w_{g1} \leq 25.8$ µm (maximum gap width (with safety factor) before wetting occurs between structures)
- $S \geq 6$ (designer preference)
- $H_0 \geq 16$ µm (based on experimental results)
- $H_1 \sim H_0$ (if $H_0 \geq 16$ µm) (based on experimental results)
- $D_0 = D_1$-9 µm (based on experimental results)
- $D_1 \leq 80$ µm (designer preference, if channel is too wide it will dominate the body of the microneedle)
- $D_i = [D_1 - (2^*H_1)] \geq 25.8$ µm (above size of maximum rib gap "w_{g1}" to ensure fluid flow)

In this list all initial parameters using a sub-reference of "0", (ie: $w_{s\text{“}0\text{”}}$) refer to the dimensions of the mask design and all secondary parameters using a sub-reference of "1", (ie: $w_{s\text{“}1\text{”}}$) refer to the dimensions of the channel after the etch has been completed. w_s is the structure width, w_g is the gap width, S is the number of structures in a particular channel, H is the height of the structures, D is the outside diameter of the channel, and D_i is the inside diameter of the channel. All parameters are measured in "µm" except for "S" which is an integer.

Based upon the parameter constraints six new channels were designed (see Figure 4-21). The cavity fraction of the channels, seen in Table 4-2, was not as high as the original channel designs due to the limitation of the constraints but they were still sufficiently high to give good expected flow results.

---

[3] $F_s \leq 50\%$ does not show significant improvement in flow rate [18] B. Woolford, K. Jeffs, D. Maynes, and B. W. Webb, "Laminar Fully-Developed Flow in a Microchannel with Patterned Ultrahydrophobic Walls," in *2005 Summer Heat Transfer Conference*, 2005.

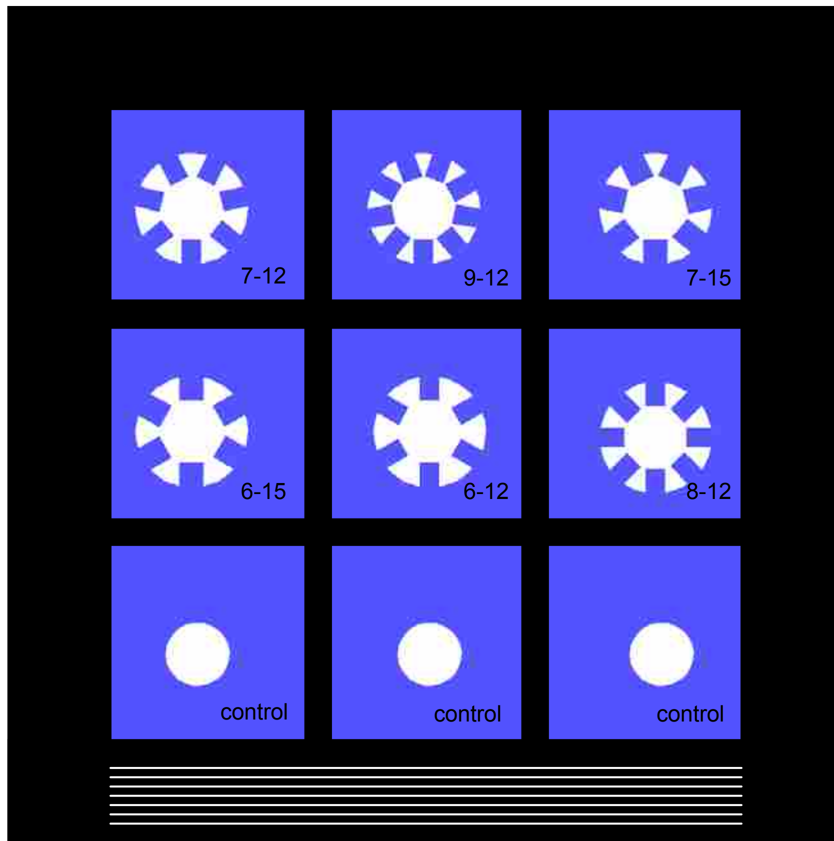

Figure 4-21: Each channel design is shown in the quadrant where an array of the corresponding channel is located. The control channels were designed to increase in diameter and thereby have an equal diameter to that of the effective inside diameter of the structured channels.

Table 4-2: The left column shows the design identification, labeled just as those in Figure 4-21, along with the predicted or desired identification number that should correspond to the fully etched channel.

Design	Predicted Size	Anticipated F_s
6-12	6-5	80%
6-15	6-8	68%
7-12	7-5	77%
7-15	7-8	63%
8-12	8-5	73%
9-12	9-5	70%

4.2.3 Microchannels Fabrication Results

The results of the etch, in Figure 4-22, yielded a satisfactory outcome from a substrate surface inspection. However, as expected from previous etch observations, the bottom of the channel profile did not match the top of the channel. Figure 4-23 shows that some tapering has occurred in the channel and that the opening on the bottom end of the channel is a much smaller diameter.

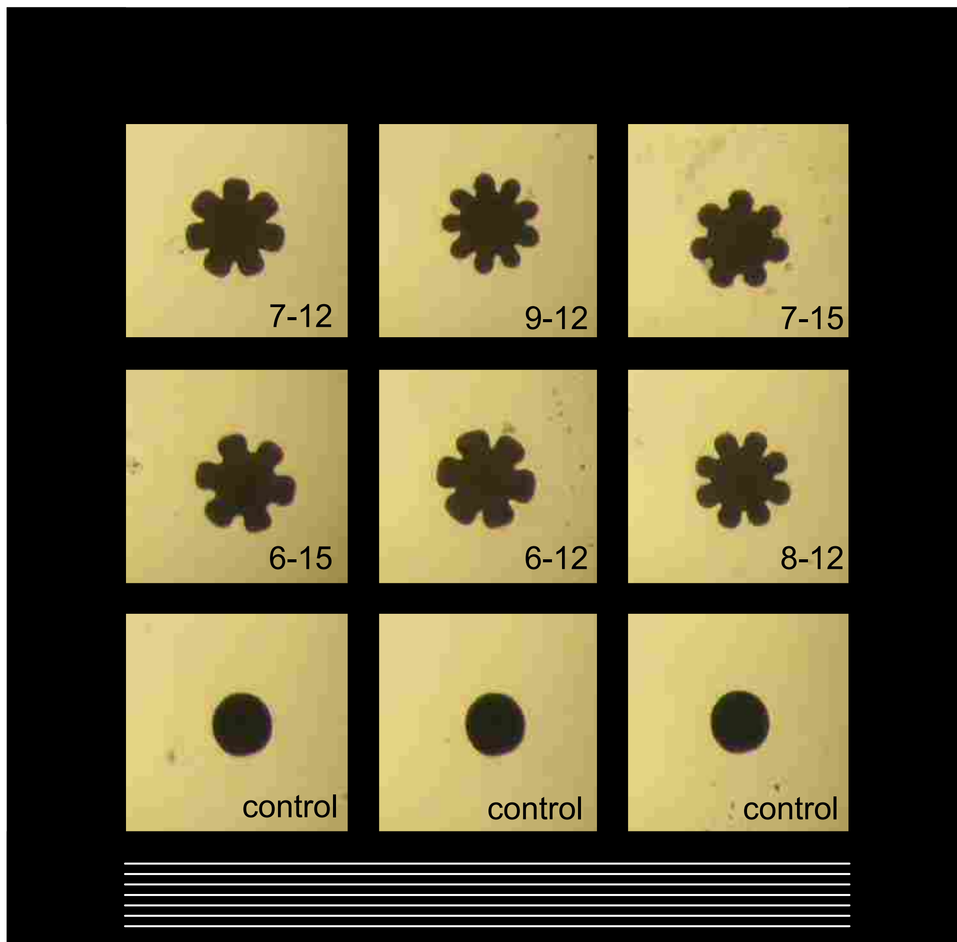

Figure 4-22: Each quadrant of the mask shows the design number (ie: 7-12 in the top left quadrant, representing 7 structures each 12µm wide) and a picture taken through an optical microscope of the surface of one of the channels.

Figure 4-23: An optical microscope view of a typical 7-12 channel on the top surface (left) and on the bottom surface (right) of the wafer. These two pictures were taken at identical magnification.

A tapered channel will not provide appropriate conditions for hydrophobic flow due to the lack of cavities at one end of the channel. An ideal hydrophobic channel is one that has a uniform cross section throughout its entire length. To obtain such channels a thin wafer (380 μm) was used to etch hydrophobic channels. After some experimentation it was found that the same recipe used to etch the thick wafers was sufficient for the thin wafers except the time was reduced to 3 hours. The resulting channels have similar cross sections on the surface just as the channels made in the thick wafer do; however, the far end of the channel is a little wider and has a little bit of "blowout" at the end. The term blowout, sometimes called the notching effect [34], refers to the characteristic shape of the bottom of a channel that is mis-formed and wider in diameter than the rest of the channel as seen in Figure 4-24 and Figure 4-25. The cross section of the channels as seen from the top view in Figure 4-26 was used to determine the general cavity fraction, F_c, of each set of channels (see Table 4-3). These were the channels eventually used for flow testing.

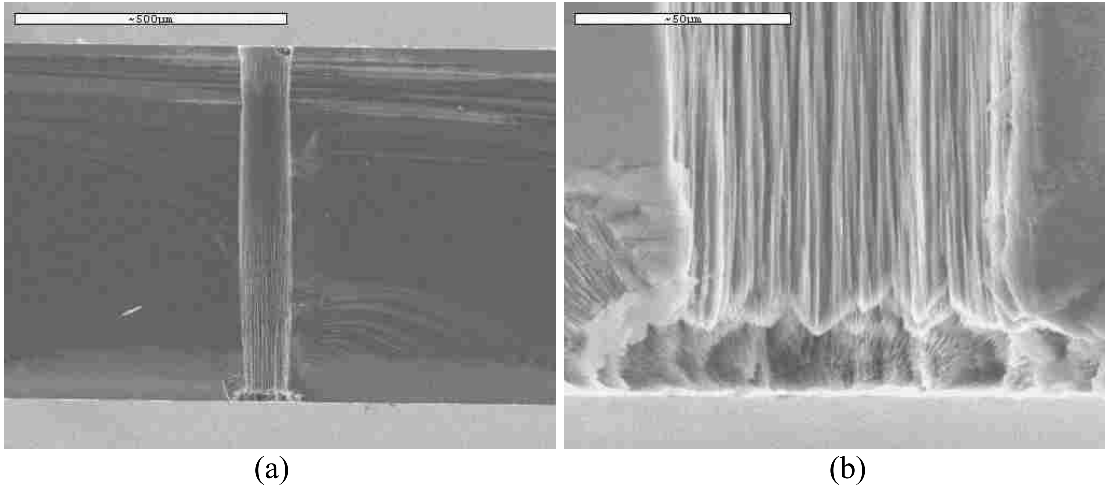

(a) (b)

Figure 4-24: A cross-sectional SEM view of a microchannel (a) 660 µm deep shows blowout at the bottom. A close-up view in (b) shows the blowout again.

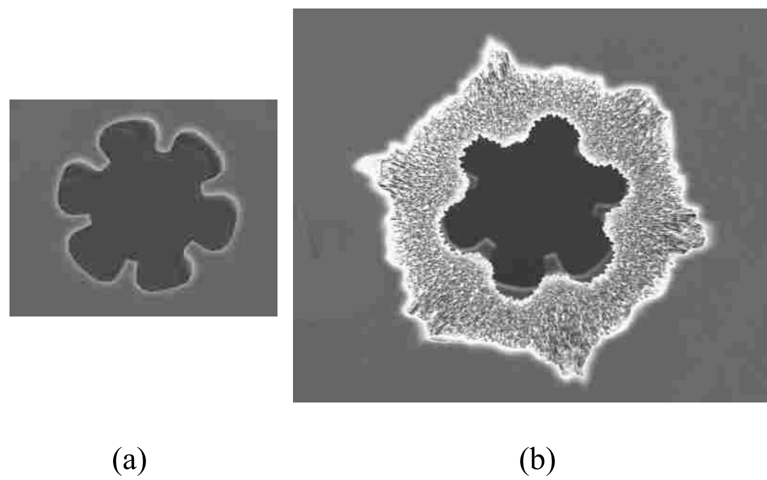

(a) (b)

Figure 4-25: Proportional SEM images of the front (a) and back side (b) of a channel in quadrant 5 of the wafer. The rough, high contrast, surface in (b) is an overhead view of the blowout that occurs in etching. Also noted is the fact that the structures will lose some of their definition by the end of the channel.

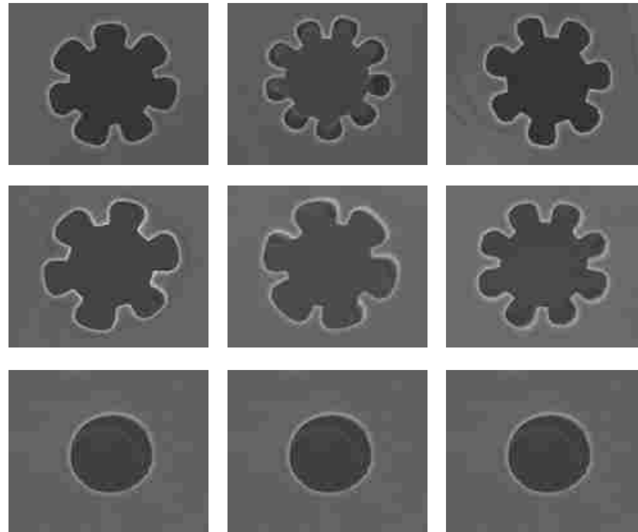

Figure 4-26: Representative SEM images of channel profiles in each quadrant space as shown in Figure 4-22 showing the general definition of the structures in each 660 μm long channel.

Table 4-3: The design I.D. of each array is shown with the quadrant number in which it is located and the calculated cavity fraction, F_c, based on the measurement of cross-section of the channel at the top of the wafer surface.

Design I.D.	Quadrant #	F_c
6-12	5	79.1%
7-12	1	76.5%
8-12	6	70.9%
9-12	2	69.8%
6-15	4	67.0%
7-15	3	63.9%

4.3 Combining Microchannels and Microneedles

4.3.1 Microneedle/Microchannel Fabrication

To create microneedles combined with microchannels both microneedle and microchannel fabrication procedures must be followed nearly in their entirety. The microchannels are made first. After all procedures in section 4.2.1 have been followed,

up to the Nanostrip bath, the wafer is rinsed and removed from the water tank but not cleaved. To prepare the channels for microneedles they must first receive an LPCVD nitride film. This deposited layer will serve as a mask for needle etching and will also serve as a protective coating on the inside of the channels to prevent them from etching away in the KOH bath. This deposition is done at the Utah Microfabrication Lab at the University of Utah. Approximately 500+ nm of LPCVD nitride is deposited onto all exposed surfaces of the wafer.

Once the LPCVD nitride layer is deposited, the wafer is ready for microneedle fabrication. The process for microneedle fabrication described in section 4.1.1 can now be followed resulting in microneedles with microchannels running vertically through the middle. Only two slight changes are needed for this process. When transferring the microneedle mask from photoresist (AZ-3330) to nitride the RIE process must be run for 10 minutes instead of 6 minutes and 35 seconds. This is because the nitride layer is a little thicker than the original coating used. The HF nitride strip at the completion of the KOH etch must also be longer than the one done previously. Again, this is because the nitride is thicker than the layer used in previous fabrication.

Some of the concerns of etching needles over microchannels revolve around the effectiveness of the nitride film protecting the inside of the channels. The film will be thinner in the middle of the microchannels than it is by the entry/exit regions. If it is too thin the KOH will eat through the protective layer and etch the silicon wafer from the inside out. Another concern is that the nitride may be thin around the edges of the

microchannels allowing the KOH to etch away at the surface of the needle mask before the needle has been etched. Both of these concerns are addressed in section 4.3.2.

4.3.2 Microneedle/Microchannel Fabrication Results

Microneedles combined with microchannels were successfully fabricated. As observed in Figure 4-27, the needles appear very similar to their predicted shapes as depicted in the CAD drawings seen in Figure 3-1.

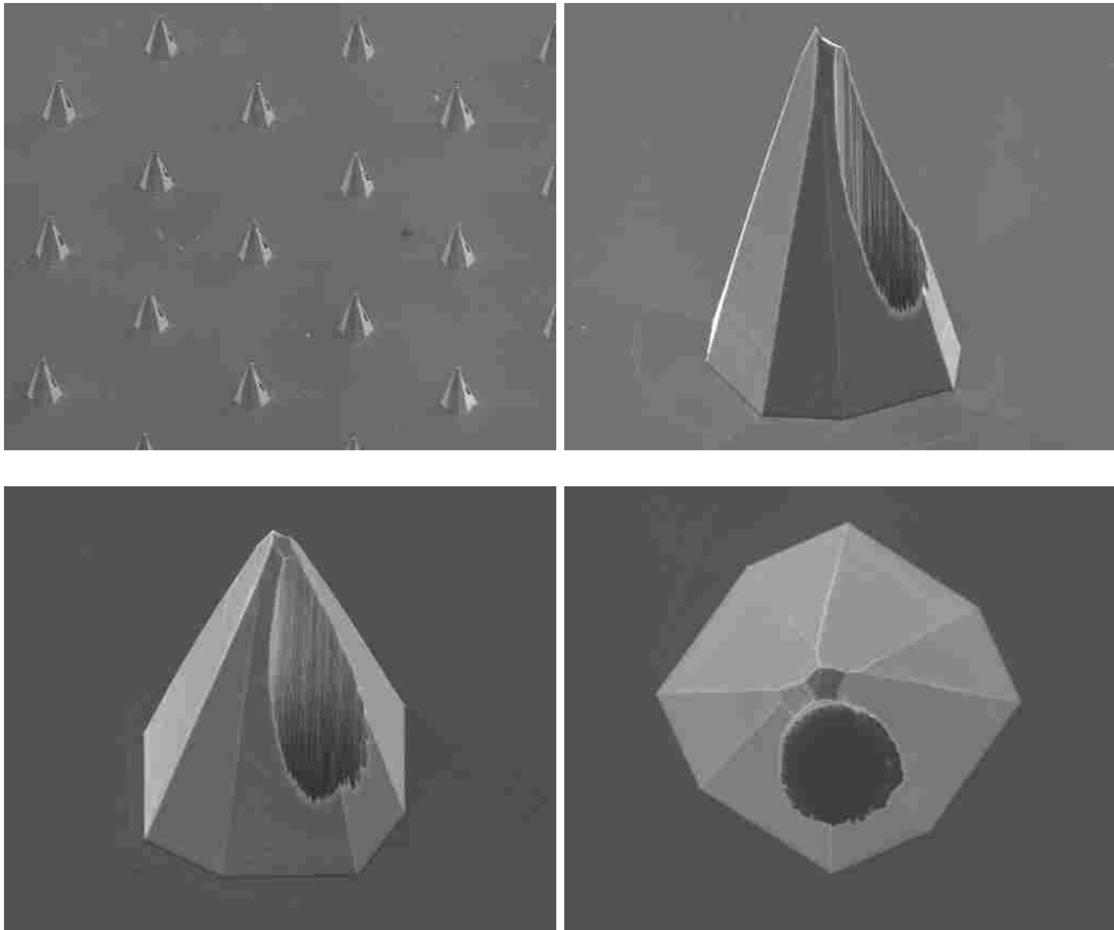

Figure 4-27: Multiple views of a microneedles combined with microchannels. The channel is about 95µm in diameter and the needle base, measuring from opposing corners, is about 295µm.

The successful combination of microneedles and microchannels depends on two factors. The first is the accurate alignment of the needle mask over the channels on the wafer. The other is that the KOH etch is stopped at the right time. If the KOH etch runs too long the needles will be etched away and the channels will dwarf the needles in size causing the two features to be proportionately awkward.

Microneedles were made that were not accurately aligned to the microchannels. Although the resulting structures were undesirable they allowed views of the channel integrity after a complete KOH etch. Figure 4-28 shows the results of this etch from a sample that did not undergo an HF rinse and therefore did not have the nitride stripped away. One of the telling observations from this image is that the nitride performed very well in the KOH bath. It can be noted, however, that this deposition is not perfect; the cylinder in the bottom right hand corner of Figure 4-28 shows some square etching in the substrate, indicative of a “pinhole” leak in the nitride which allowed KOH to etch through to the silicon.

It was found that the integrity of the LPCVD nitride at the edges of the microchannels was also exceptional. One wafer was viewed through an optical microscope several times during the KOH etching process. It was observed that KOH did not penetrate the needle mask at the points where the channels were located.

It is observed that the needles in Figure 4-27 have no surface roughness around the base as is common in other microneedle samples without channels. It is believed that this is due to the new mask material used. In most needle etches the mask was comprised of 150 nm LPCVD nitride on top of 300 nm thermal oxide. The new mask is 500+ nm of

LPCVD nitride. Most likely the faster etching (relative to the etching of the LPCVD nitride mask) of the underside of the thermal oxide mask causes a certain amount of surface roughness at the base of the needle.

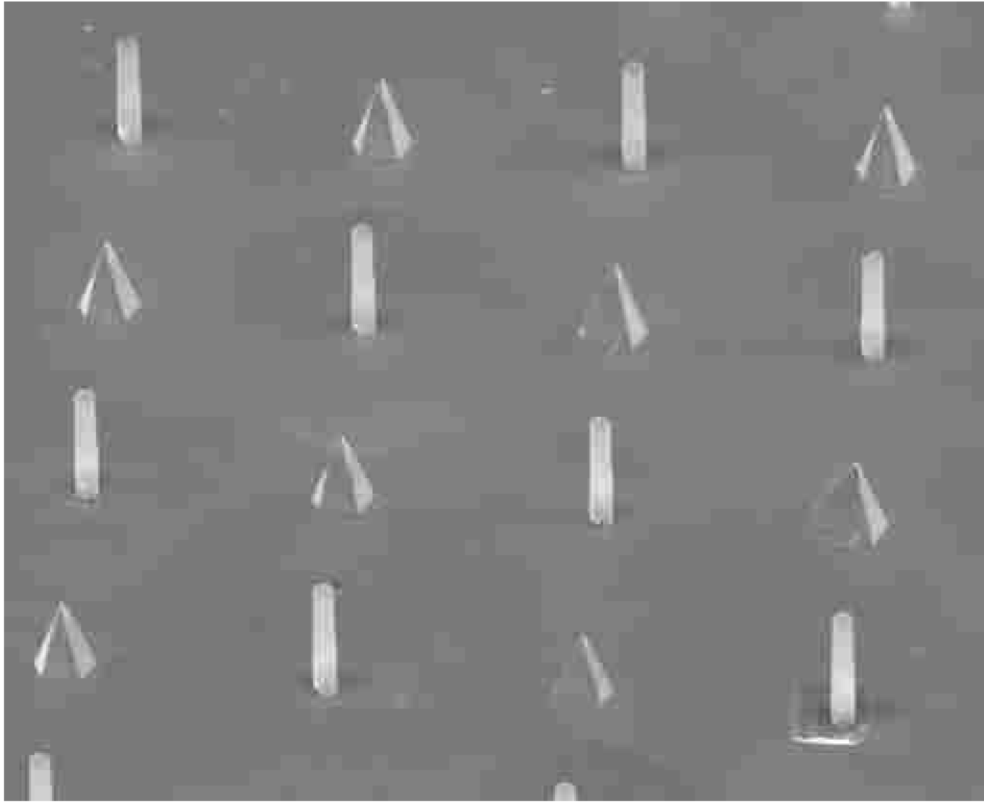

Figure 4-28: The needle and channels masks were not accurately aligned in this sample. This revealing SEM image (of sample that did not undergo an HF rinse to strip the nitride) shows long thin nitride cylinders where microchannels once were. This sample was etched in KOH to a depth of about 435µm.

Chapter 5 - Experimental Flow Results

5.1 Test Stand

The microchannels are tested in a test stand (see Figure 5-1) built to record timed volume flow under various flow pressures. The microchannels are sandwiched between two identical miniature reservoirs. One reservoir is fed by a large tank reservoir and the other flows out to a solenoid valve that regulates the flow through the system. The small reservoirs are connected to either end of a pressure transducer which measures the pressure difference between the two reservoirs. The pressure transducer and solenoid valve are powered by a power supply. Each of the small reservoirs also has a thermocouple inserted into them to read the temperature of the water in each reservoir. A Labview program is used to start and stop the solenoid valve at specific times and also records the pressure transducer output. Each portion of the test stand will be described in detail.

The small reservoirs, seen in Figure 5-1 and Figure 5-2, are used to provide steady flow of water through the microchannels while maintaining a similar pressure on either end of the channel. This system insures that the channels are immersed in water and will have no adverse effects due to surface tensions that might otherwise take place at the entry or exit region when transitioning between air and water. Each reservoir has four sealed inlets.

Figure 5-1: The complete test stand used to test the flow rates through the microchannels

The inlet at top allows flow in or out of the reservoir system. Water flows in from the tank reservoir to the small reservoir on the right and water flows out to the solenoid valve from the top inlet on the left. The second set of inlets, on the back side of the small reservoirs, leads in and out of the pressure transducer. The third set of inlets, on the front side of the small reservoirs, allows a thermocouple to be fed into each reservoir to monitor the temperature of the water within the reservoirs. The fourth set of inlets is located on the mating surfaces of the small reservoirs. A small hole, approximately ¼ inches in diameter, leads from the cavity of the reservoir to the wafer with the microchannels. The hole needs to be at least this large because a 100/1 ratio should exist between the reservoir hole cross-sectional area and the total cross-sectional area of the

test microchannels. Water is prevented from flowing around the test wafer by sealing it on either side with two rubber slabs cut with a diamond-shaped hole in the center to allow flow through them. The two reservoirs are clamped together during a test run to keep everything in place. A close up view of these small reservoirs can be seen in Figure 5-2.

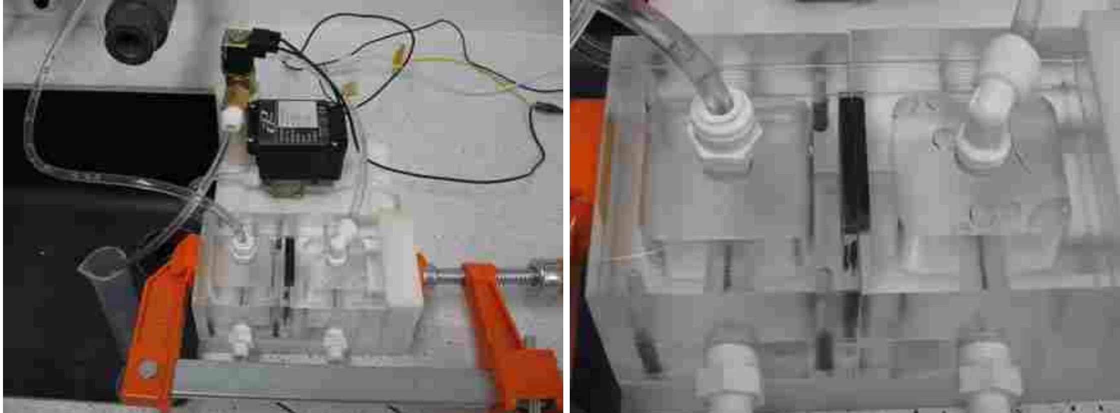

Figure 5-2: The picture on the left shows the reservoirs, pressure transducer behind them, and solenoid valve behind and to the left of the pressure transducer. The picture on the right is a close up view of the small reservoirs. The black strip in the middle of the two reservoirs is the two rubber inserts with an array of microchannels in between them.

To provide a better understanding of these small reservoirs, which is the core portion of the test stand, Figure 5-3, Figure 5-4, and Figure 5-5 show detailed descriptions of the small reservoir system.

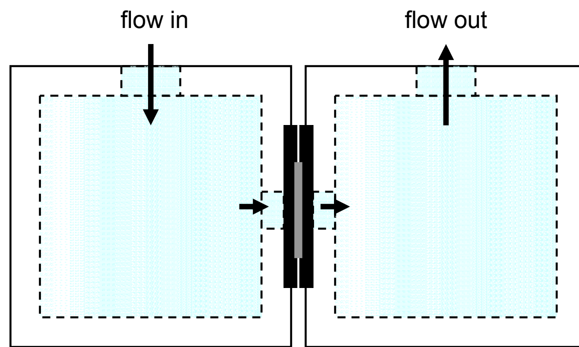

Figure 5-3: A side view of the two small reservoirs with an array of microchannels in between. The water flows into the top on the left side, through the channel in the middle of the system, and back out on the right hand top side.

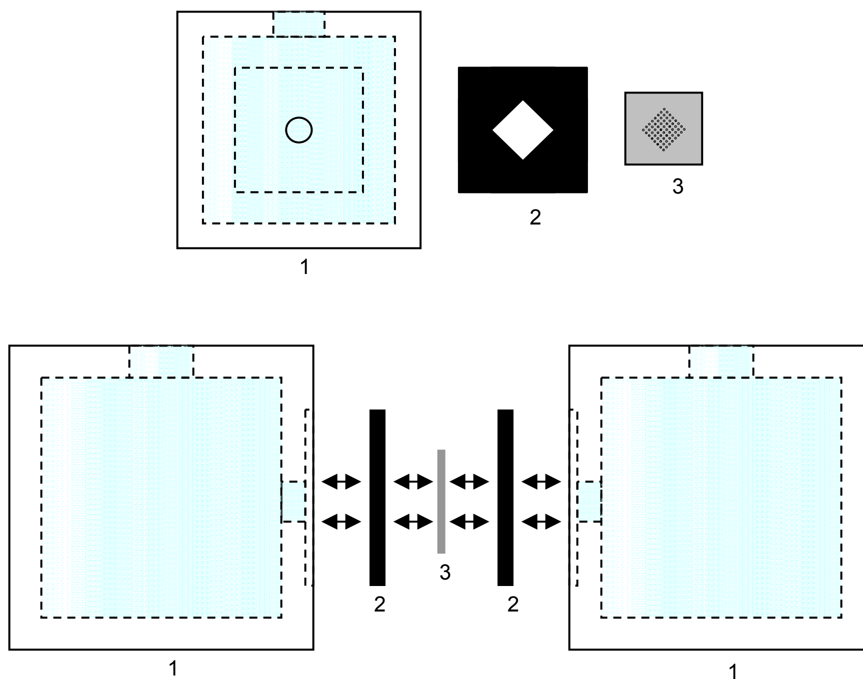

Figure 5-4: Views of mating surfaces of the (1) reservoir, (2) rubber sealer, and (3) microchannel array can be seen above, while the exploded assembly view of these components can be seen below.

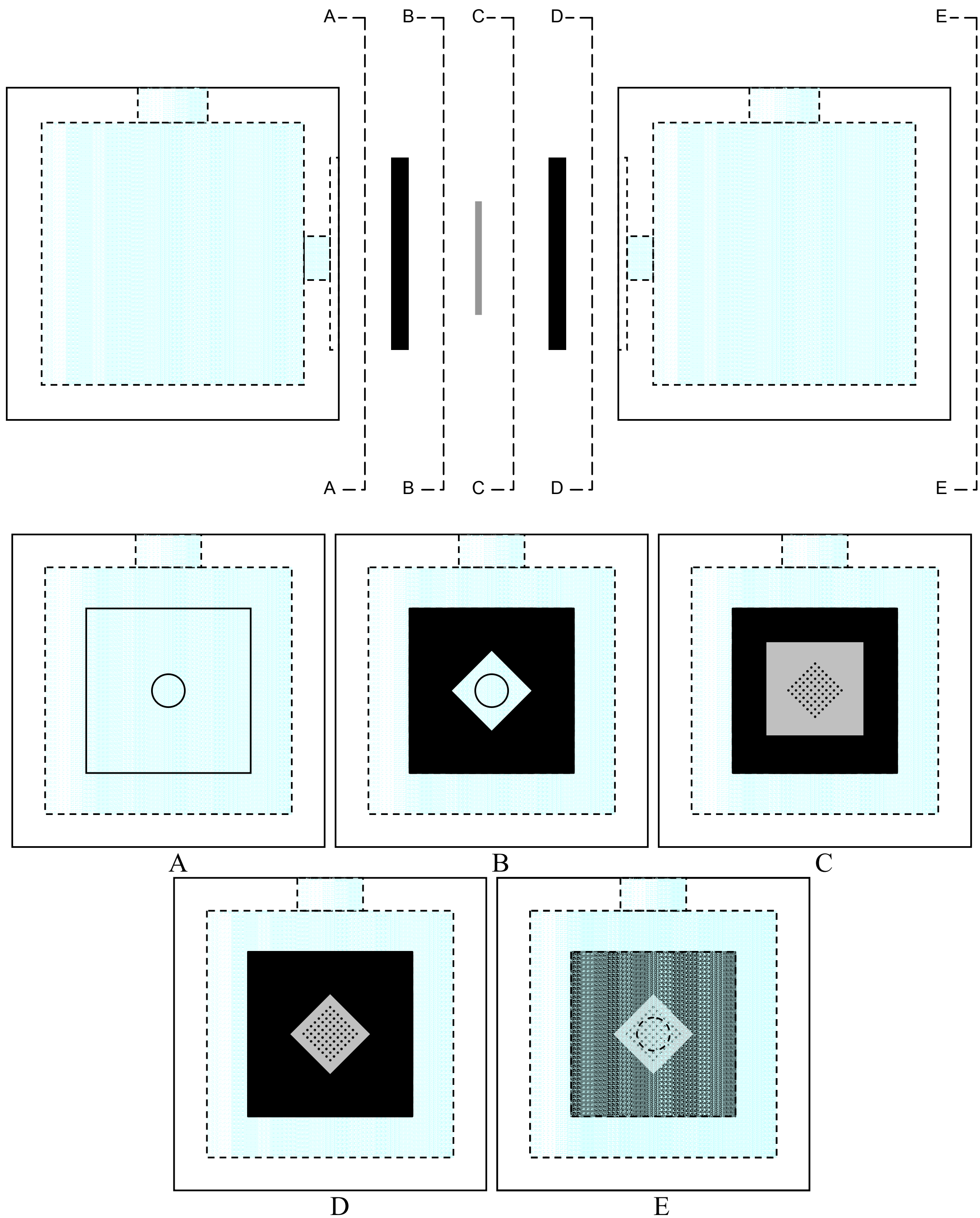

Figure 5-5: The reservoir assembly is sectioned out (above) views A-E and the cross-sectional cutaways are show (below). (A) Shows the "in-flow" reservoir, a rubber seal is in place in (B), the microchannel array is added in (C), in (D) the other rubber seal sandwiches the array, and in (E) the "out-flow" reservoir is put into position.

The test stand is comprised of a fluid system and an electrical system. The fluid system, seen in Figure 5-6, consists of the tank reservoir, the small reservoirs, the pressure transducer, the solenoid valve, and a graduated cylinder for water collection. The thermocouples are also included in the schematic of the fluid system since they operate independently of the electrical system and the data is recorded manually. The graduated cylinder is used to measure water volume for a test run. The volume flow rate through the microchannels is determined by the volume of water collected during a test run and the duration of the test run. The volume flow rate will vary depending upon the pressure of the water. The pressure is either determined by the height of the water level in the tank reservoir or by the pressure transducer. It was found in experimentation that the transducer would sometimes give questionable results so usually the pressure was found based on the height of the water in the tank reservoir which had only negligible variation.

The electrical system, seen in Figure 5-7, consists of both the pressure transducer and solenoid valve as well as a breadboard, DAQ board, electrical relay, physical ground, and a Labview program run by a computer. The pressure transducer data is collected and the solenoid valve switched on through a data acquisition board running to the computer. The board is also grounded on the same line that common ground is found on the bred board. The grounding significantly reduces the signal noise from the pressure data.

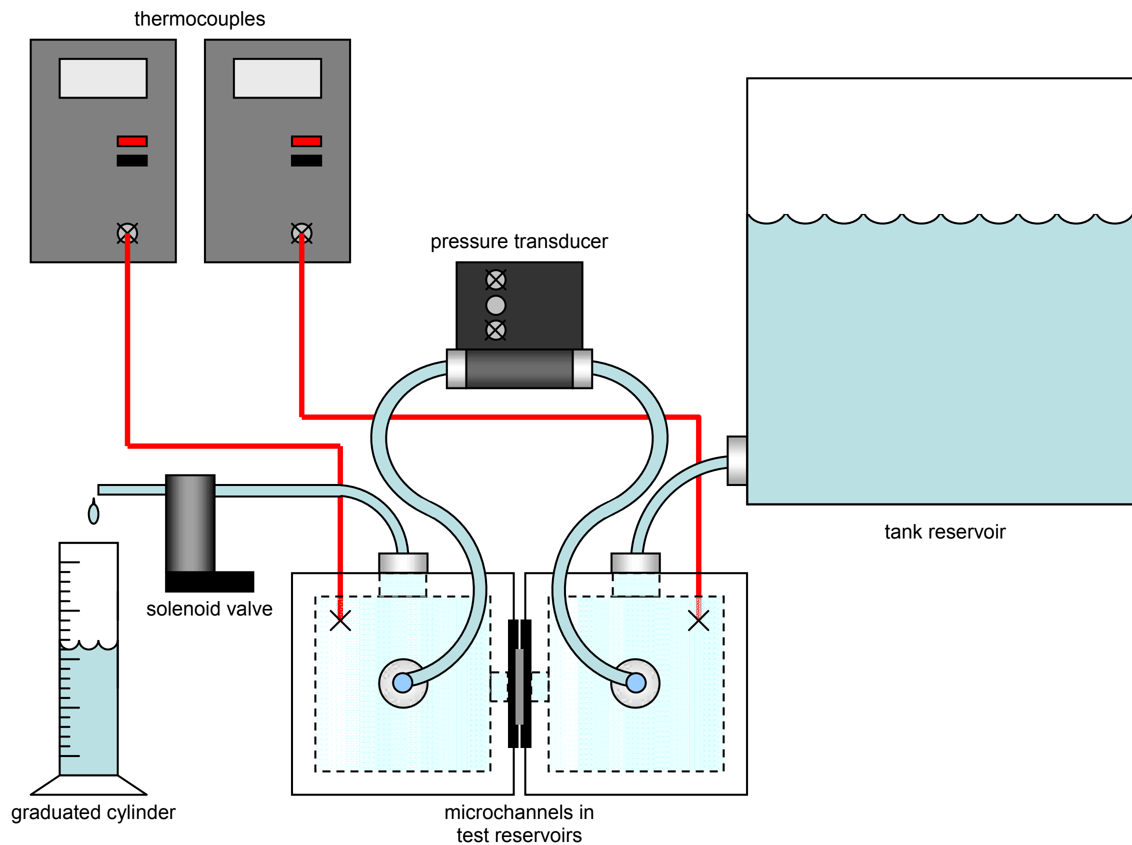

Figure 5-6: A schematic of the small reservoirs and all interacting equipment.

The pressure transducer used is a 0-5 psi Cole Parmer[4] brand transducer. The pressure transducer measures the pressure difference between reservoirs but does not influence the inter-reservoir flow at all. The pressure transducer is powered by a 24 volt power supply and the pressure difference data is collected and recorded with a Labview program. In general, ten to one hundred data points per second are collected. Except for significant and unexpected pressure changes the pressure is meant to be averaged over the duration of an entire test run.

[4] **Specifications**
Part Number: 68071-56
Range: 0-5 PSID
Excit.: 24 VDC
Output: 4-20 MA

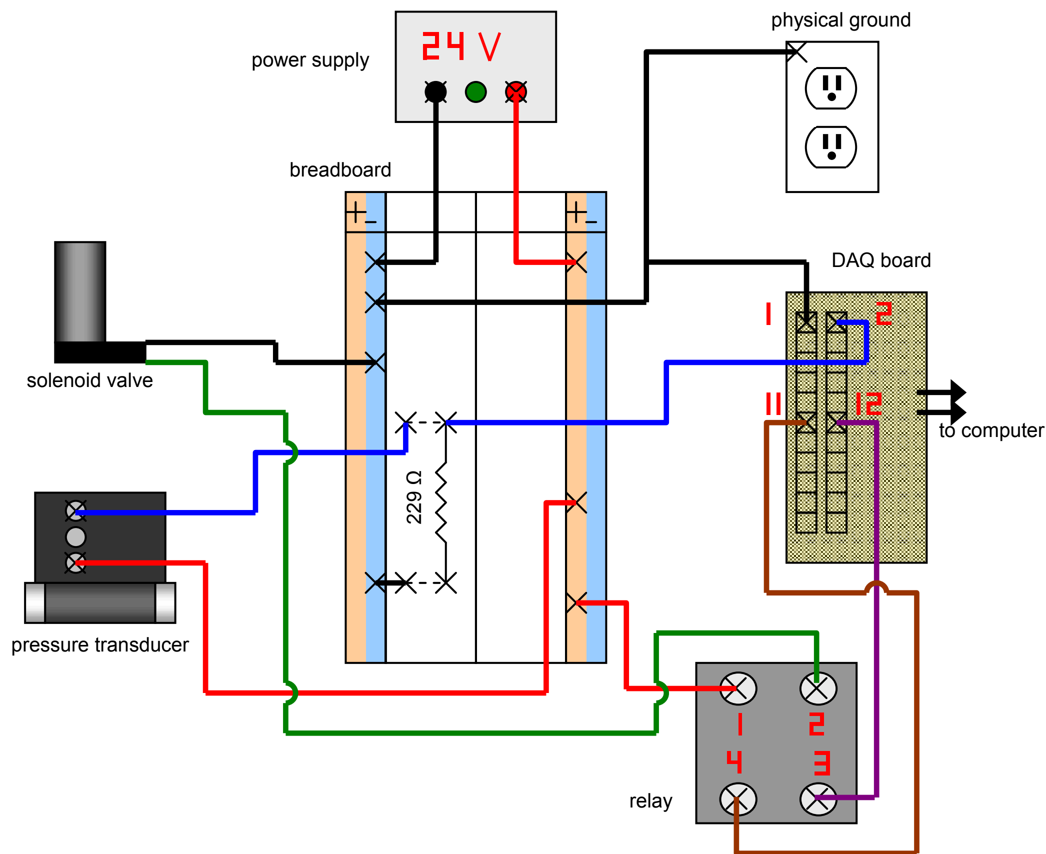

Figure 5-7: A physical wiring schematic of all equipment used in the test stand.

The solenoid valve is a Snap Tite/Allied[5] valve and controls the flow of water through the entire system. The only time the solenoid valve is turned on is during a test run, allowing water to flow freely through the microchannels. The water flow is gravitational and is simply the result of water draining from a higher to a lower level in the system. The solenoid valve is turned on and off with the same Labview program that records the pressure transducer data. The solenoid valve uses a relay to trigger its operation. The

[5] **Specifications**
Part Number: 2W13W-1NB-A6D6
ORIF: 3/32
V: 24 VDC
PSI: 60
Watts: 6.0

computer signals the relay with a 3 V signal that runs through the relay allowing the 24 V power to open or close the solenoid valve. The solenoid valve receives 0 V when turned off. The relay, along with the breadboard and DAQ board used in the test stand, can be seen in Figure 5-8.

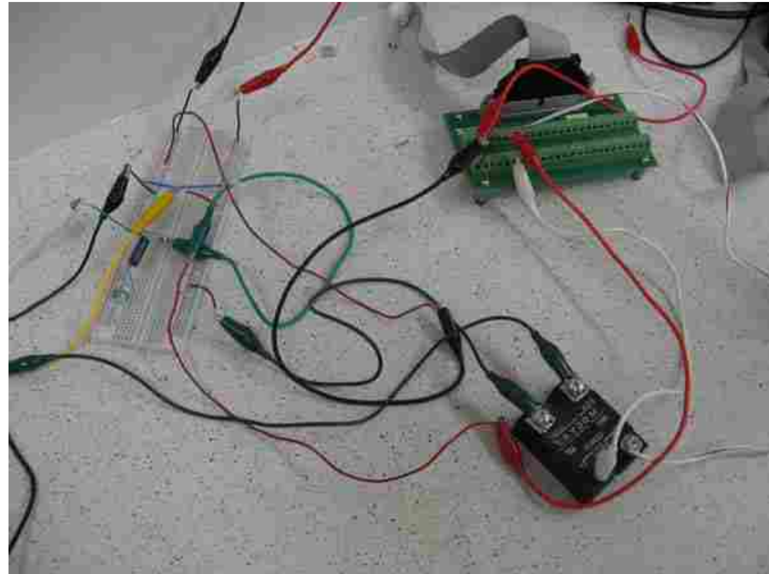

Figure 5-8: A photograph of the wiring necessary to run and monitor the equipment used in the test stand.

Labview version 6.1 is used for this test stand. It is simply meant to turn on the solenoid valve for a prescribed amount of time and collect pressure transducer data during that time. The operating window, seen in Figure 5-9, used allows the user to start and stop the run or set the desired run time and let it run and stop automatically. The pressure data is recorded on the waveform chart and written to a data file.

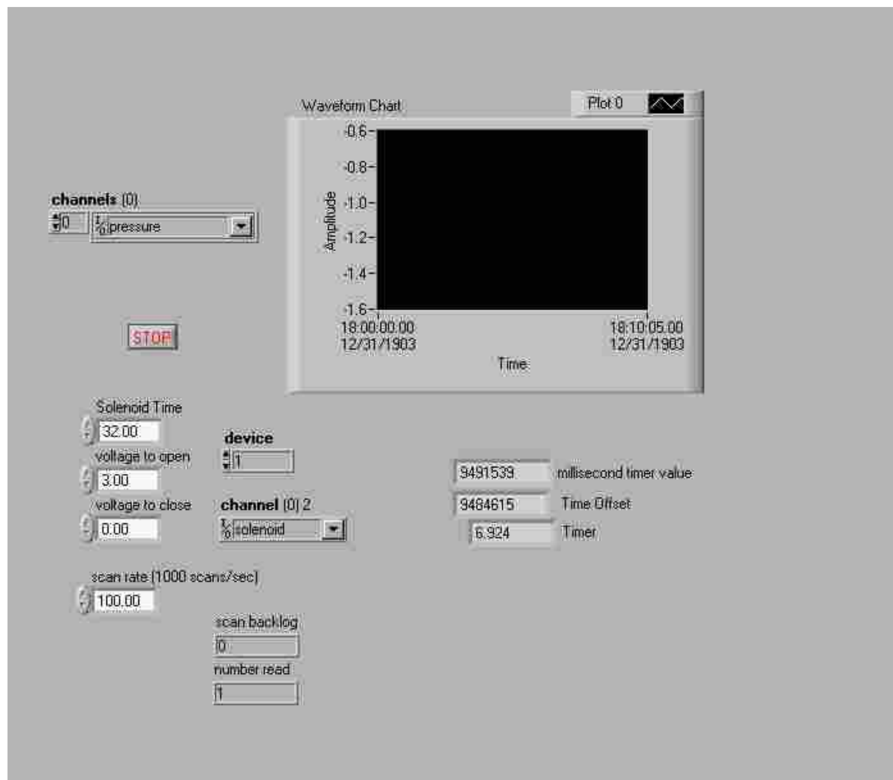

Figure 5-9: A view of the operating window used for experimental test runs.

The schematic for the Labview program, seen in Figure 5-10, is fairly basic to an experienced Labview programmer. It was created specifically for the experimental test stand in this research by Kevin Cole, a staff member of the department of mechanical engineering at BYU, with assistance from the author.

The test stand and its accompanying Labview program was built to be robust in anticipation of expected but unforeseen modifications to the types of experiments run or the types of channels being tested.

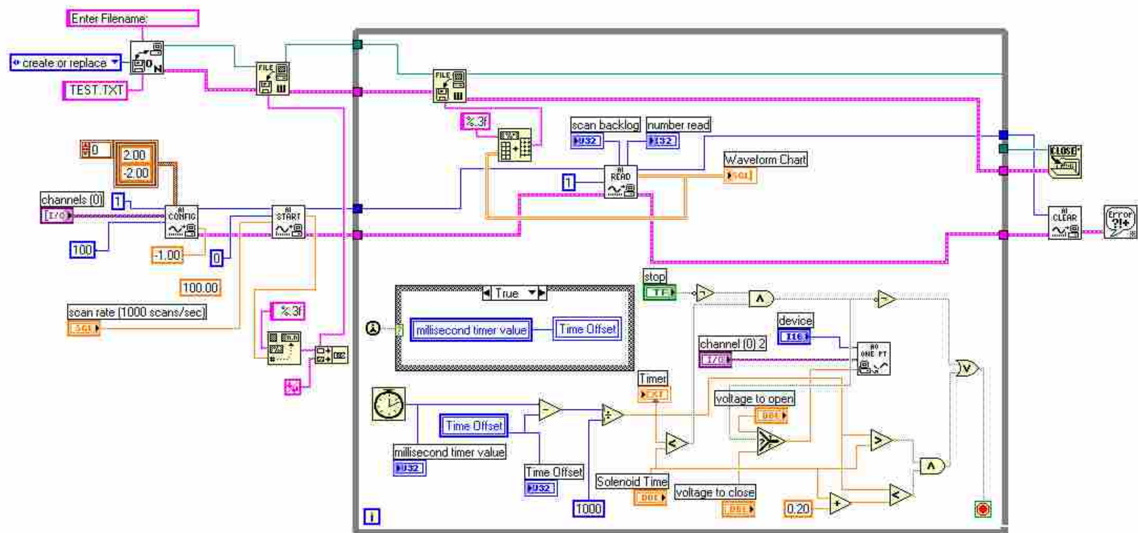

Figure 5-10: The schematic diagram of the Labview program used to operate and record data from the test stand.

5.2 Testing Procedure

The purpose of the flow testing was to be able to compare results from one microchannel to the next simply to show that a difference in the frictional factor that would exist as a function of the cavity fraction of the channel. Comparison of the experimental results to numerical computations is outside the scope of this work.

The typical test run was accomplished by first inserting a sample microchannel array into the test stand. The stand itself is turned onto its side and the top small reservoir and rubber seal removed so that the array may be lined up with the rubber seal on the bottom reservoir. The top rubber seal and reservoir are then placed back on top of the tilted test stand and the reservoir system (with the microchannel array in the middle) is clamped

together. The test stand is then place right side up again. The level of the tank reservoir is checked and filled, if necessary, to the desired height with distilled water and the tank reservoir valve is manually opened. The power supply is checked so that it is turned on and the Labview is used to open the solenoid valve to allow flow. The flow data is not recorded immediately because the system must run for 30-60 seconds to get air bubbles out of the lines. This must be done after changing each microchannel array. Once the air bubbles are out the Labview program is run again and the temperature in each small reservoir is recorded. At the end of the run the tank reservoir valve is manually closed and the array is removed so that another one may be tested.

Sometimes a silicon chip with a microchannel array will have a rogue hole in it. This is a hole that was etched from an imperfection in the photoresist mask. Such an imperfection is usually caused from a bubble that came to the surface during softbake of the photoresist. The rogue hole is covered up with tape (usually masking tape) to prevent unwanted flow through the hole which would influence the results of the test.

A small oil-like film could be seen concentrated around the microchannel openings after their removal from the test stand and it was concluded that oils from the rubber gaskets are entering the water. There may have been other oil sources as well such as machining oil used for reservoir manufacture which still resided within the small reservoirs of the test stand. The reservoirs and all the lines were rinsed out with soapy water and the channels were rinsed in an ultrasonic cleaner before and after each test run to ensure an oil and debris-free surface within the channels. After this the oil residues diminished significantly.

5.3 Flow Results

Based on Equation 3-1 if the contact angle of a droplet of water is 90° or smaller then liquid will wet all small cavities. Because silicon-water interfaces are hydrophilic as is the natural oxide growth on silicon, the conclusion is that the gaps in between the structures of the plain silicon channels are wetting. To be able to model this flow appropriately, the concept of a hydraulic diameter of the channel was utilized [28]. The hydraulic diameter takes into account the increased cross-sectional area as well as surface area contributing to drag. The hydraulic diameter, D_h, is equal to 4 times the cross sectional area divided by the cross-sectional perimeter of the channel. Some uncertainty exists in the calculation of D_h as can be seen in Table 5-1.

Table 5-1: Hydraulic diameter, D_h, for five different cavity fractions including three standard deviations accuracy. These measurements were taken from the "sample 12" arrays, "sample 13" are about 90% this size.

Sample	cavity fraction (F_c)	average D_h (µm)	99% confidence +/- (µm)
5	79.1%	46.0	6.2
1	76.5%	44.6	2.3
6	70.9%	41.4	8.6
4	67.0%	42.4	2.6
3	63.9%	41.0	1.2

Uncertainty exists not only from the variation from channel to channel in a given array but also from a difference in diameter from the entrance to the exit of the channels. In fact, the channel diameters vary to such a degree as to rendering numerical modeling of the channels impractical. To demonstrate the difficulty in finding a correct value for

either the diameter of a hydrophobic channel or the hydraulic diameter of a non-coated channel, Figure 5-11 shows a simple diagram of the channels at their entry and exit regions. Just as the SEM images of the entry and exit of the microchannels in Figure 4-25 depict, the non-uniformity of the channel cross-section is much too large and when the diameter to the fourth power is used in the *f*Re equations, an inconsistent diameter creates significant uncertainty in the results. Due to the inconsistencies of the diameter measurement, no valid trends for *f*Re could be found and instead all results were focused on the resulting volume flow of the channels over time and a loss coefficient K_L.

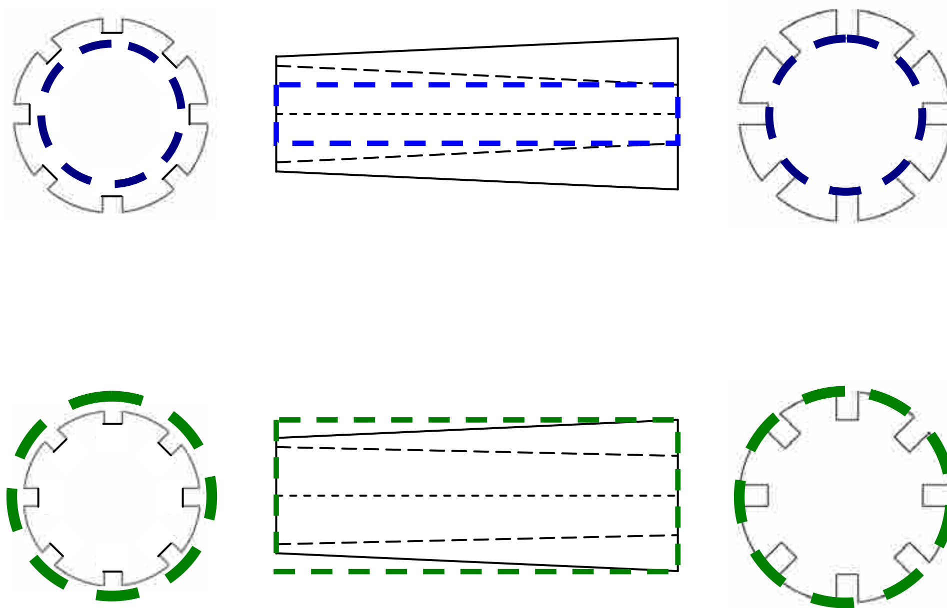

Figure 5-11: An exaggerated depiction of the channel entry region on the left and the exit on the right. The top channel measures inside diameter for a hydrophobic channel. Because the channel walls taper this diameter is smallest at the exit. The bottom channel measures the outer limits of the cross-section for calculating hydraulic diameter. Again, an inaccurate calculation due to the tapering of the walls.

When testing with hydrophobically coated channels, the samples were coated with a layer produced by C_4F_8 gas in the ICP machine. The passivation plasma was left on for 50

seconds. Based upon knowledge of the etching and passivation cycles as well as other experimentation done in the microfluidics lab it was determined that a coating applied for this duration in the machine was more than ample to give a good hydrophobic coating on the surface of the channel walls. According to experience the contact angle of a droplet of water on a smooth silicon surface coated with C_4F_8 gases is about 120° and on a structured surface yields contact angles in the rage of 150-165°.

Non-coated channels had been previously tested at 3.65 kPa. However, attempts to test the hydrophobically coated channels at this same pressure failed because flow could not be achieved through the channels. The height difference in the water level was increased to bring the pressure up to 4.75 kPa at which point flow through the channels was observed, although at a visibly slower rate than expected based upon previous experiments of non-coated channels. After reviewing Equation 3-1, it was found that the diameter of the channels was just barely large enough to allow water to pass through them at this pressure (4.75 kPa) due to the resistance to wetting a space this small. The data for the smallest diameter control channel employed could not be recorded because flow through them could not be achieved at this pressure. By increasing the pressure by a little more than 1 kPa it was found that a reliable flow could be achieved through the channels.

A series of comparative tests were run in which five different samples of structured channels were tested, at a pressure of 5.84 kPa, until they reached near steady state flow conditions. The flow rate gradually decreases through the channels over time. When the flow rate is relatively the same over a long period of time then the flow conditions are

determined to be at steady state conditions. Each sample has different cavity fraction and structure geometry and thus has different flow conditions associated with it.

Since the channels have different diameters at one end versus the other end, the channels were run to steady state with the flow going in one direction. Subsequently the array was dried out and run to steady state with flow going the opposite direction. The volume of fluid that passed through the array was recorded at five minute intervals and the two flow results for the configurations are plotted together. The above described tests were done for both hydrophobically coated and non-coated channels.

The test results of each array sample are shown accompanied with an SEM image of the front and the back of a single channel, which represents fairly well what each of the 64 channels in the sample looks like. Plots of both the non-coated test runs and the hydrophobically coated test runs are also shown for each sample with water flowing through the large diameter entrance (large opening) of the channel and flow entering through the small diameter entrance (small opening) as described in Figure 5-12.

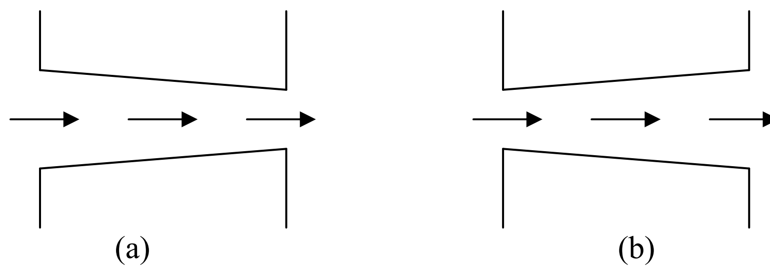

Figure 5-12: The large diameter entrance to the channel is shown in (a), while (b) shows the small diameter entrance to the channel. The arrows show the directionality of fluid flow through the channels.

Sample #1, (see Figure 5-13), has a nominal cavity fraction of 76.5%. The results of the steady state test runs can be seen Figure 5-14.

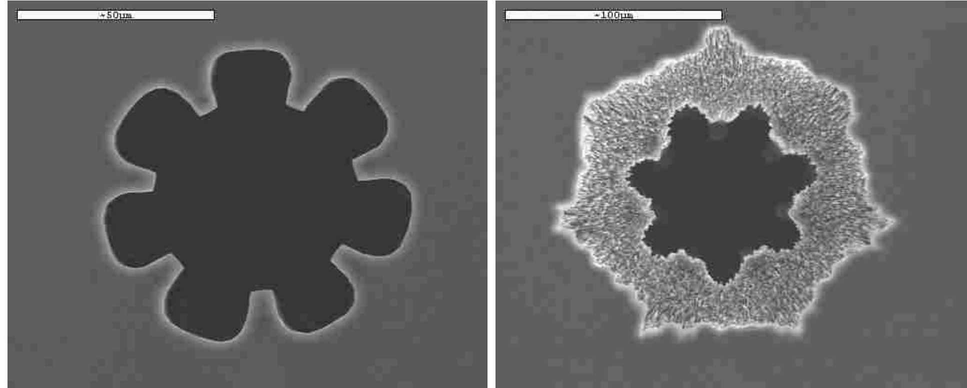

Figure 5-13: This SEM image shows the front and back side of one of the channels in the sample #1 array. Note that the scale of the two images is not the same.

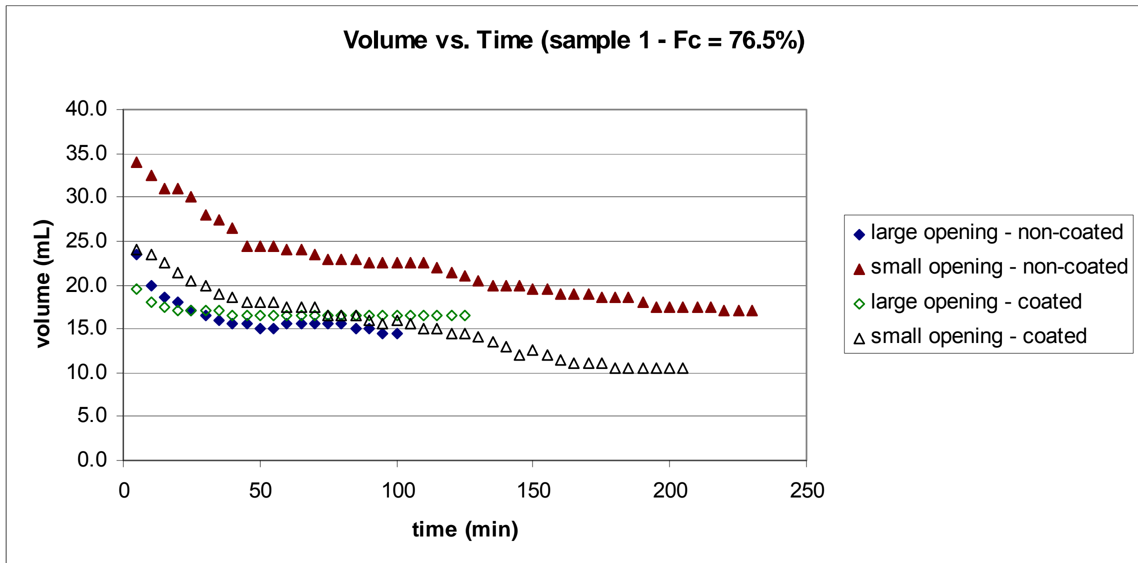

Figure 5-14: The steady state testing for sample #1 showing hydrophobically coated and non-coated test runs for flow entering both the large diameter opening and small diameter opening of the channels.

In sample #1, the curves for both small opening tests are notably similar although the non-coated does show significantly higher flow. The large opening coated channel shows

strong indication of having reached steady state while it appears that perhaps the other test runs may still decrease in flow over time.

Sample #3, (see Figure 5-15), has a cavity fraction of 63.9%. The results of the steady state test runs can be seen in Figure 5-16.

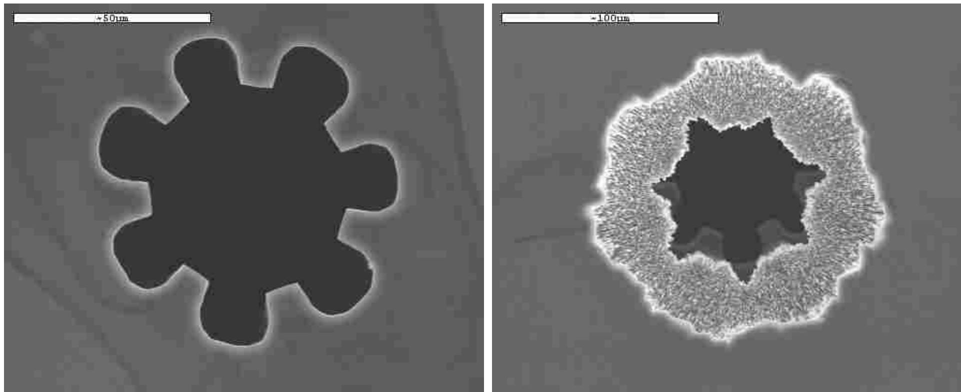

Figure 5-15: This SEM image shows the front and back side of one of the channels in the sample #3 array. Note that the scale of the two images is not the same.

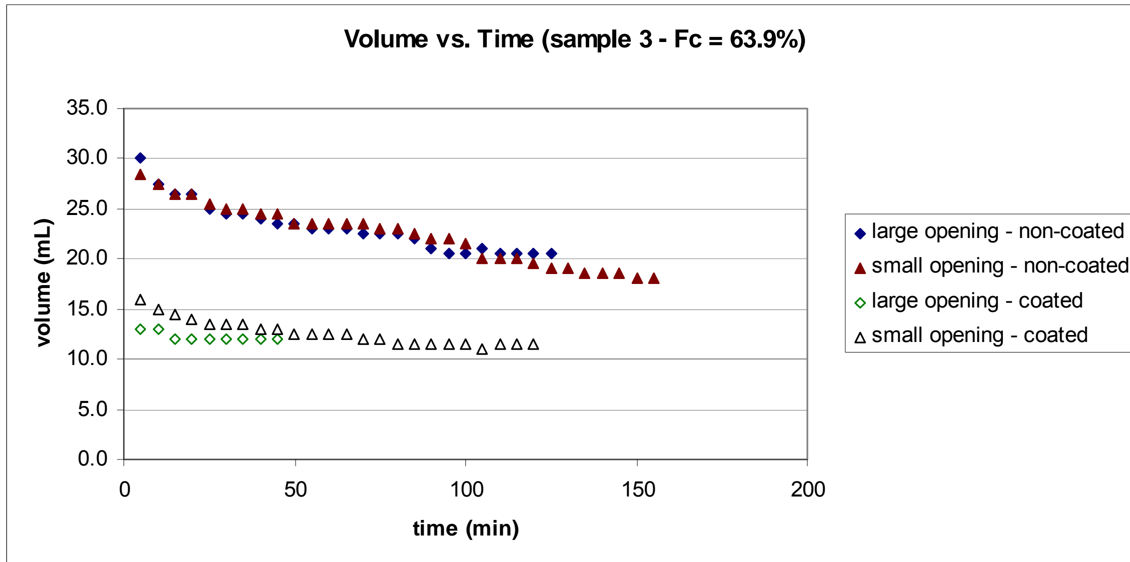

Figure 5-16: The steady state testing for sample #3 showing hydrophobically coated and non-coated test runs for flow entering both the large diameter opening and small diameter opening of the channels.

In sample #3, the non-coated curves are nearly identical while the coated curves although slightly different still display similar steady state flow. The non-coated steady state flow seems to be much higher than the coated steady state flow.

Sample #4, (see Figure 5-17), has a cavity fraction of 67.0%. The results of the steady state test runs can be seen in Figure 5-18.

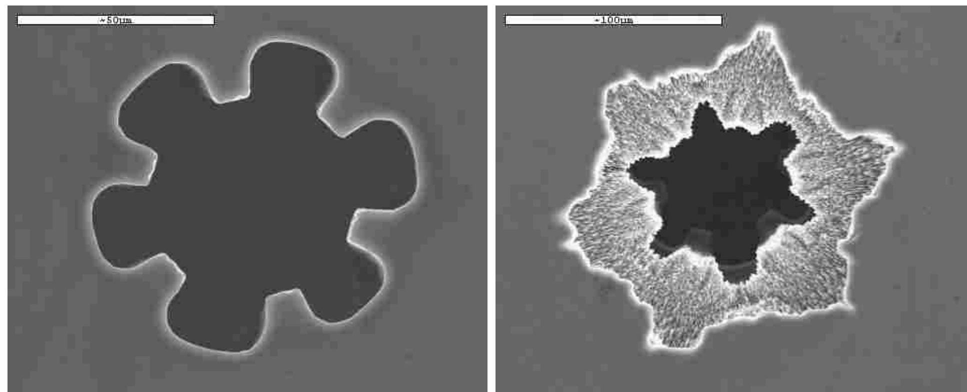

Figure 5-17: This SEM image shows the front and back side of one of the channels in the sample #4 array. Note that the scale of the two images is not the same.

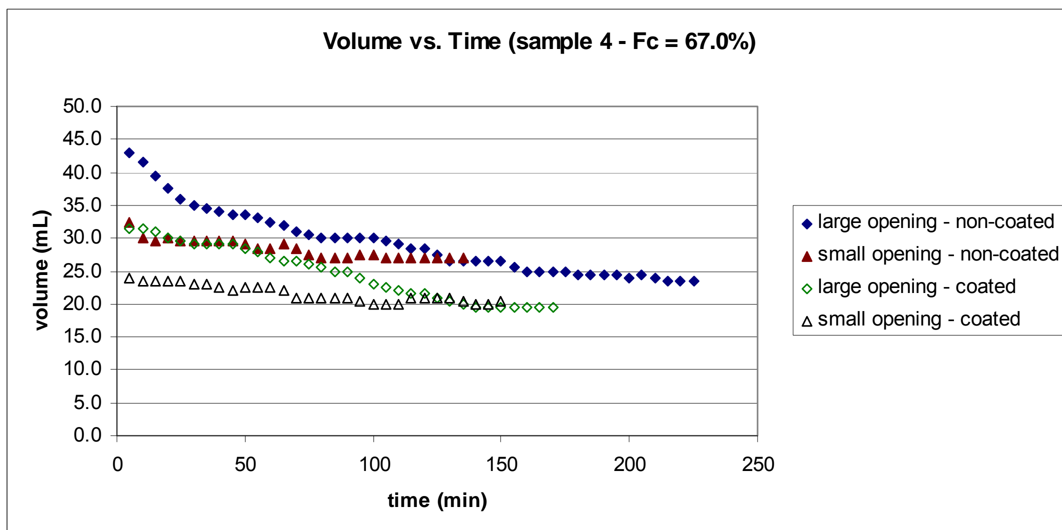

Figure 5-18: The steady state testing for sample #4 showing hydrophobically coated and non-coated test runs for flow entering both the large diameter opening and small diameter opening of the channels.

The test runs for sample #4 show that the large diameter curves are similar to each other and the small diameter opening curves are similar to each other; however, in each comparison the non-coated tests display a higher flow than the coated tests.

Sample #5, (see Figure 5-19), has a cavity fraction of 79.1%. The results of the steady state test runs can be seen in Figure 5-20.

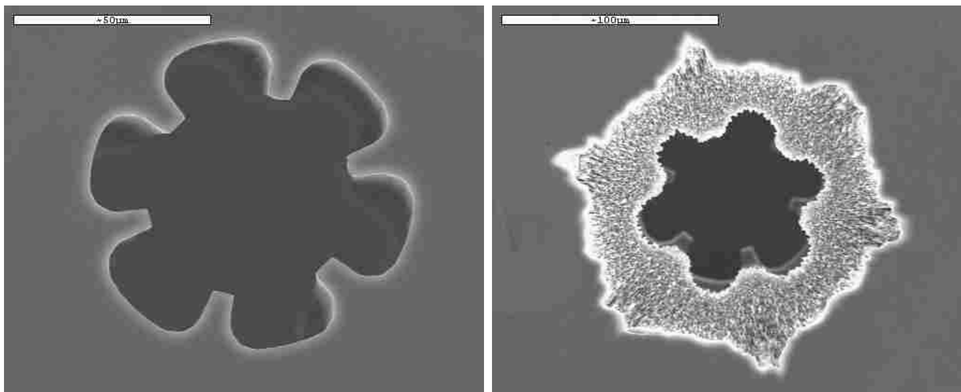

Figure 5-19: This SEM image shows the front and back side of one of the channels in the sample #5 array. Note that the scale of the two images is not the same.

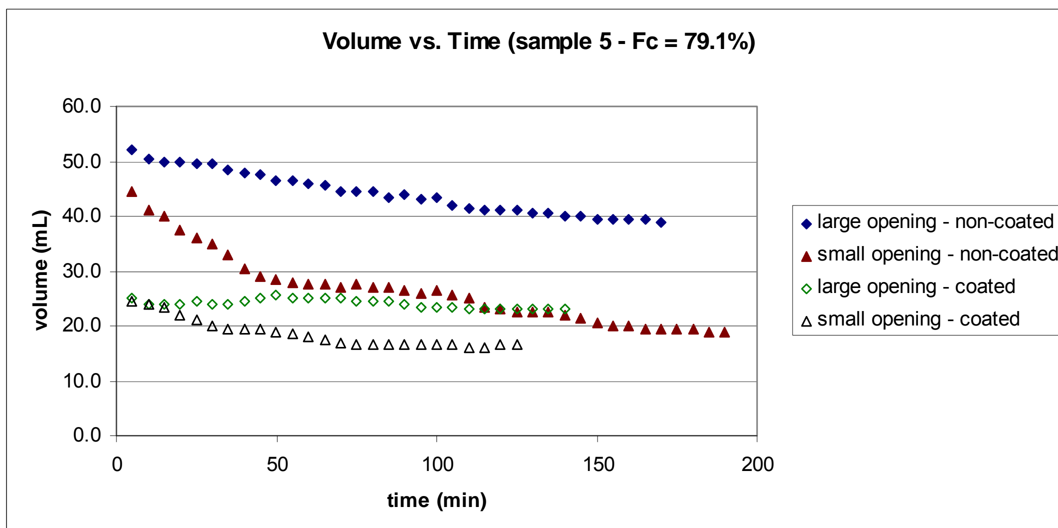

Figure 5-20: The steady state testing for sample #5 showing hydrophobically coated and non-coated test runs for flow entering both the large diameter opening and small diameter opening of the channels.

The sample #5 test runs seem to be a bit unique from other samples in that there are no similar trends between curves. They do show a trend identified in the data for other samples in that the non-coated flow is significantly higher than the flow for the coated channels.

Sample #6, (see Figure 5-21), has a cavity fraction of 70.9%. The results of the steady state test runs can be seen in Figure 5-22.

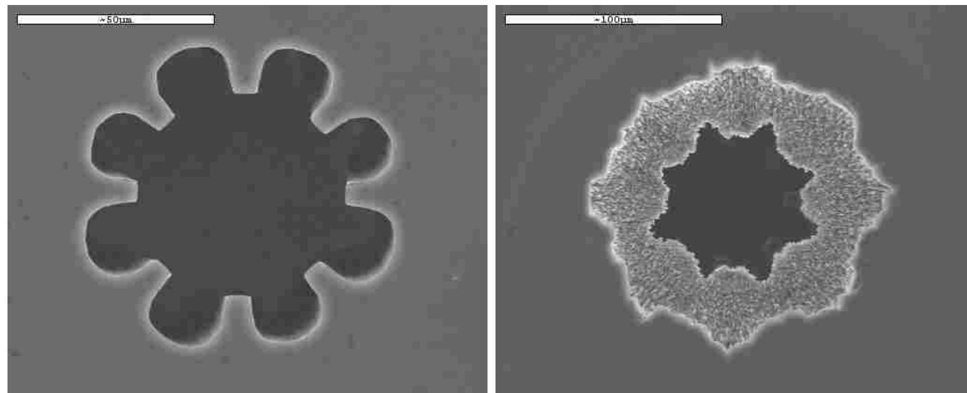

Figure 5-21: This SEM image shows the front and back side of one of the channels in the sample #6 array. Note that the scale of the two images is not the same.

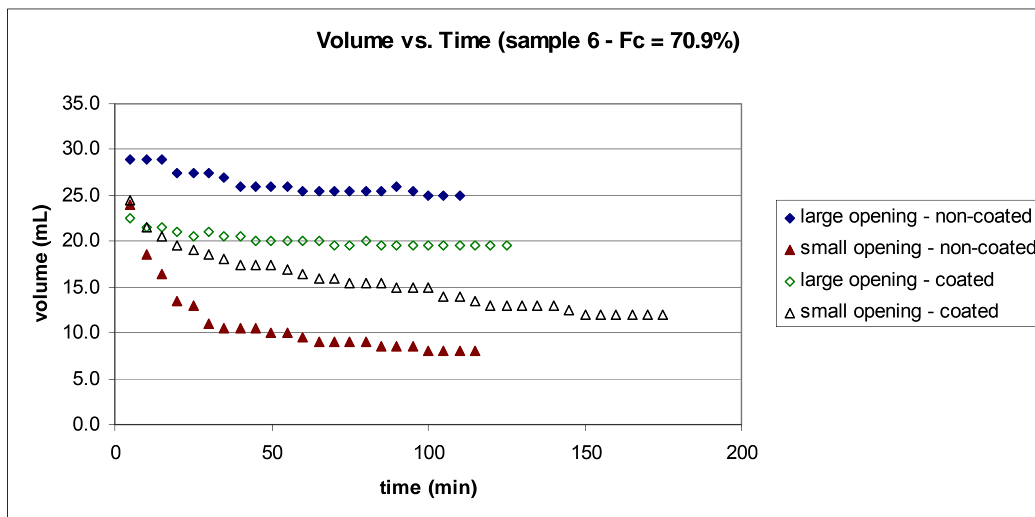

Figure 5-22: The steady state testing for sample #6 showing hydrophobically coated and non-coated test runs for flow entering both the large diameter opening and small diameter opening of the channels.

In sample #6, the two large opening curves seem to match each other in decline although the non-coated flow is, as usual in other cases, higher than the coated flow. An exception to the phenomenon that is observed in most all other test runs in all other samples is that the non-coated small opening test run displays a lower flow than the coated small opening test run.

The control channels were tested just like the structured channels for flow through the large and small diameter entry regions and with or without a hydrophobic coating. The results are discussed below.

Sample #9, (see Figure 5-23), is a smooth walled channel without any structures so the cavity fraction is considered to be zero. The results of the steady state test runs can be seen in Figure 5-24.

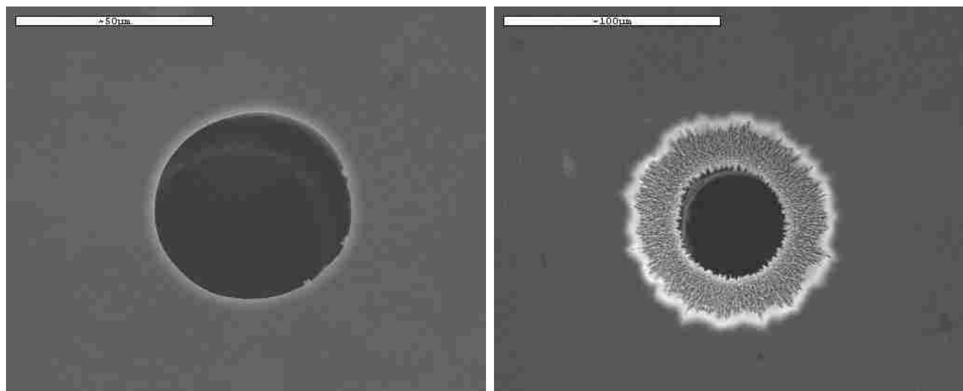

Figure 5-23: This SEM image shows the front and back side of one of the channels in the sample #9 array. Note that the scale of the two images is not the same.

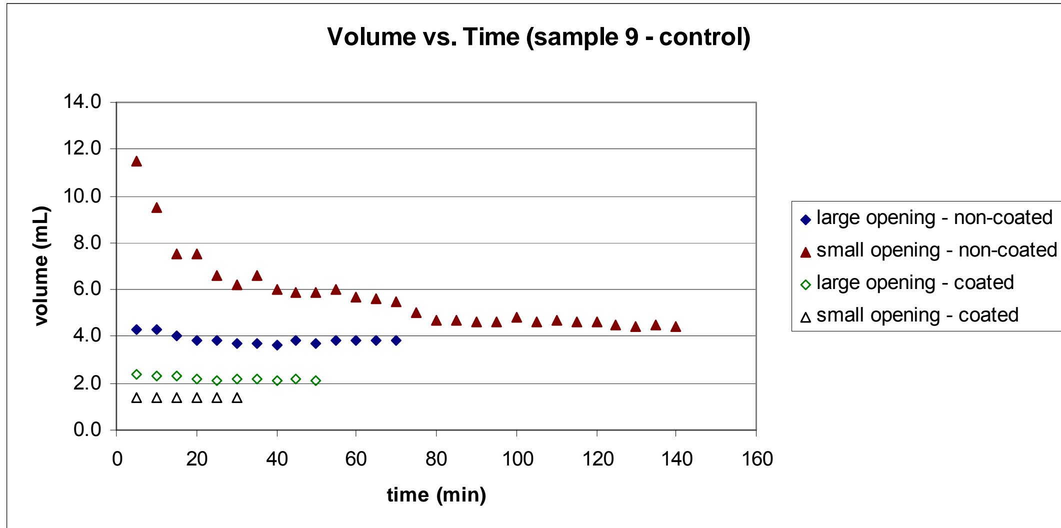

Figure 5-24: The steady state testing for sample #9 showing hydrophobically coated and non-coated test runs for flow entering both the large diameter opening and small diameter opening of the channels.

The test results for the control channels in sample #9 show that even without a difference in practical diameter between coated and non-coated test runs, the non-coated channels exhibit a higher flow through them than do the hydrophobically coated channels. This suggests that somehow the hydrophobic coating somehow prohibits flow through the channel. At this point the reason remains unexplained.

The steady state data of all the samples has been collected and compared to bring out some of the most relevant trends. This comparison can be found in Table 5-2.

Table 5-2: A comparison of steady state flow rates. For each sample the channel characteristic is identified that has the highest flow rate. ie: the coated and non-coated sample #1 curves were compared against each other; for the two large opening curves, the coated data set had the higher steady state flow rate. The symbol, "--" means that both curves have matching steady state flow rates.

	Surface Treatment		Channel Opening	
Sample	**Large Opening**	**Small Opening**	**Non-coated**	**Coated**
1	coated	non-coated	small	large
3	non-coated	non-coated	--	--
4	non-coated	non-coated	--	--
5	non-coated	non-coated	large	large
6	non-coated	coated	large	large
9	non-coated	non-coated	--	large

Having compared all the data together, a hypothesis can be formed to give explanation to the phenomena that are taking place in the channels during the test runs. The hypothesized cause of the characteristic decrease in flow rate with time for virtually all the samples, coated or non-coated, is small bubbles on the surface of the channel walls that decrease the amount of drag on the flowing water. Over time, these small bubbles are shed from the surface of the channel walls and surface drag increases, decreasing the flow rate of water through the channels.

It is interesting to note that generally the better flow rates come from the channels that are not coated rather than those that are coated. This opposes the original reason for using the hydrophobic coating which was to increase flow rate. It could be argued that differences in practical channel diameters may be causing the higher steady state volume flows for the non-coated channels. Although it is believed that this does influence the results, it is not believed to be the only contributor in this phenomenon, due to the results found from the testing of smooth walled control channels. However, a brief discussion of the practical diameter is given.

The volume flow will vary between coated and non-coated channels due to the characteristic change in diameter of the flow regime. A hydrophobically coated channel will have a theoretical channel diameter fitting within the limits of the structures that run the length of the channel, whereas a non-coated channel will have a much larger cross sectional area at any given point along the channel where more fluid can pass by in a given amount of time (see Figure 5-25).

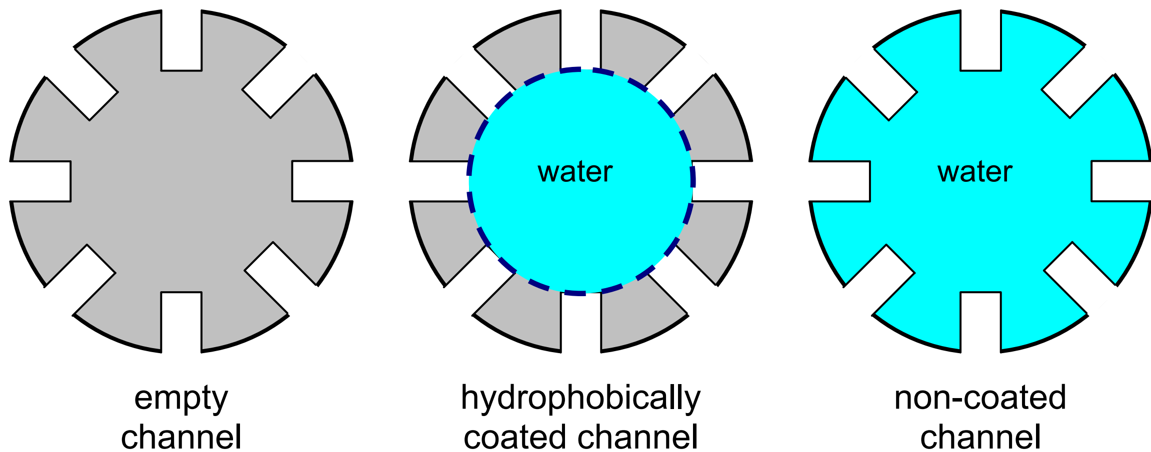

Figure 5-25: Three channel profiles show an empty channel cross section on the left, a hydrophobically coated channel with water running through in the middle, and a non-coated channel with water running through on the right.

Again, it is not believed that the differences in practical diameter are the only cause for higher steady state volume flow in the non-coated channels. This is because of the evidence given by testing in the control channels where the practical diameter in the channel is the same regardless of whether the channel is coated or not.

Another experiment that was performed on the control channels was to test flow going through the small diameter entry and then through the large diameter entry without drying it out first. The results of the testing can be seen in Figure 5-26.

The results of this testing show that flow through a hydrophobically coated large diameter entry (small diameter exit) will provide a higher flow than flow through a small diameter entry. The hypothesized reason is that the hydrophobically coated smaller diameter entry does not wet as easily due to its small "gap" spacing (see Equation 3-1) and thus provides only sporadic or uneven flow through the channels. The testing of hydrophobically coated and non-coated control channels was repeated and gave similar results every time, thus giving strong evidence of the repeatability of this phenomenon.

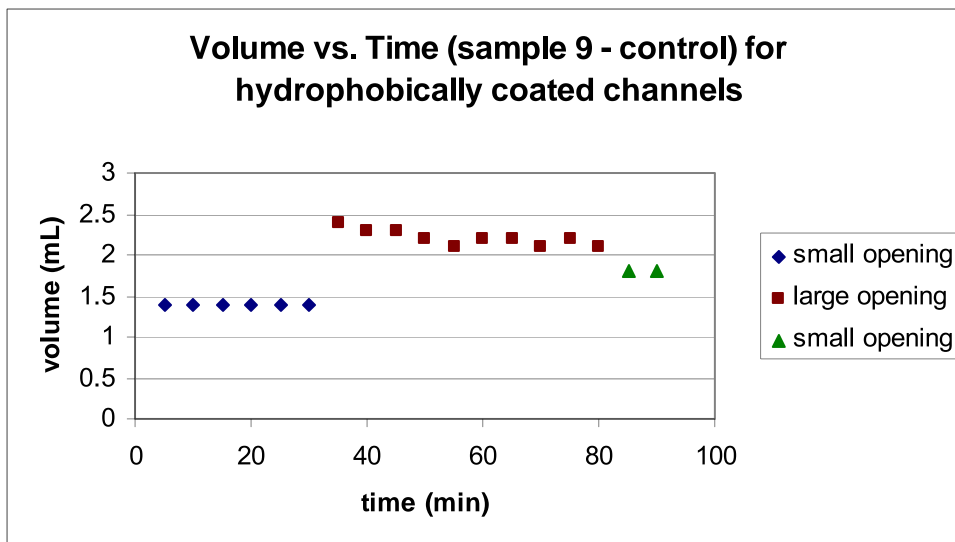

Figure 5-26: The steady state results of the hydrophobically coated control channels. The first and third runs were done through the small diameter entry and the second run was done through a large diameter entry. This test run was unique in that the channels were not dried out between runs of different flow directions.

This structured channel data also shows signs that support the fact that a higher flow rate is achieved going through the large diameter opening of a channel instead of the small. Although the results are not as consistent from one sample to the next, in general, if there is a noticeable difference between the large and small diameter entrance flows, it is the large diameter entry flow that shows the higher results.

The last analysis performed from the test data was the computation of a loss coefficient, K_L, as shown in Equation 5-1.

$$K_L = \frac{\Delta p}{\frac{1}{2}\rho V^2} \quad \textbf{(5-1)}$$

In this equation Δp is the pressure drop, ρ is the density of water, and V is the velocity of the water flow through the microchannels. This loss coefficient was computed to help identify any prevailing trends in the data collected in improved fluid flow due to structured channels despite the high amount of uncertainty in the data. The K_L data is plotted against cavity fraction, where the control channels are assumed to have a zero cavity fraction. The results can be seen in Figure 5-27.

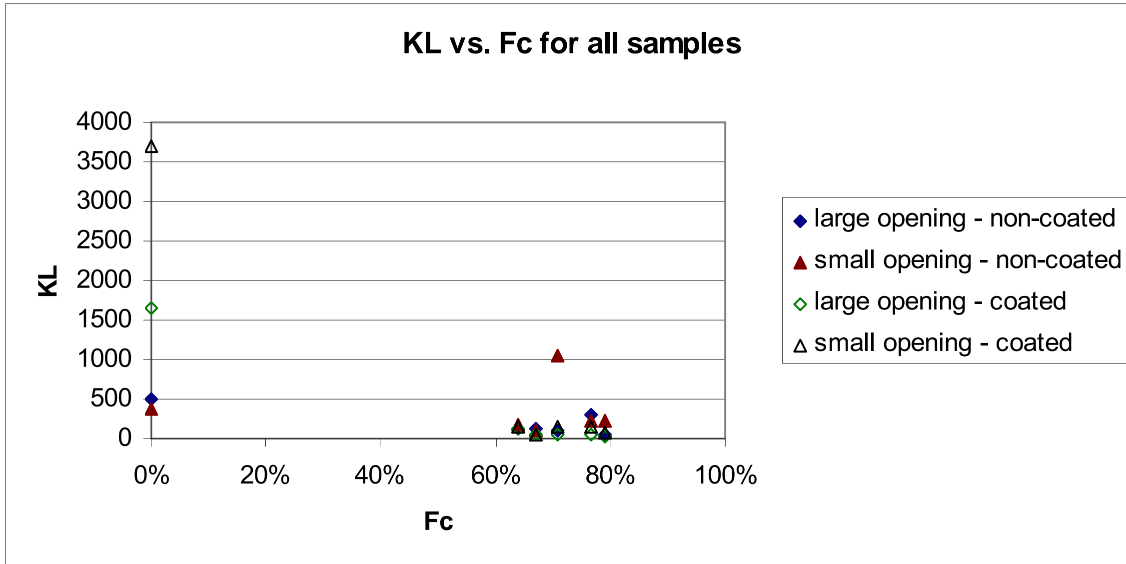

Figure 5-27: Plot showing the steady state K_L results for all test samples including control channels.

Based on the results of the K_L plots it can be seen that the K_L values for the control channels are much larger in comparison to the structured channels. This is expected because K_L values naturally decrease as the channel diameter gets smaller. It is difficult to see all the data points well in Figure 5-27 so a view of the K_L results for just the structured channels can be seen in Figure 5-28.

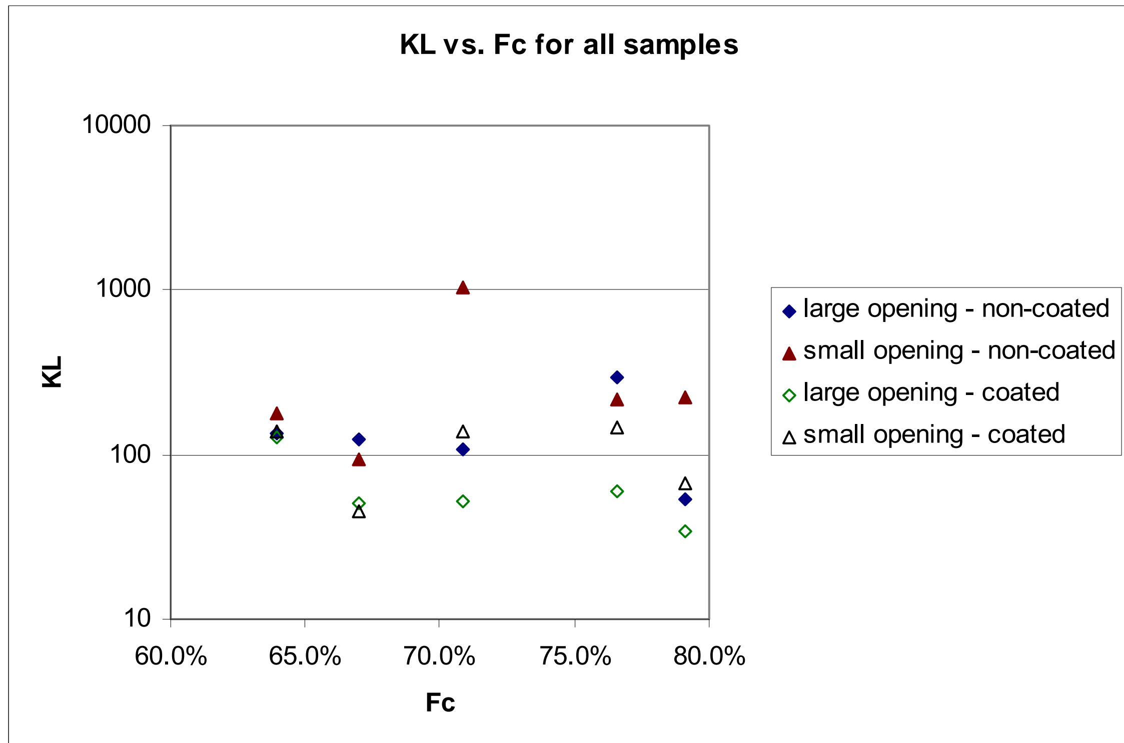

Figure 5-28: Plot showing the steady state K_L results, on a log scale, for all test samples except the control channels. This plot without the control channels allows for a more detailed view of the structured channel K_L results.

It can be seen from the data that the hydrophobically coated control channels have a higher loss than the non-coated and the coated structured channels have a lower loss than the non-coated structured channels. When channels are hydrophobically coated there is an advantage to having structured channels in that the losses are significantly reduced compared to the smooth walled coated control channels. However, there is still no evidence that applying a hydrophobic coating to the channels is beneficial to an increased flow rate.

The flow testing results have given rise to several hypotheses to the interaction between the channels and the water flowing through them. First, a characteristic decrease in flow over time is expected to be caused by small bubbles on the rough surface of the channel

walls which are shed over time, slowly increasing drag on the fluid and thus reducing the flow rate. Second, the non-coated channels tend to have a higher flow rate than the hydrophobically coated channels. It is believed that this is due, in part, to the large practical diameter that exists in the non-coated channels. The other reason for this is because the hydrophobic coating hinders flow in some way that as yet remains unexplained. Third, the large opening flow entrances sometimes allow for higher flow rates than do the small diameter entrances. This is believed to be because the small diameter entrances, especially when hydrophobically coated, are too small for the water to wet. It has also been observed that a hydrophobically coated channel will benefit greatly if it also has hydrophobic structures, supporting the hypothesis that the structures help to reduce drag by preventing complete wetting of the channel walls. Lastly, no evidence has been found to suggest that a hydrophobically coated channel, structured or smooth walled, will provide higher flow rates than a non-coated channel.

Chapter 6 – Conclusion

6.1 Conclusion of Results

The successful fabrication of out-of-plane silicon microneedles with inner microchannels has been demonstrated. The results of this research will benefit the medical community, administrators as well as patients, in the ongoing pursuit of improving medical treatments and assuaging the pain typical of hypodermic injections.

In addition, cylindrical microchannels with structures have been tested for hydrophobicity. It has been found that good measurements of reduction in friction are extremely sensitive to diameter measurements in microchannels as small as those used in this research. However, a loss coefficient was calculated to demonstrate an improvement in flow of a hydrophobically coated channel with the addition of structures to the surface of the walls. No evidence was found to suggest that hydrophobically coated channels, structured or non-structured, will give better flow rates than non-coated microchannels.

6.2 Recommendations for Future Research

6.2.1 Protective Needle "Cap" Over Channels to Prevent Clogging

A few suggestions are offered for future endeavors involving this research. The first, regarding the microneedle design, is to prevent the channel from extending all the way through the needle, as seen in Figure 6-1. The protective needle tip above the channel would help prevent clogging of the channel as the needle is inserted into the stratum corneum. Clogging is a concern with some microneedle designs and is currently addressed by relying on the fact that an array of microneedles will increase the chances that at least some of the microneedles will be unclogged by skin matter and able to deliver fluid freely [5-7, 30, 35]. A variation of this design using hydrophobic microchannels is shown in Figure 6-2 and Figure 6-3.

The fabrication would probably be made possible by stopping the ICP etch of the microchannels before it had gone all the way through the wafer. A double-sided polished wafer would be necessary so that the needle masks could be patterned on the back side of the wafer. A unique method for aligning the needles to the channels would be necessary since the channels would not be visible on the back side of the wafer. One possibility is an infrared aligner that will show patterns all the way through a wafer. Another option is to etch a very large feature at the same time as the channels. Large features tend to have faster etch rates than small constricted ones so it is possible that the large feature would etch all the way through the wafer in the same time that the channels were etched only part way.

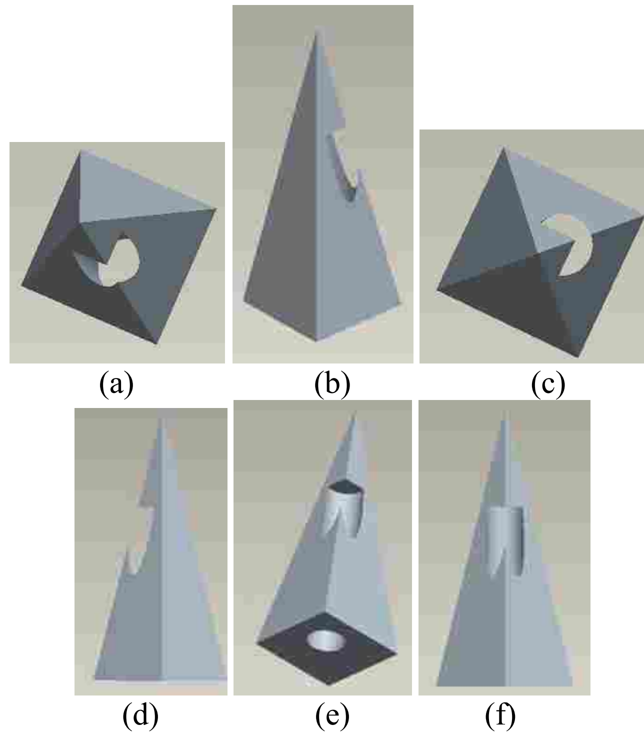

Figure 6-1: Microneedle concept with a lumen diameter of 48 µm opening up about half way up the structure. (a) and (b) are angled views from above, (c) is a view from directly overhead, (d) and (f) are side views, and (e) is an angled view from underneath.

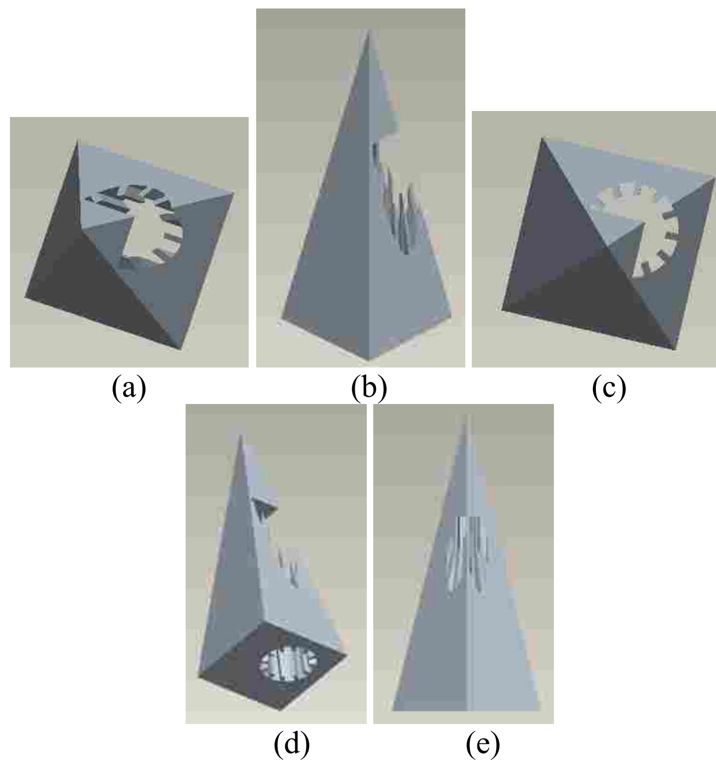

Figure 6-2: Microneedle design concept with structured lumen. (a) and (b) are angled views from above, (c) is a view from directly above, (d) is an angled view from underneath, and (e) is a side view.

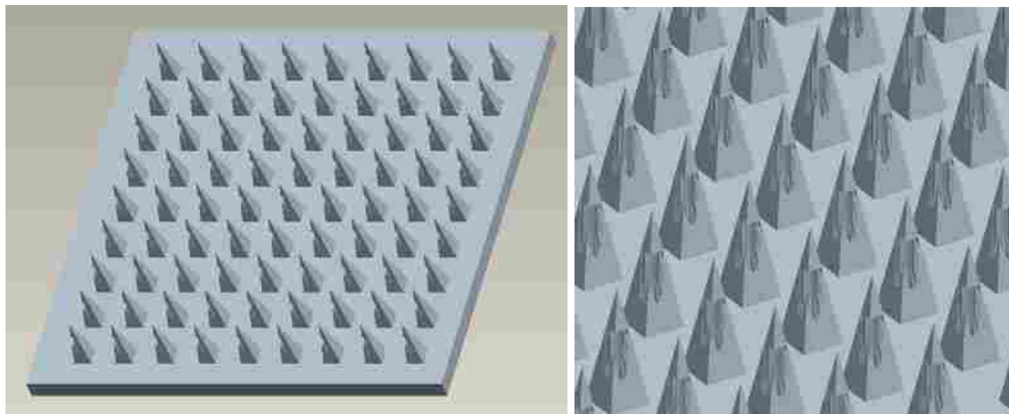
(a) (b)

Figure 6-3: Images showing (a) a conceptual array of microneedle protruding from the base of a silicon substrate and (b) a magnified version of the same array.

One concern would be that the LPCVD nitride would deposit deep enough into the channels to protect the very end of the channels where the KOH would first be exposed to the channels during the needle etch. Experimentation with this or another protective coating would be necessary. The KOH etch of the needles would also need to be controlled well as the needles are easily etched away in a matter of minutes when the temperature is high.

6.2.2 Testing of Transdermal Fluid Delivery Rates

The needles in this research were designed to a height that would not penetrate deep enough into most injections sights to cause pain. Although, as mentioned in chapter 2, others have reported that a 400 μm penetration depth should not be deep enough to cause any significant pain, the needles in this research have not been officially tested or documented to be painless. In order to test for any possible pain associated with these needles testing needs to be approved through the Institutional Review Board (IRB) directed by the Office of Research and Creative Activities at BYU. Complete

documentation is required and the testing must be thoroughly planned. Through discussions with an IRB chairperson, a few of the precautions and stipulations for testing procedures have been established and are presented in Appendix F as taken from unfinished documentation supporting the IRB application and approval process.

In addition to the knowledge to be gained through "pain" testing it will also be necessary to know the nature of injection into the epidermal, and perhaps dermal, regions of human skin using the microneedles. In particular, the biggest unknown factor is the absorption rate of specific medications in the top layers of the skin. This type of data is not well documented in the medical community and even if it were, the specific application of the needles in this research would most likely have its own unrecorded trends. A low absorption rate in the skin could easily nullify the advantages of hydrophobic channels in a microneedle application.

6.2.3 Silicon Micro-milling

A form of microchannel fabrication that may prove to be fast and cheap is silicon micro-milling. A company in contact with Dr. Brian Jensen has begun testing micro-milling technologies on brittle materials such as silicon. Initial communications with this testing have been positive and with success, needles with smooth walled channels could be manufactured much cheaper and with a higher channel anisotropy than current methods have been able to produce.

6.2.4 Improved Channel Testing

A few suggestions are offered for future work with microchannels. Firstly, the ICP recipe has potential for refinement which will hopefully give a more uniform cross-section throughout the length of the microchannels. If at all possible it is recommended that a design be found that allows for the increase in hydraulic diameter of the microchannels. Cross-sectional uniformity will be easier to control and lower pressures can be used to induce fluid flow through the channels.

A means for reducing surface roughness on the channel walls is also recommended as this will improve flow rates generally and will also lessen the possibilities of vapor bubbles forming on the surface.

References

[1] C. o. P. A. o. C. a. F. Health, "The Assessment and Management of Acute Pain in Infants, Children, and Adolescents," *Pediatrics,* vol. 108, pp. 793-797, 2001.

[2] I. Luzinov, P. Brown, G. Chumanov, and S. Minko, "Ultrahydrophobic Fibers: Lotus Approach," Nation Textile Center November 2004.

[3] L. Lin and A. P. Pisano, "Silicon-Processed Microneedles," *IEEE Journal of Microelectricalmechanical Systems,* vol. 8, pp. 78-84, March 1999.

[4] S. Chandrasekaran and A. B. Frazier, "Characterization of Surface Micromachined Metallic Microneedles," *Journal of Microelectromechanical Systems,* vol. 12, pp. 289-295, June 2003.

[5] H. J. G. E. Gardeniers, R. Luttge, E. J. W. Berenschot, M. J. d. Boer, S. Y. Yeshurun, M. Hefetz, R. v. t. Oever, and A. v. d. Berg, "Silicon Micromachined Hollow Microneedles for Transdermal Liquid Transport," *Journal of Microelectromechanical Systems,* vol. 12, December 2003.

[6] B. Stoeber and D. Liepmann, "Arrays of Hollow Out-of-Plane Microneedles for Drug Delivery," *Journal of Microelectromechanical Systems,* vol. 14, June 2005.

[7] P. Griss and G. Stemme, "Side-Opened Out-of-Plane Microneedles for Microfluidic Transdermal Liquid Transfer," *Journal of Microelectromechanical Systems,* vol. 12, June 2003.

[8] D. V. McAllister, F. Cros, S. P. Davis, L. M. Matta, M. R. Prausnitz, and M. G. Allen, "Three-Dimensional Hollow Microneedle and Microtube Arrays," in *Transducers 99, Int. Conf. Solid-State Sens. Actuators, 10th, Sendai* Japan, 1999.

[9] S. J. Moon and S. S. Lee, "A novel fabrication method of a microneedle array using inclined deep x-ray exposure," *Journal of Micromechanics and Microengineering,* March 2005.

[10] http://www.elwoodstudio.com/key_pages/illustration_fr.htm, "skin anatomy," 2005.

[11] M. Alper, A. Kavak, A. H. Parlak, R. Demirci, I. Belenli, and N. Yesildal, "Measurement of epidermal thickness in a patient with Psoriasis by computer-

supported image analysis," *Brazilian Journal of Medical and Biological Research,* vol. 37, pp. 111-117, January 2004.

[12] H. L. Offereins, K. Kuhl, and H. Sandmaier, "Methods for the Fabrication of Convex Corners in Anisotropic Etching of (100) Silicon in Aqueous KOH," *Sensors and Actuators A,* pp. 9-13, 1991.

[13] R. Dizon, H. Han, A. G. Russell, and M. L. Reed, "An Ion Pattern Transfer Technique for Fabrication of Three-Dimensional Micromechanical Structures," *Journal of Microelectromechanical Systems,* vol. 2, December 1993.

[14] H. Sandmaier, H. L. Offereins, and K. a. W. Lang, "Corner Compensation Techniques in Anisotropic Etching of {(100)}-Silicon Using Aqueous KOH," in *Tranducers '91, the 6th International Conference on Solid State Sensors and Actuators Digest of Technical Papers* San Francisco, CA: IEEE Press, 1991.

[15] G. K. Mayer, H. L. Offereins, H. Sandmaier, and K. Kuhl, "Fabrication of Non-Underetched Convex Corners in Anisotropic Etching of (100)-Silicon in Aqueous KOH with Respect to Novel Micromechanic Elements," *Journal of the Electrochemical Society,* vol. 137, pp. 3947-3951, December 1990.

[16] R. P. v. Kampen and R. F. Wolffenbuttel, "Effects of (100)-oriented corner compensation structures on membrane quality and convex corner integrity in (100)-silicon using aqueou KOH," *Journal of Micromechanics and Microengineering,* vol. 5, pp. 91-94, 1995.

[17] D. Oner and T. J. McCarthy, "Ultrahydrophobic Surfaces. Effects of Topography Length Scales on Wettability," *Langmuir 2000,* vol. 16, pp. 7777-7782, 2000.

[18] B. Woolford, K. Jeffs, D. Maynes, and B. W. Webb, "Laminar Fully-Developed Flow in a Microchannel with Patterned Ultrahydrophobic Walls," in *2005 Summer Heat Transfer Conference*, 2005.

[19] J. Ou, B. Perot, and J. P. Rothstein, "Laminar drag reduction in microchannels using ultrahydrophobic surfaces," *Physics of Fluids,* vol. 16, pp. 4635-4643, December 2004.

[20] J. Kim and C.-J. C. Kim, "Nanostructured Surfaces for Dramatic Reduction of Flow Resistance in Droplet-Based Microfluidics," in *IEEE Conf. MEMS* Las Vegas, NV, 2002.

[21] N. J. Shirtcliffe, S. Aqil, C. Evans, G. McHales, M. I. Newton, C. C. Perry, and P. Roach, "The use of high aspect ratio photoresist ({S}{U}-8) for super-hydrophobic pattern prototyping," *Journal of Micromechanics and Microengineering,* vol. 14, pp. 1384-1389, 2004.

[22] H. Yabu, M. Takebayashi, M. Tanaka, and M. Shimomura, "Superhydrophobic and Lipophobic Properties of Self-Organized Honeycomb and Pincushion Structures," *Langmuir,* vol. 21, pp. 3235-3237, 2005.

[23] B. He, N. A. Patankar, and J. Lee, "Multiple Equilibrium Droplet Shapes and Design Criterion for Rough Hydrophobic Surfaces," *Langmuir,* vol. 19, pp. 4999-5003, 2003.

[24] J.-G. Fan, X.-J. Tang, and Y.-P. Zhao, "Water contact angles of vertically aligned Si nanorod arrays," *Nanotechnology,* vol. 15, pp. 501-504, 2004.

[25] D. C. Tretheway and C. D. Meinhart, "Apparent fluid slip at hydrophobic microchannel walls," *Physics of Fluids,* vol. 14, pp. L9-L12, 2002.

[26] K. Watanabe, Y. Udagawa, and H. Udagawa, "Drag reduction of Newtonian fluid in a circular pipe with a highly water-repellent wall," *Journal of Fluid Mechanics,* vol. 381, pp. 225-238, 1999.

[27] C.-H. Choi, K. Johan, A. Westin, and K. S. Breuer, "Apparent slip flows in hydrophilic and hydrophobic microchannels," *Physics of Fluids,* vol. 15, pp. 2897-2902, October 2003.

[28] B. R. Munson, D. F. Young, and T. H. Okiishi, *Fundamentals of Fluid Mechanics*, 4th ed.: John Wiley and Sons, 2002.

[29] E. Mukerjee, S. D. Collins, R. L. Smith, and R. Isseroff, "Microneedle Array for Transdermal Bio-Fluid Sampling and Drug Delivery," *Micro Total Analysis Systems 2001,* pp. 379-380, 2001.

[30] E. V. Mukerjee, S. D. Collins, R. R. Isseroff, and R. L. Smith, "Microneedle array for transdermal biological fluid extraction and in-situ analysis," *Sensors and Actuators A,* vol. 114, pp. 267-275, 2004.

[31] S. Rajamaran and H. T. Henderson, "Silicon MEMS-Based Development and Characterization of Batch Fabricated Microneedles for Biomedical Applications," in *Department of Electrical and Computer Engineering and Computer Science*: University of Cincinnati, 2000.

[32] M. Elwenspoek and H. Jansen, *Silicon Micromachining*: Cambridge University Press, 1998.

[33] A. A. Ayon, R. Braff, C. C. Lin, H. H. Sawin, and M. A. Schmidt, "Characterization of a Time Multiplexed Inductively Coupled Plasma Etcher," *Journal of the Electrochemical Society,* vol. 146, pp. 339-349, 1999.

[34] D. Rosen, J. Olsson, and C. Hedlund, "Membrane Covered Electrically Isolated Through-Wafer Via Holes," *Journal of Micromechanics and Microengineering,* vol. 11, pp. 344-347, 2001.

[35] B. Stoeber and D. Liepmann, "Design, Fabrication and Testing of a MEMS Syringe," in *Solid State Sensor and Actuator Workshop* Hilton Head, SC, 2002.

Appendix A - Fabrication Precautions and Details

Spin Coating

Spin coating is the process used to apply photoresist onto the wafer. Although a fairly simple process, a good application of photoresist will only be achieved with careful attention to the spinning characteristics and cleanliness of the wafer.

A good spinner will allow variable steps and speeds at which a photoresist can be spun onto a wafer. For an acceptable application of photoresist the following rules generally apply: 1) keep the wafer clean; contaminants and particles will cause striations of uneven thickness in the coating 2) be sure to put a sufficient amount of photoresist on the wafer before spinning, too little resist will leave portions of the wafer uncoated 3) controlled acceleration of the spin speed is often necessary to evenly distribute the resist over the wafer 4) an adhesion material, such as HMDS, will often need to be spun on prior to the resist to help the resist adhere to the wafer surface 5) heating of the wafer, or soft bake, after the resist has been spun on is necessary but can hurt the coating. A softbake is typically done in an oven or on a hotplate if the resist is strong enough to withstand the direct heat, and can cause bubbles or other imperfections in the resist layer if not done with proper timing and temperatures.

Mask

When designing a layout in L-Edit a few design rules are important to know. Each cell in L-Edit has a four quadrant coordinate system. All design features must be kept in the positive x and y region so that they can be read by the pattern generator or e-beam lithography machines. Although e-beam lithography can handle any feature size, pattern generation must have a feature size of 3 μm if done at BYU and about 1 μm if outsourced somewhere else. Accuracy of pattern generation feature placement is also limited to around 0.5-1 μm. Pattern generators cannot have any angles smaller than 90° in a feature. When designing a mask in L-Edit, only one color should be used. The designer is also responsible for centering the design relative to where they want it on the mask. The (0,0) point of the layout will typically be placed at the bottom left corner of the mask. L-Edit will automatically save the file as a GDS II if requested. This makes for quick and reliable data transfer to those who are making the physical mask.

Although the lithography masks in this research are outsourced to BYU or outside vendors, an understanding of the mask making equipment is valuable in the design stage. With both methods a square piece of soda lime glass, 5 inches wide and about 1/8 inch thick is covered with chrome on one side and then with a photoresist over that. The mask design is imprinted on the photoresist then transferred to the chrome. The quality of the mask will depend upon the design of the mask layout, the feature sizes on the design, and the method used for making the mask.

Pattern generation is the preferred method for making a mask because it is less expensive but for relatively large features will give the same general quality. A pattern generator creates a mask by orienting an aperture so that a localized section of the mask is flashed

with light. The aperture can be reoriented and resized so that many shapes can be made by overlapping the areas that have been exposed through the aperture. The features cannot have acute angles and a minimum feature size of 1-2.5 μm is possible.

E-beam lithography is used when the feature size or angles prohibit pattern generation. It is a more expensive process but will ensure a high quality mask if feature size is what counts. E-beam lithography works much like a printer, scanning back and forth, sometimes on and sometimes off to recreate a digital design of the mask onto the photoresist of the physical mask. There are fewer restrictions on designing a mask for this process so this can be another savings advantage as well.

Lithography

The exposure of a pattern onto photoresist is done at BYU with a piece of equipment made by Karl Suss. First the wafer is loaded onto a platform and a vacuum is applied to hold it down. The platform is lowered and the mask is placed above it. A vacuum holds the plate down as well. The wafer is then raised to a point just underneath the mask for mask alignment relative to the wafer. Two microscopes offer a fairly wide range of viewable area over the mask and wafer so that the user can look through the transparent (free of chrome masking) portions of the mask to be able to align it as desired relative to the wafer. Typically, a wafer is meant to be placed with the major flat toward the user as seen in Figure A-1.

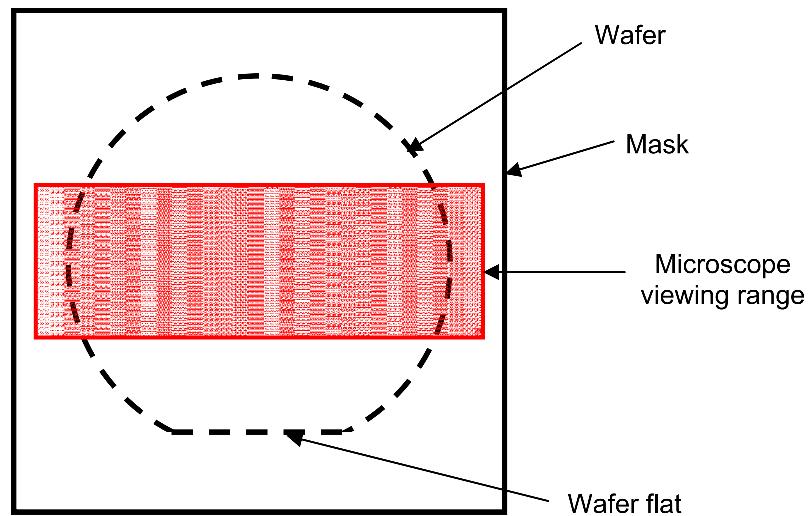

Figure A-1: The viewing range through a mask is shown with the outline of a typically oriented wafer inside the Karl Suss lithography machine.

As can be seen, the major flat of the wafer is not located within the viewing range of the microscope. For some of the applications in this research the mask must be aligned relative to the major flat of the wafer. As this is not possible with standard procedures the mask and the wafer must both be turned 90° either clockwise or counterclockwise before being placed in the Karl Suss so that the wafer can be aligned to the major flat of the wafer as seen in Figure A-2.

Once the mask is aligned relative to the wafer the photoresist can be exposed with light through the transparent portions of the mask. The wafer is moved upward until it is in contact with the underside of the mask. The wafer is then exposed to a concentrated specific frequency light. The duration of the exposure will depend upon the type of photoresist, its thickness, and the minimum feature size among other things.

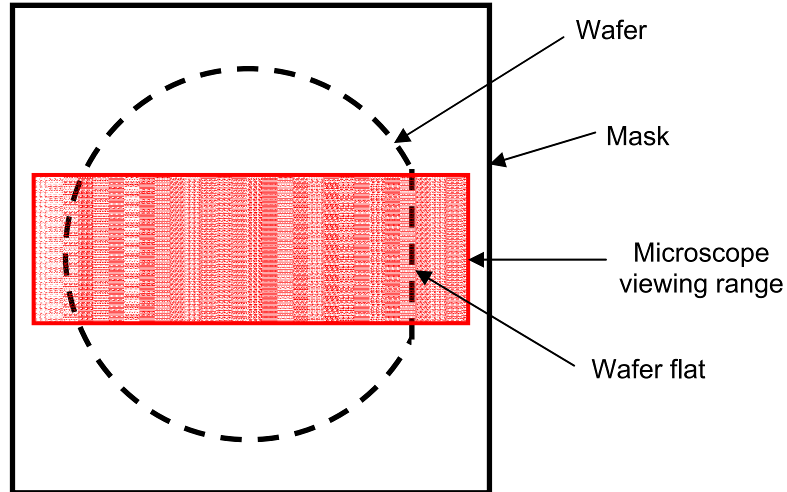

Figure A-2: The viewing range through a mask is shown with the outline of a re-oriented wafer modified for alignment with the mask inside the Karl Suss lithography machine.

ICP Etch

The etching of the channels will need to undergo extensive testing as changing elements in the etch recipe can drastically alter the shape of the channels. The ICP process has many parameters that need to be tuned for a successful etch. These parameters include the flow rates of both SF_6 and C_4F_8, the cycle time, overrun time, coil power, platen power, pressure, and total etch time. Most of these parameters will need to have settings for both etch and passivation cycles (see Table A-1).

Table A-1: The units used in each parameter setting of an ICP process for both the etch and passivation cylces.

<table>
<tr><th></th><th>SF_6</th><th>C_4F_8</th><th>cycle time</th><th>overrun</th><th>coil power</th><th>platen power</th><th>APC (pressure)</th><th>total time</th></tr>
<tr><td>Etch</td><td>(sccm)</td><td>(sccm)</td><td>(sec.)</td><td>(sec.)</td><td>(Watts)</td><td>(Watts)</td><td rowspan="2">(degrees)</td><td rowspan="2">(min.)</td></tr>
<tr><td>Passivate</td><td>(sccm)</td><td>(sccm)</td><td>(sec.)</td><td>(sec.)</td><td>(Watts)</td><td>(Watts)</td></tr>
</table>

Flow rates are typically high for SF_6 during the etch cycle and low (usually zero flow) during the passivation cycle. Conversely, flow rates for C_4F_8 are low or zero during the etch cycle and high during the passivation cycle. Cycle time refers to how many seconds the etch or the passivation cycle will run. The overrun time refers to the amount of time that the flow of one gas stays high while changing cycles and turning the other gas on to the high flow. The coil power refers to the power used to generate the plasma inside the chamber. A higher coil power will produce more ions in the plasma. The platen power is the power used to pull the ions down toward the wafer. Typically in the Bosch process the coil power is relatively high creating a lot of ions and the platen power is relatively low gently tugging the ions down toward the sample surface. The automatic pressure control (APC) is a butterfly valve in the main pressure line. It is fixed at a certain angle which regulates the pressure that will generally be held in the chamber. The total time is the full amount of time that the sample wafer will be etched in the chamber. The total time can be set using hours and minutes or it can be set with a number of etch/passivation cycles to run.

Each of these parameters will affect the results of the etch in different ways. The main etch characteristics to be aware of are the anisotropy of the etch, the etch rate, the percent variation in uniformity of the etch from one location on the wafer to another, the selectivity of the photoresist etch rate compared to the silicon etch rate, micromasking and striation effects that occur on the side walls, and aspect ratio dependant etching (ARDE) (see Table A-2).

Table A-2: The desired outcome of several etching attributes is shown next to the necessary adjustment that need to be made to several parameters of the ICP machine.

Attribute	Desired Outcome	Platen Power	SF_6 Flow Rate	Etch Cycle Time	Passivation Cycle Time	APC (pressure)
Etch Rate	↑	↑	↑	↑	↓	
ARDE	↓		↑			
Selectivity	↑	↓		↓	↑	↑
Uniformity (%)	↓		↓			
Anisotropy	↑	↑	↓			↓
Micromasking	↓		↓			↓

The etch rate refers to the amount of vertical distance that is etched for a given amount of time. Most researchers use the average etch rate however the etch rate gets slower the deeper an etch goes into the substrate therefore the rate of change of the etch rate is usually not taken into account [33]. The ARDE refers to the fact that smaller spaces will etch slower than large ones. A very large hole (on the order of hundreds of micron) will etch much quicker than a narrow trench. Similarly, a slender well with diameter equal to that of the width of a trench will etch slower than the trench. Selectivity is a ratio of the silicon etch rate over the photoresist etch rate. Although a layer of thick photoresist will remain for quite some time during an etch, the side walls of the resist that determine the shape of a features will recede during the etch. The receding of a photoresist mask may need to be compensated for in the mask design. Percent variation in uniformity across the wafer is of only minor concern but should be addressed. Changing etch parameters can cause variation in the etch rate across the wafer so that similar features in one point on the wafer will take longer to etch than on other points of the wafer. Anisotropy refers to the ability to maintain a constant cross section of a feature from top to bottom. This is one of the most critical etch characteristics when creating microchannels. Micromasking

happens when small (submicron size) spots of masking material prevent etching by blocking ion bombardment from the SF_6 plasma. This results in what is known as “grass” as well as stalagmite looking features in the middle and on the side walls of a well or hole. [33]

There are other considerations that need to be taken into account as well. The total surface area of the wafer being etched should only add up to about 10 %. Too much surface etching can lead to poor heat transfer from the wafer to the cooled mounting plate and will give poor etch results. It is also a characteristic of ICP etching that wells and trenches begin to taper inward the deeper they get. Only through careful control of the etching parameters can this effect be partially avoided.

Appendix B - Microneedle Fabrication Details

Preprocessing steps include a dehydration bake at 120 °C for 20 minutes followed by a rinse in acetone and isopropyl to clean off dust, oils, or other contaminants. The wafer is then ready for photoresist.

To apply a photoresist layer to the wafer it is first placed inside the spinner and HMDS is applied. This is a chemical that helps photoresist adhere to the surface of the wafer. About 10 drops of HMDS are spun on at 3000 rpm for 10 seconds after which the photoresist, AZ-3330, is applied. A minimum of 60-70 drops of AZ-3330 is needed and it is spun on at 6000 rpm, with an acceleration setting of 015, for 60 seconds. This gives a 1-2 µm thick layer of photoresist. Once the photoresist is applied the wafer is placed on a hotplate for a soft bake. The hotplate should be at 90 °C and the wafer should remain on the hotplate for at least 60 seconds.

After the soft bake the light sensitive photoresist on the wafer is ready to have a pattern exposed onto it. The Karl Suss lithography machine in the clean room will allow the user to create specific recipes for many types of photoresists and processing procedures. Some of the parameters are simply standard settings and rarely change for any work done in the clean room while others are specific for the job being done. The parameter settings for the work done on the microneedles in this research are found below.

Karl Suss AZ3330 Settings

Type:	Hard Contact	Resist:	Positive
		Mode:	Manual Align
Max Exposure:	500	WEC:	Contact
Exposure:	9.0 sec	Align Check:	On
Alignment Gap:	40µm	Prealigner Type:	o
Max Contacts:	500		
Hard Contact Delay:	5 sec	Mic/Mask Teach:	Default
		Data Logging:	On

The most important settings for this exposure are the “Exposure”, “Alignment Gap”, “Mode”, “WEC”, and “Align Check” settings. The rest of the parameters are usually set by default and do not need to be adjusted. The “Exposure” setting of 9.0 seconds is the time that the photoresist on the wafer will be exposed to direct high frequency light. The “Alignment Gap” setting of 40 µm is the distance between the wafer and the mask in the machine. If this gap is too small the bottom of the mask will scrape against the top of the wafer as the mask is adjusted into position relative to the wafer. The “Mode” setting allows the user to manually align the mask to the wafer. This is necessary, as explained in chapter 3, so that the mask can be perfectly aligned to the [100] major flat of the wafer. The “WEC” setting of contact means that at the time of exposure the wafer will be pressed to the bottom side of the mask. This limits the amount of light diffraction undergone during exposure. The “Align Check” setting allows the user to view the alignment of the mask over the wafer while in contact but before exposure so that realignment can be made, if necessary, prior to exposure to light. The masks used have been made at BYU and, for improved mask quality, at IC Photomask[6].

[6] IC Photomask
3498 North San Marcos Place, Suite 5, Chandler, AZ 85225
Tel: (480) 892-2420
Web: www.icphotomask.com

After the photoresist has been exposed through the mask the pattern can be developed. The wafer is submersed in developer, AZ300 MIF, for about 45 seconds then rinsed off in deionized water for about half a minute. After it is dried off, the wafer is placed on the hotplate again for a hard bake. The settings are the same as for the soft bake, 90 °C for 60 seconds.

At this point the pattern in the photoresist is ready to be transferred into the oxide/nitride layer underneath. This is done with Reactive Ion Etching (RIE). The RIE etch is done with the RF power supply set to 300, a pressure of 100 mTorr, and the reflective power set to 2. The etch is run for 6 minutes 35 seconds and should be done with just one wafer at a time. Although the machine can etch several wafers at once the recipe may need to change to get the same results. A complete set of instructions for this etch is found in Appendix B. After the RIE etch is complete the photoresist will look slightly burnt and should be removed by simply rinsing the wafer in acetone and isopropyl. At the completion of this step, the wafer will have a “hard mask” of oxide/nitride and the sample is now ready to be etched in potassium hydroxide (KOH) to create the microneedles.

Appendix C - RIE Operation Instructions

- Turn on RIE pump in the pump room (1st roughing pump, wait 1-2 seconds then blower)
- Turn on "start" button for pump
- Open CF_4 tank (both valves)
- Turn on RIE (switch is located on bottom right hand side)
- Vent chamber and open it to place sample (if needed, support wafers scraps can be included to keep sample wafer stable)
- Close chamber and hold down to pump

- Slowly turn etching valve (counter-clockwise) until gauge reads **14** then open the rest of the way
- Switch CF_4 on mass flow meter to the "up" position (this is the "open" regulator) and turn knob to channel 3 (so you can see what the flow is if you need to)
- Set RF power supply to **300** (do this by holding down "setpoint" button and turning knob to the right)
- Purge air
    - When "roughing gauge" gets down to **100** open baratron valve
    - When "baratron etching valve" reads **20** close both "baratron valve" and "etching valve"
    - Switch on CF_4 until rough gauge reads **3000**
    - Turn off CF_4 and "vent", pump down to **14** on the round gauge
    - Open etching valve all the way
- Repeat "purge air" instructions (purge air cycle is done twice for better etching results)
- Switch CF_4 (on mass flow meter) to "middle" position (for regulated flow)
- Open baratron valve (etching valve should be open already) and turn on CF_4 and chiller
- At this point both etching and baratron valves should be open and CF_4 and chiller on
- Close etching valve until the baratron gauge reads about **80** (desired **pressure** minus 20)
- Make sure timer is set to appropriate time (for the current layer of nitride on thermal oxide that is deposited on our wafers this should be around **6 min 35 seconds**, for a 500 nm thick layer of pure LPCVD nitride this should be **10 min 00 sec**.

- Start the etch (red button underneath timer and "RF on" button on RF power supply)
- Immediately adjust etching valve and tuner to keep baratron pressure at **100** and reflective power at **2**
- You will need to stay attentive during the entire etch to make sure that pressure and reflective power are set appropriately

- When etch is over turn off chiller and CF_4 (switch mass flow meter to "down" position)

- Purge CF_4
  - Open etching valve all the way
  - When "roughing gauge" gets down to **100** open baratron valve
  - When "baratron etching valve" reads **20** close both "baratron valve" and "etching valve"
  - Switch on "vent" and pump down to **14** on the round gauge
  - Turn off "vent"
- Repeat "purge CF_4" instructions
- Repeat "purge CF_4" instructions again but this time allow chamber to vent all the way down
- Remove sample
- Do next etch *or* if finished turn off RIE, pump (box next to wall and pump in the pump room), and CF_4 gas (make sure to close both valves)

Appendix D - KOH Etch Experimentation

The following shows the chronological design steps and experimental results that led to the fabrication recipe ultimately used for this research. Although only the major findings are briefly highlighted, a significant amount of literature review and analysis of results was involved and is left unrecorded in this summary of findings.

Etch #2

Initially a pinwheel shaped mask was used in attempt to create square cross-section needles. The long slender compensation beams extending from a square center were calculated from some misinterpreted equations in a paper highlighting KOH etching with compensation beams [12]. The temperature was set at 70 °C and was etched for 9½ hours.

This etch resulted in little nubs about 8µm high like the one shown in Figure D-1.

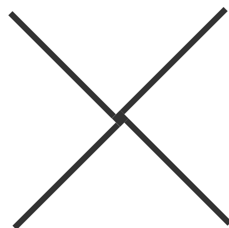

(a)

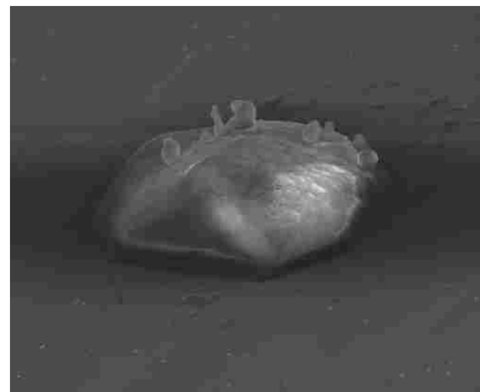

(b)

Figure D-1: The slender pinwheel shaped mask in (a) created nubs like the one seen in (b).

Etch #3

The pinwheels were modified by filling in certain portions to see what would happen. One paper suggested that a square with dimensions that filled the entire space as the pinwheel would give the same results but was not preferred because it was not space efficient [13]. The dimensions of the initial pinwheel stayed the same with the modifications and accompanying results as shown in figure D-2 – Figure D-7.

The temperature was set to 70 °C and the etch lasted about 13½ hours. Many smooth faces emerge in these structures and close observation will show that many of the faces are identical from one structure to the next.

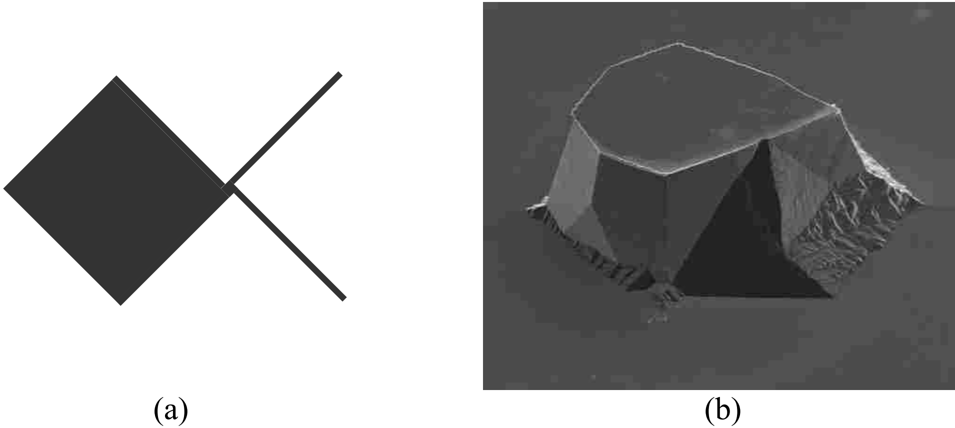

(a) (b)

Figure D-2: The mask in (a) created the structure in (b)

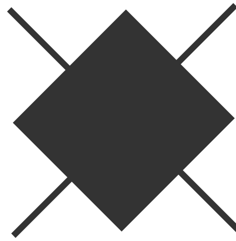

(a)

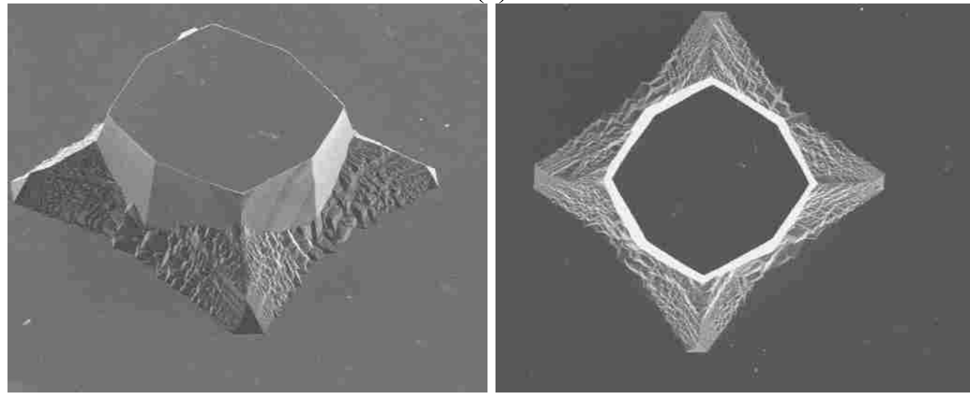

(b) (c)

Figure D-3: The mask in (a) created the structures in (b), an angled view and (c), an overhead view of the same structure.

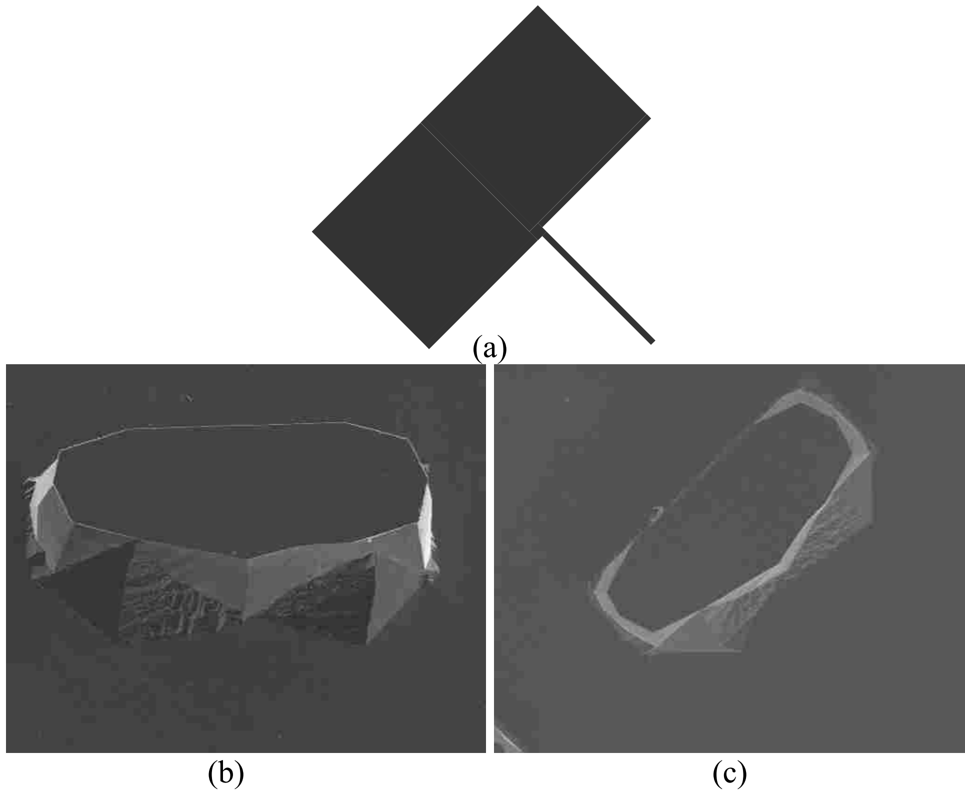

Figure D-4: The mask in (a) created the structures in (b), an angled view and (c), an overhead view of the same structure.

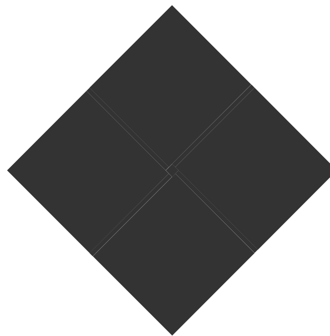

(a)

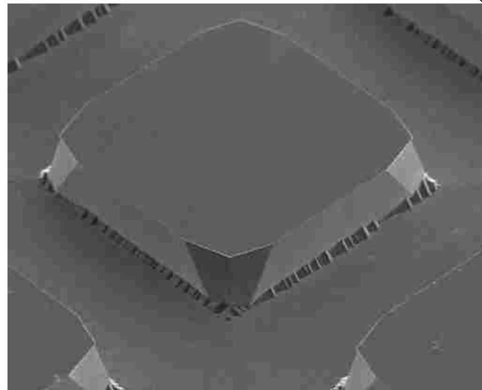

(b)

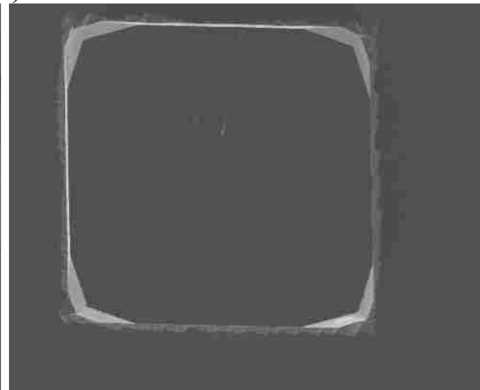

(c)

Figure D-5: The mask in (a) created the structures in (b), an angled view and (c), an overhead view of the same structure.

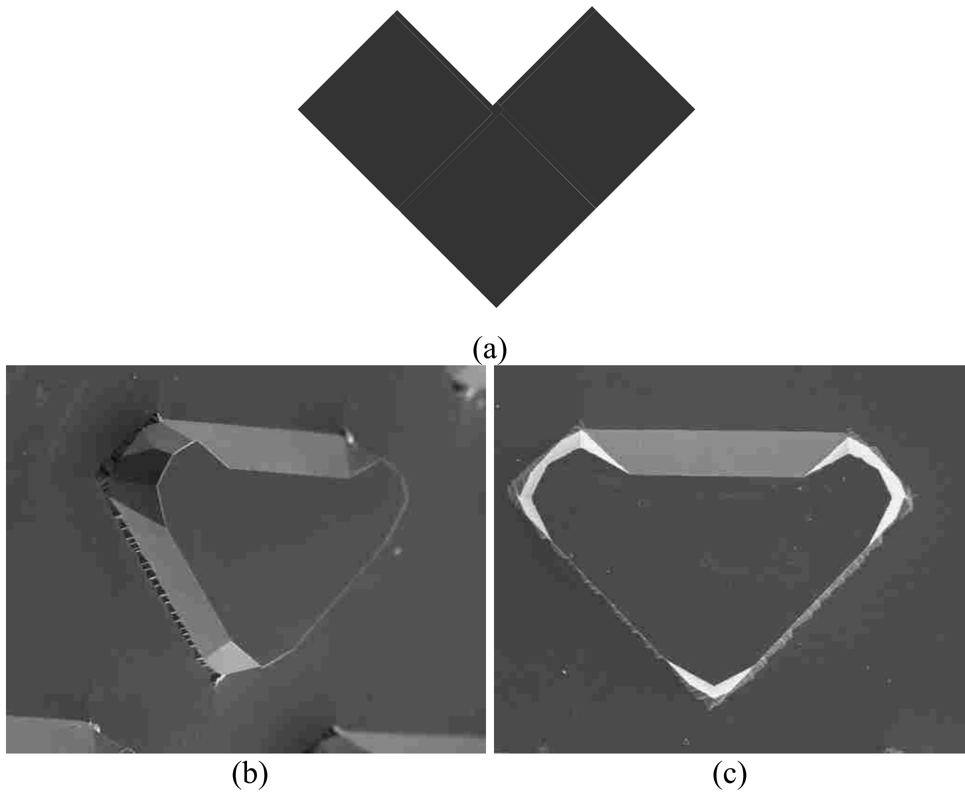

Figure D-6: The mask in (a) created the structures in (b), an angled view and (c), an overhead view of the same structure.

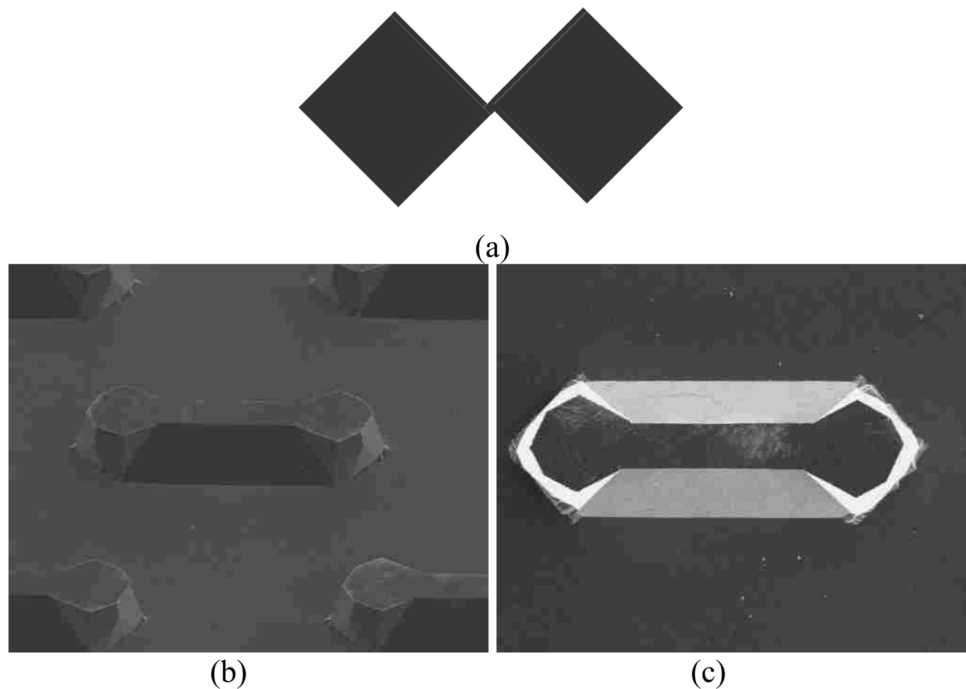
(a)

(b) (c)

Figure D-7: The mask in (a) created the structures in (b), an angled view and (c), an overhead view of the same structure.

Etch #4

This etch has multiple variations of the pinwheel. The intent was to compensate for the etching away of the mask by making the mask larger. The distance from the center of each compensation beam was extended by 175, 200, 250, 300, and 325 μm, some examples of which are shown in Figure D-8 – Figure D-10. There was also a set of squares rotated at a 45 degree angle. This turned out to be the lucky etch resulting in needles from the square mask (see Figure D-11).

The temperature was set to 70 °C and the etch lasted about 13½ hours. The first set of images shows the results of the pinwheel mask extended by 325 μm, the second set shows

the results of the pinwheel mask extended by 175 μm and the third by 250 μm. The last shows octagonal cross-sectioned needles about 180 μm high.

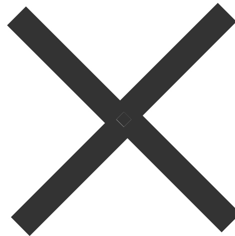

(a)

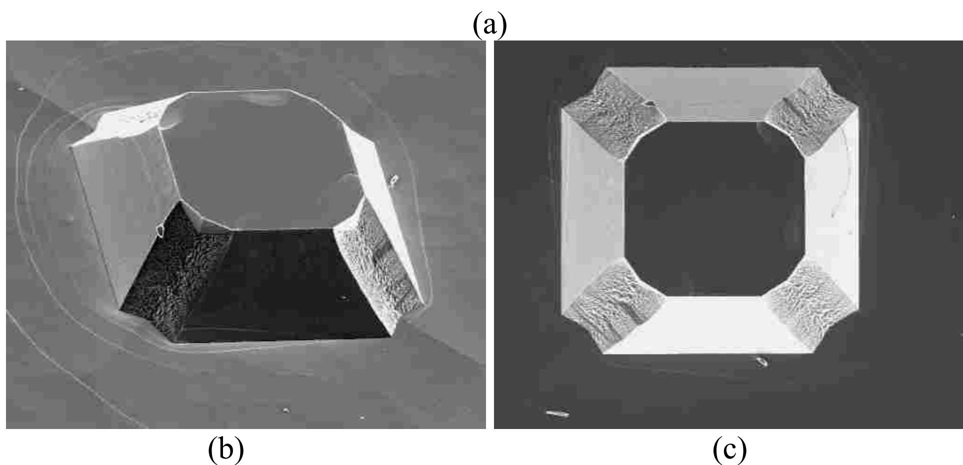

(b) (c)

Figure D-8: The mask in (a) created the structures in (b), an angled view and (c), an overhead view of the same structure.

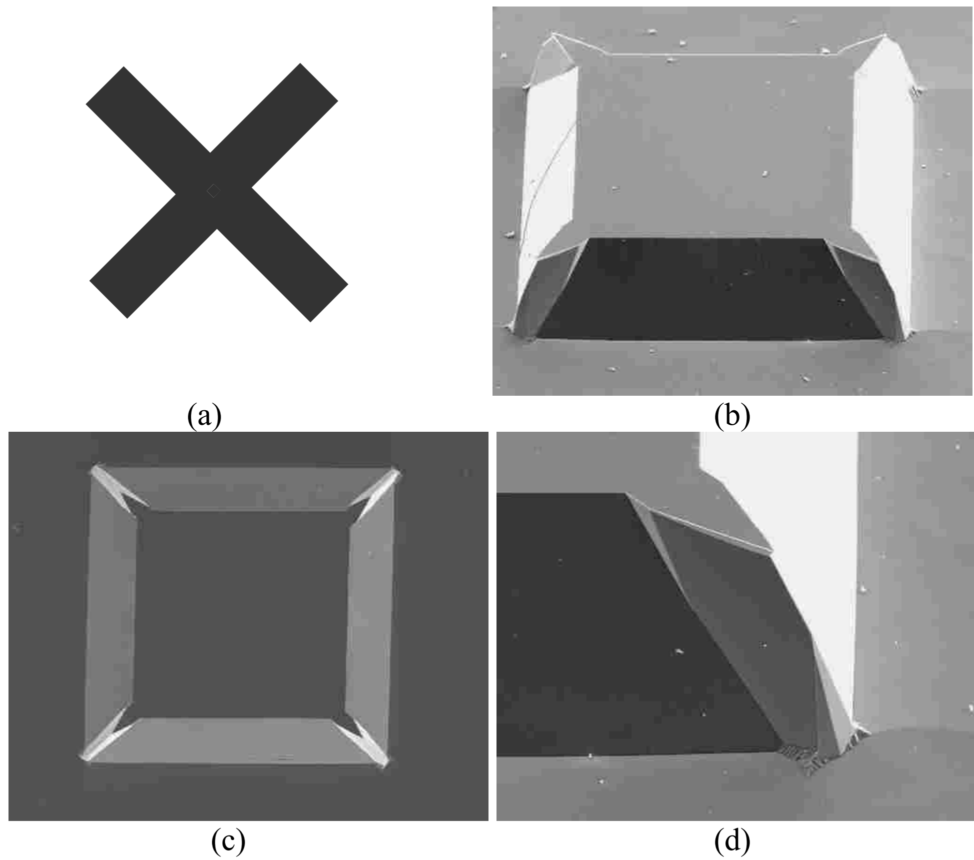

(a) (b)

(c) (d)

Figure D-9: The mask in (a) created the structures in (b), an angled view, (c), an overhead view, and (d) a close up view of the same structure,

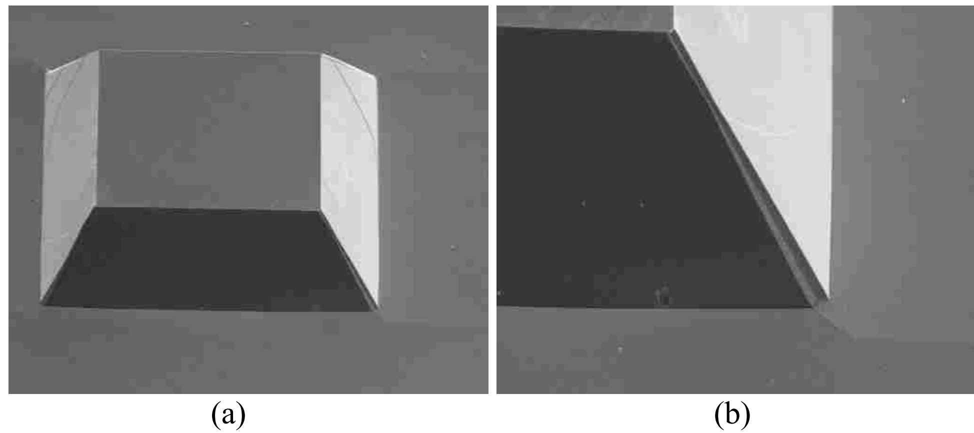

(a) (b)

Figure D-10: A mask with member widths greater than that of Figure D-8 and smaller than that Figure D-9 was used to create the structures seen in (a) and (b).

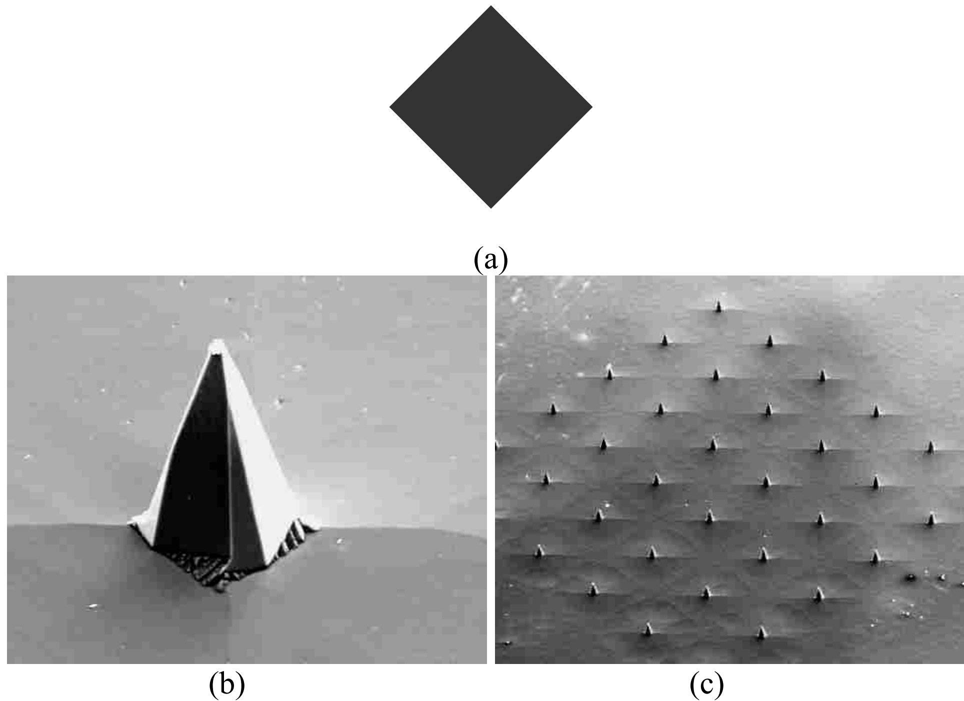

(a)

(b) (c)

Figure D-11: The mask in (a) was used to create the needle seen in (b). An array of these same needles can be seen in (c).

Etch #5

The next etch was done with a series of squares of varying dimensions. There was also a uniquely shaped pinwheel (see Figure D-12). The squares ranged in dimensions 800, 900, 950, 1000, 1050, 1100, and 1150 μm.

The temperature was set to 70 °C and the etch lasted 13 hours 20 minutes. The images below show the results of the slotted pinwheel as well as the small needle that was etched from the 800 μm square mask and the large capped needle that was etched from the 1150 μm square mask (see Figure D-13). There are eight separate {411} planes that can be etched in the silicon and they all emerge in the needle. The cap is interesting because it is mirrors each {411} plane that has been etched on the needle.

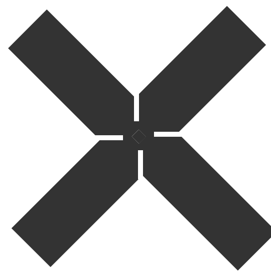

(a)

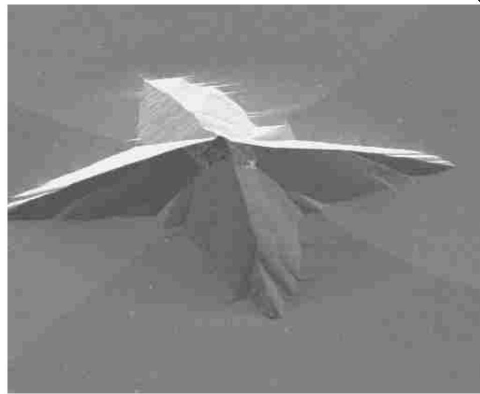

(b)

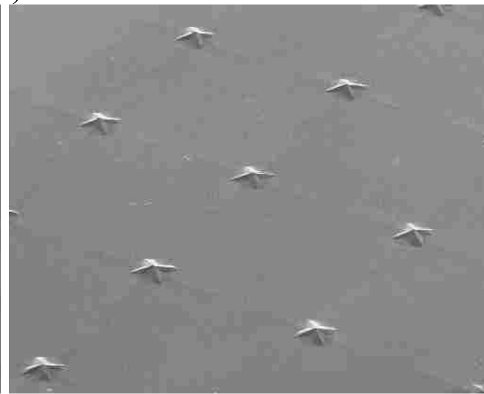

(c)

Figure D-12: The mask in (a) was used to create the structure in (b). An array of these structures can be seen in (c).

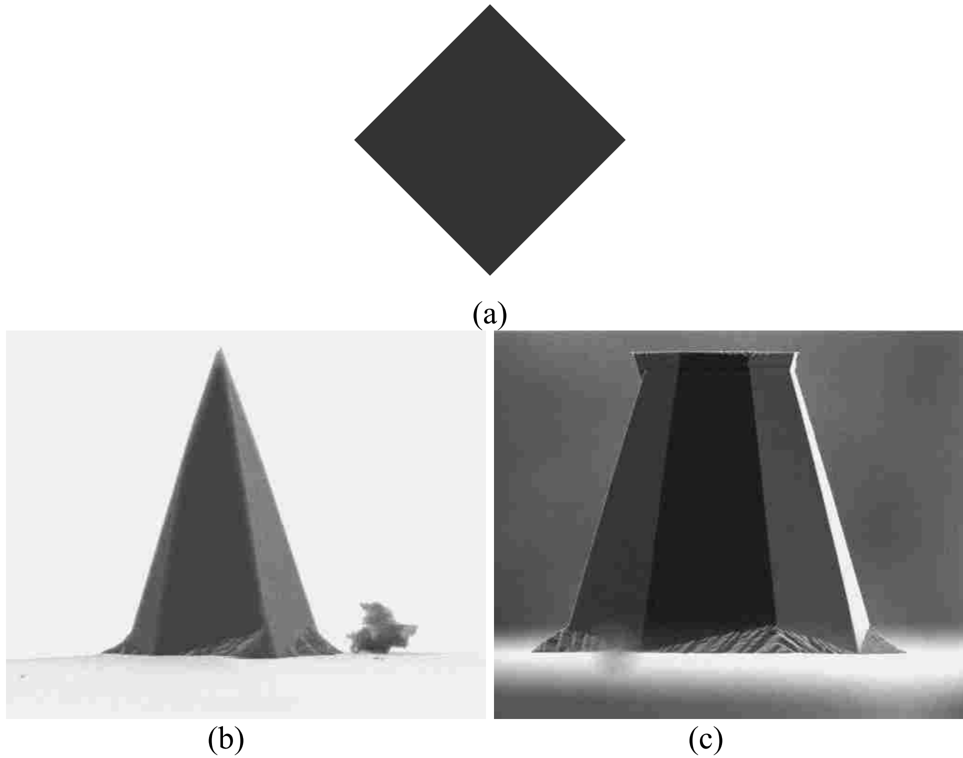

Figure D-13: The various sizes of the mask in (a) were used to create various needles (b) or "unfinished" needles (c).

Etch #7

This etch was the same except it shows some anomalies and variations in the features (see Figure D-14). The temperature was set to 79 °C and the etch lasted 7 hours and 50 minutes.

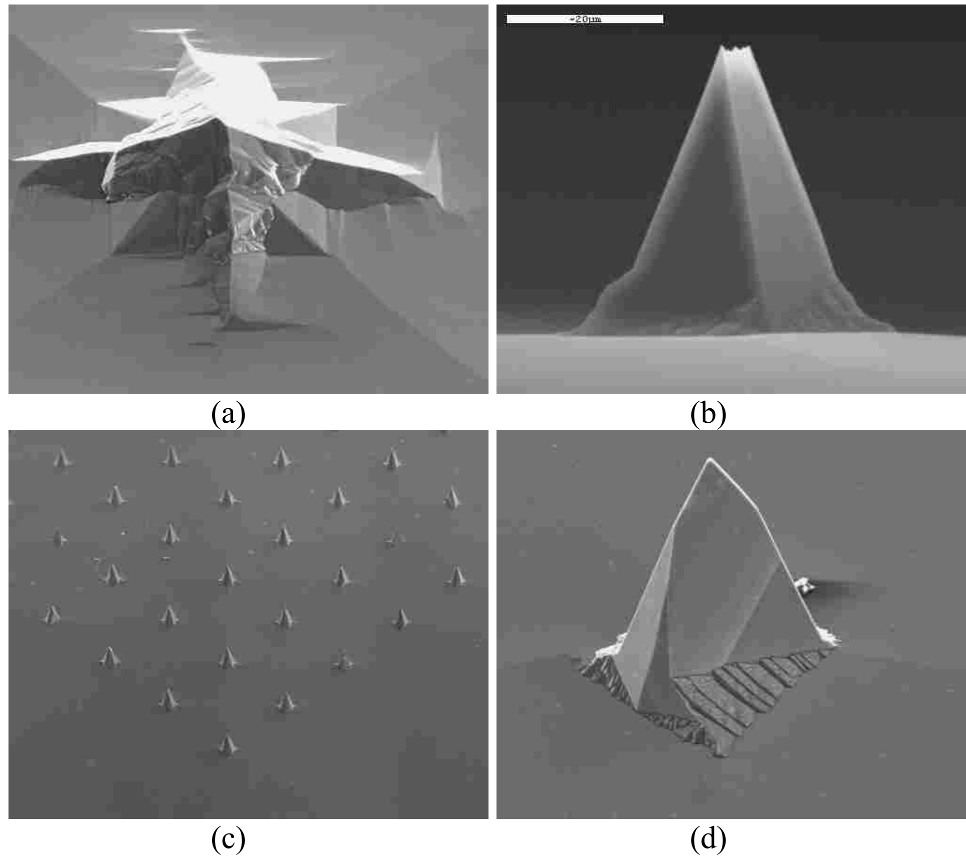

Figure D-14: The structure in (a) was formed with a mask similar to that in Figure D-13. The needle in (b) was etched to the point that it almost disappeared altogether. An array of needles is shown in (c) and a mis-formed needle due to a mask with a poor pattern transfer from a blemish in the photoresist is shown in (d).

Etch #8

This etch was the same except as well. The images in Figure D-15 show how the cap size can vary. It also shows an overhead view of a needle with a cap. The temperature was set to 79 °C and the etch lasted 8 hours and 13 minutes.

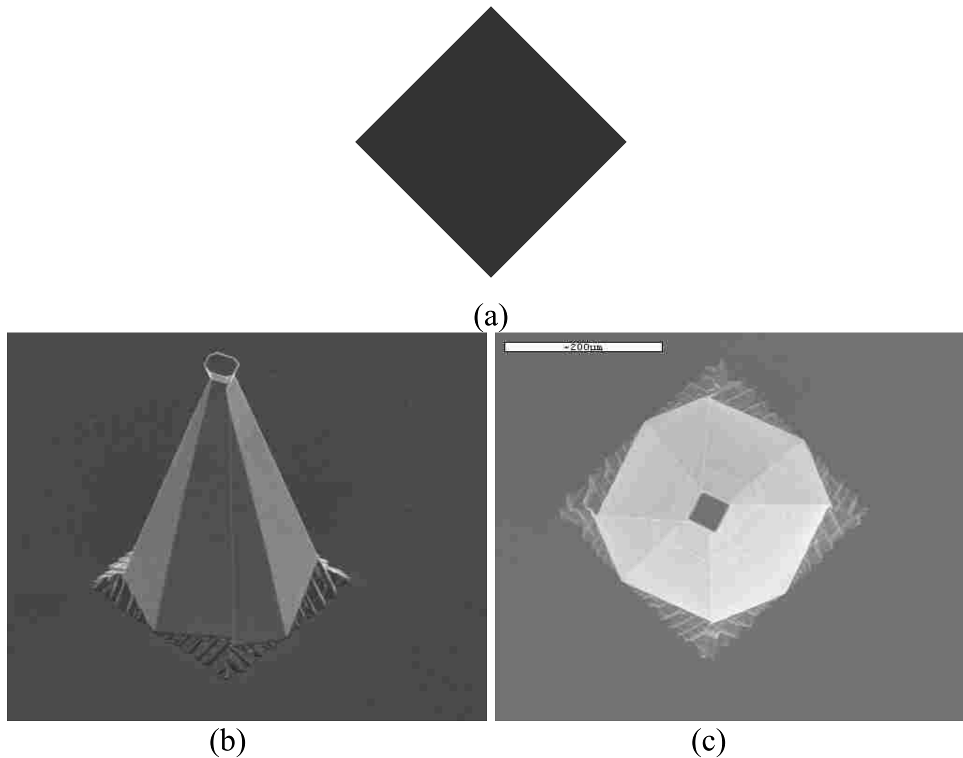

Figure D-15: The square mask in (a) was used to create the unfinished needles seen in (b) and (c).

Etch #9

This etch had new squares on it ranging in these sizes; 970, 985, 1000, 1015, 1030, 1050, 1070, 1085, and 1100 µm square (see Figure D-16). It also had some pinwheel shaped masks on it. The general shape for these masks was found using a simulation program called ACES. There were six different pinwheel shapes. There were three different sized core squares of 900, 945, and 990 µm each with two different sizes of protruding squares as the pinwheel like members these squares were either 20 µm square or 40 µm square. All of the pinwheels with 20 µm square members formed square cross-sectioned needles like those shown in Figure D-17. All of the pinwheels with 40 µm square members formed mesas that would eventually be needles with further etching as shown in Figure D-18. The temperature was set to 79 °C and the etch lasted 8 hours and 2 minutes.

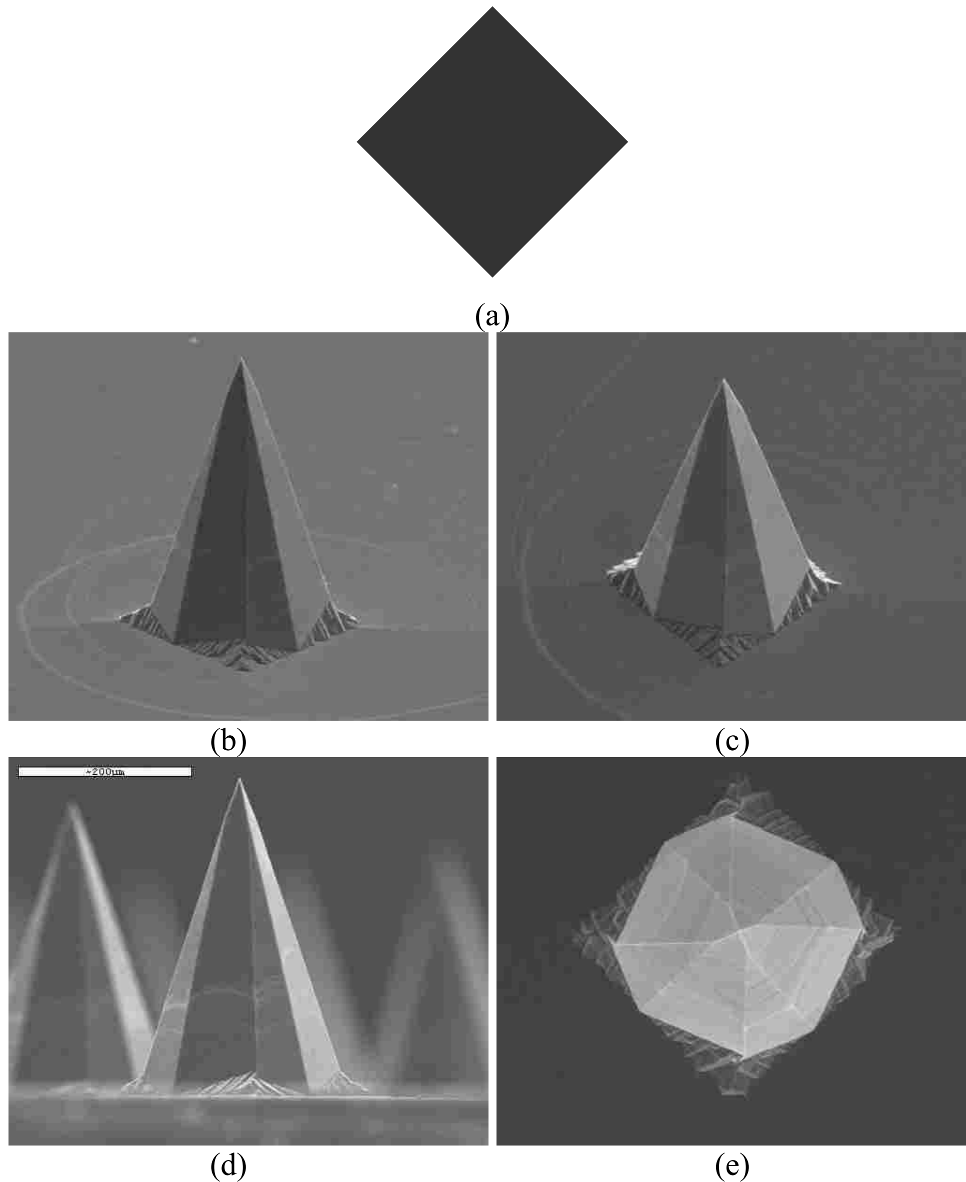

Figure D-16: The 1100µm square mask in (a) created the needles in (b) – (e) shown from various angles.

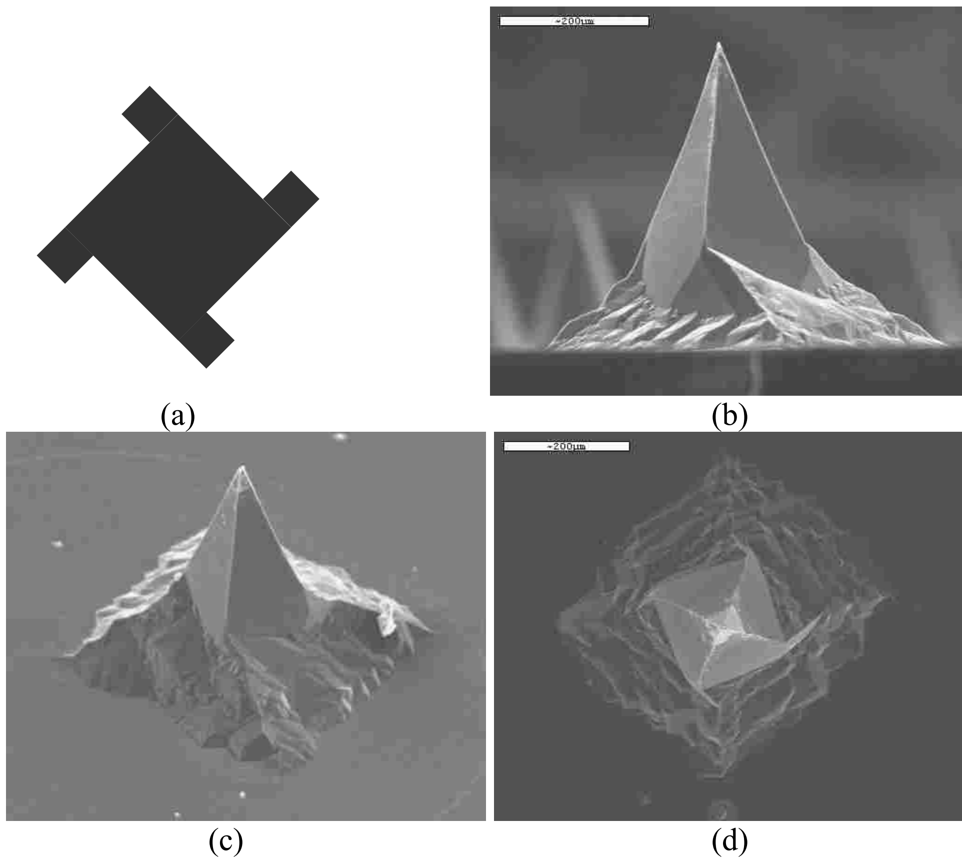

Figure D-17: The mask in (a), with 20µm square pinwheel members, created square needles like those seen in (b), (c), and (d). The height of the needles varied depending on whether the body of the mask was a 900, 945, or 990µm square.

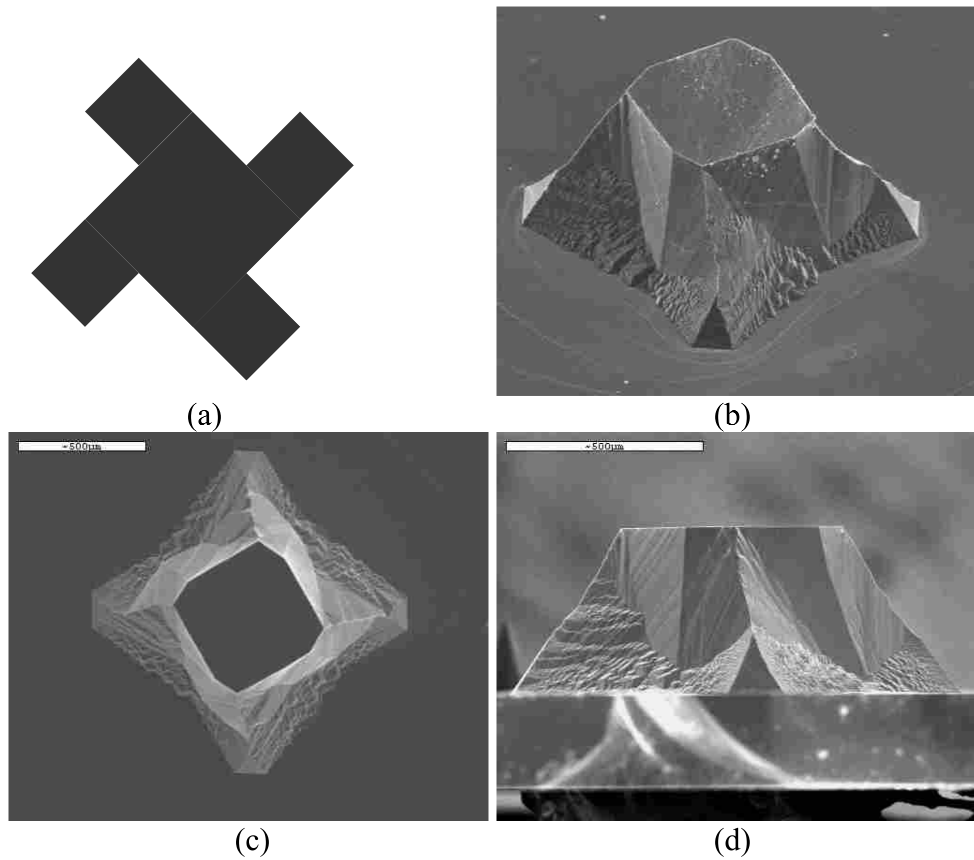

Figure D-18: The mask in (a), with 40µm square pinwheel members, created structures like those seen in (b), (c), and (d). The width of the structures varied depending on whether the body of the mask was a 900, 945, or 990µm square, but all heights of these structures were the same.

Appendix E - Microchannel Fabrication Details

Process steps for the creation of microchannels are described in detail to aid in the repeatability of the fabrication.

When a wafer is prepared it first receives a photoresist coating. HMDS was applied (10 drops, 3000 rpm, 10 seconds) and then the photoresist was applied. This time the photoresist used was SPR-220 7.0. This is a photoresist that will spin on thicker than AZ3330. The photoresist was poured onto the center of the wafer until a pool about 2/3 – 3/4 of the wafer diameter was formed. The photoresist was spun on at 1000 rpm with an acceleration setting of 003 for 60 seconds. This leaves a coating 10-12 μm thick on the top surface of the wafer.

The softbake was done on the hotplate at 110 °C for a minimum of 90 seconds. The softbake had to be done carefully due to the sensitivity of SPR-220. A hotplate is meant to replace the use of an oven, creating the same effect an oven would but in a much quicker time frame. The rapid change in heat can cause bubbles to form in the photoresist which will ruin patterns in the resist and create uneven thicknesses so the wafer must be slowly heated to the softbake temperature. To do this, the wafer is placed on a clean room paper towel and slowly lowered, for about ten seconds, onto the surface of the hotplate. Doing this will help the resist gradually reach its softbake temperature.

After the softbake the resist must cure for about 24 hours. SPR-220 produces toxic fumes when freshly applied so caution must be exercised when using it. The wafer with SPR-220 on the surface should always be stored in a ventilated area until the resist has cured. After curing the resist no longer gives off any fumes so no precautions are necessary to avoid toxicity.

Once the curing is complete the resist will have a pattern exposed onto it. The recipe used in the Karl Suss machine for SPR-220 is very similar to the one used with AZ3330. The two changes are in the "Exposure" settings and the "Alignment Gap" setting which can be seen in the complete recipe listed below.

Karl Suss SPR-220 Settings

Type:	Hard Contact	Resist:	Positive
		Mode:	Manual Align
Max Exposure:	500	WEC:	Contact
Exposure:	50.0 sec	Align Check:	On
Alignment Gap:	90µm	Prealigner Type:	o
Max Contacts:	500		
Hard Contact Delay:	5 sec	Mic/Mask Teach:	Default
		Data Logging:	On

Once the resist has had the mask pattern exposed it must sit for another 2 hours before it can be developed. Once ready the resist is developed in MF 24A for 3 minutes. It is then rinsed for about half a minute in deionized water. After this the wafer receives a hard bake on the hotplate set to 110 °C for 90 seconds. Again the wafer is slowly lowered onto the hotplate to avoid damaging the photoresist layer.

With the completion of the hard bake the wafer will be prepared for the ICP etch. The wafer being etched must be resting on a base wafer. The base wafer should be silicon

without any films or contaminants. This will help preserve the life of the ICP equipment. The base wafer should be no smaller in diameter than the sample being etched and must have a fairly uniform flatness. This will help reduce variations in the heat transfer from the sample wafer to the base wafer.

The two wafers are attached or "glued" together with AZ3330. This is a photoresist that is easy to work with, is removed fairly easily, and is safe to use inside the ICP chamber. To glue the wafer together 11-14 drops of photoresist are randomly dropped on each mating side. A clean room swab is used to "paint" the surface with the resist giving each mating a uniform coating. The two wafers are then gently pressed together to remove any air pockets. The two wafers are then placed on a hotplate set to 90 °C for 60 seconds to help cure the glue. It is better if the photoresist glue can set for 24 hours but not critical. No difference in etch results has been observed from wafers that have or have not had the glue set before etching.

With a base wafer attached to the sample wafer, the ICP etch can be performed. The recipe used for this etch is modified from the default Bosch recipe provided by the manufacturer. The settings for each relevant parameter are shown in Table E-1.

Table E-1: The most up-to-date recipe used in the ICP process for etching microchannels.

<table>
<tr><th></th><th>SF6</th><th>C4F8</th><th>cycle time</th><th>overrun</th><th>coil</th><th>platen</th><th>APC</th><th>total time</th></tr>
<tr><td>Etch</td><td>120</td><td>0</td><td>9</td><td>0</td><td>600</td><td>15</td><td rowspan="2">84.2</td><td rowspan="2">4 hr 20 min</td></tr>
<tr><td>Passivate</td><td>0</td><td>85</td><td>6</td><td>0</td><td>600</td><td>0</td></tr>
</table>

This recipe was found by several experimental etches and observation of performance. A history of this experimentation can be found in Appendix F. The current recipe still has

limitations and can probably be improved with greater effort and time dedicated to its enhancement.

The ICP process is automatic and can be left alone for the entire duration of the etch, however, sometimes a problem can occur, whether it be a drop in gas pressure or a power loss. This kind of event will automatically stop the etch so it is recommended that the user check on the etch status from time to time. At the end, after the sample is removed from the chamber, a blank wafer will be placed in the chamber for a 20 minute oxygen cleaning. This cycle will purge out the chamber so that it can be used by others. More complete instructions on how to use and run the ICP equipment are found in Appendix G.

Appendix F - ICP Etch Experimentation

The following gives a chronological account of the recipes and experimental changes that were made to be able to etch the microchannels currently being fabricated. Etches #1-9 show a recipe, the procedure, a discussion of the results and conclusions, as well as SEM images to illustrate the results.

Etch #1

In this etch the recipe is given in Table F-1, followed by a brief statement of procedure, results, and conclusion (with any other pertinent information added as well), after which the results in Figure F-1 – Figure F-4 can be seen.

Table F-1: Recipe used in etch #1

<table>
<tr><th></th><th>SF6</th><th>C4F8</th><th>cycle time</th><th>overrun</th><th>coil</th><th>platen</th><th>APC</th><th>total time</th></tr>
<tr><td>Etch</td><td>130</td><td>0</td><td>8</td><td>0</td><td>600</td><td>15</td><td rowspan="2">84.2</td><td rowspan="2">30 min</td></tr>
<tr><td>Passivate</td><td>0</td><td>85</td><td>5</td><td>0</td><td>600</td><td>0</td></tr>
</table>

Photoresist: AZ3330 about 1-2 µm thick
Procedure: Two etches were done
Etch 1A was a thirty minute etch
Etch 1B: some of the samples from Etch 1A were recoated with AZ3330 and etched for another 30 min
Results: Etch 1A ~ 110 µm, Etch 1B ~ 200 µm
Conclusion: two separate etches with two separate coatings of photoresist will not give an adequate channel profile

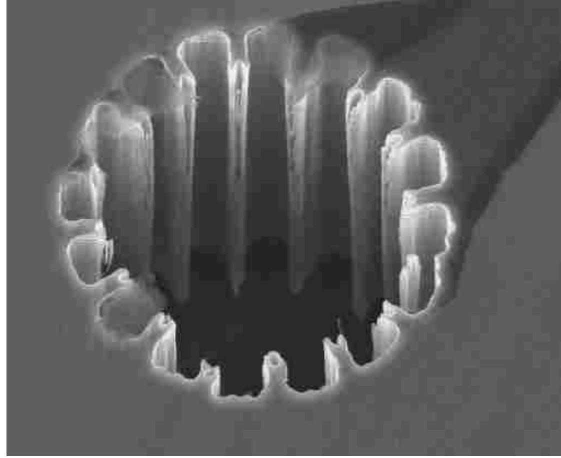

Figure E-1: This channel is 110µm deep and shows the ridges of the channel just as they appear on the mask. A polymer residue has been left on the surface of the wafer.

Figure F-2: When the photoresist for the second etch was spun on, it flowed around existing hole like water around a rock. Three levels can be seen here. The top level is the egg shaped hole that etched from the top surface during the second etch period. The second level is the last remnants of hole from the first etch period. This is estimated to be about 10µm thick. The hydrophobic structures can still be seen along the perimeter. The third level is the rough walled circle in the middle. This is about 100µm deeper than the initial etch so it reaches about 210µm into the wafer substrate. It was etched during the second etch period.

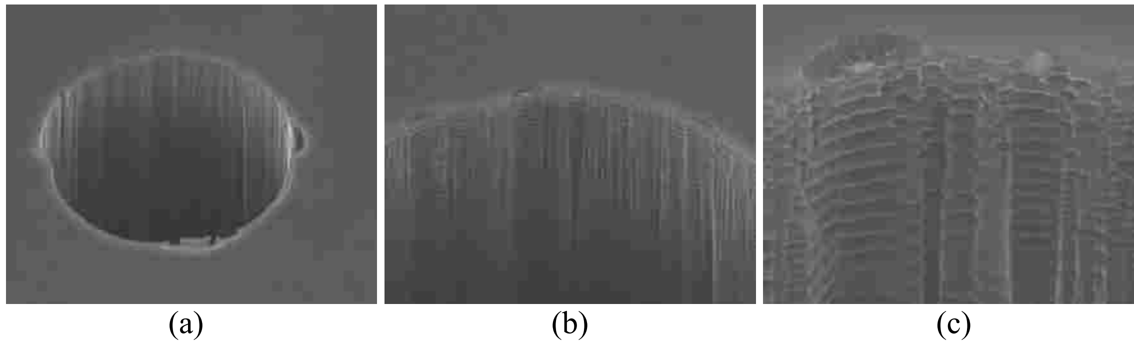

(a) (b) (c)

Figure F-3: The three images here show sequentially zoomed-in portions of the same hole. Small ridges can be seen clearly when zoomed in sufficiently indicating the distance that is etched during each etch/passivation cycle of the ICP process.

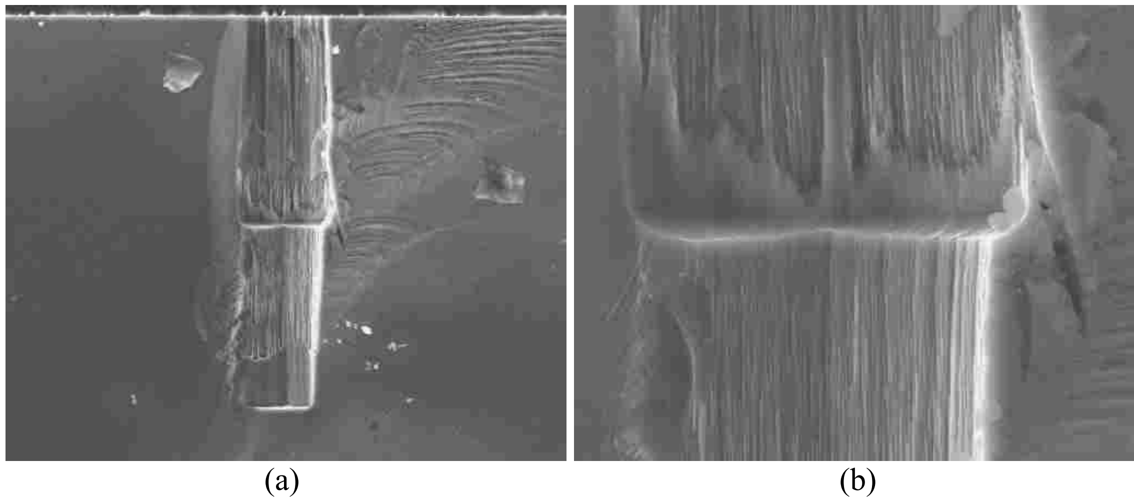

(a) (b)

Figure F-4: Here, a close-up view of a single channel that has undergone the double etch process shows the effects that take place after long periods of etching. In the image on the right, the small ridges that indicate a good sidewall are being etched away and large sidewall striations are left in their place.

Etch #2

In this etch the recipe is given in Table F-2, followed by a brief statement of procedure, results, and conclusion (with any other pertinent information added as well), after which the results in Figure F-5 can be seen.

Table F-2: Recipe used in etch #2

	SF6	C4F8	cycle time	overrun	coil	platen	APC	total time
Etch	130	0	8	0	600	15	84.2	45 min
Passivate	0	85	6	0	600	0		

Photoresist: SPR-220, 7.0 ~ 10 µm thick (all subsequent etches will use this photoresist at this thickness unless otherwise stated)
Procedure: glued (photoresist as adhesive) two-thirds of a full wafer to the base wafer, not all clamps were holding down the etch wafer
Results: etched stopped prematurely due to burnt looking surface on wafer and bubbles forming in photoresist
Conclusion: Etch wafer not clamped down solidly to base wafer, poor heat transfer between wafers led to burning and bubbles in photoresist

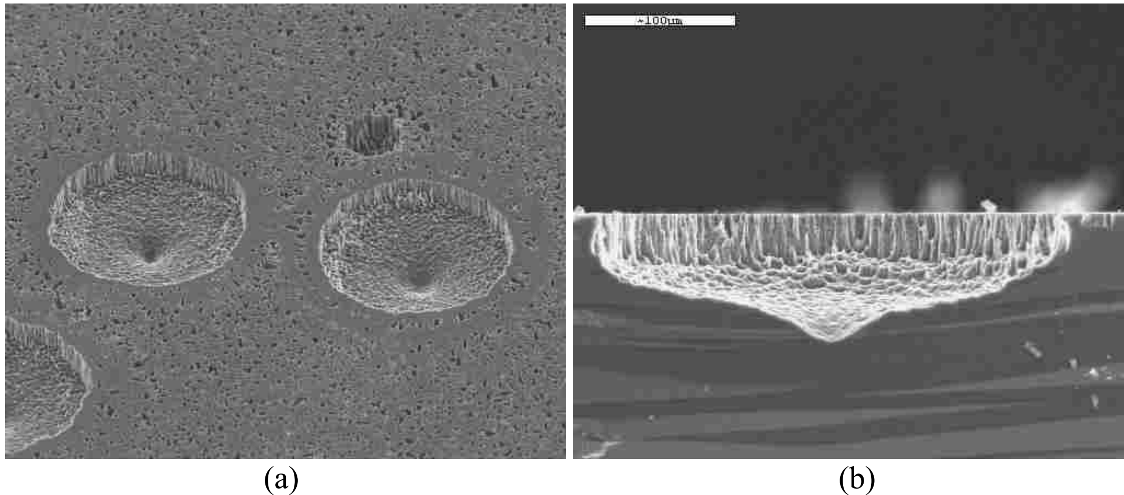

(a) (b)

Figure F-5: A top and side view shows where bubbles formed in the photoresist and created large holes in the substrate. The left image shows a small hole intentionally created from the mask just above the two accidental holes.

Etch #3

In this etch the recipe is given in Table F-3, followed by a brief statement of procedure, results, and conclusion (with any other pertinent information added as well), after which the results in Figure F-6 can be seen.

Table F-3: Recipe used in etch #3

	SF6	C4F8	cycle time	overrun	coil	platen	APC	total time
Etch	130	0	8	0	600	15	84.2	3 hr 30 min
Passivate	0	85	6	0	600	0		

Procedure: a repeat of the previous etch with a whole wafer. The photoresist was only exposed for 20-30 seconds in the Karl Suss
Results: shallow channels (not very deep), a lot of "grass", diameter too small
Conclusion: could not etch as deep because there was a thin layer of photoresist covering the feature area

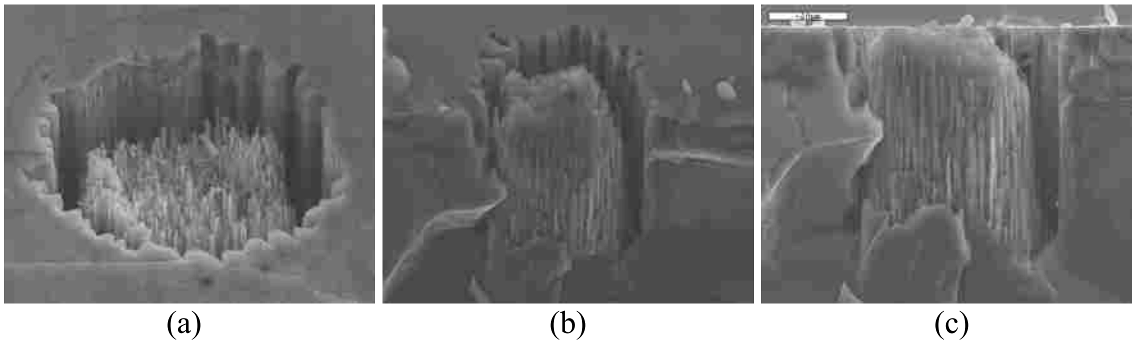

(a) (b) (c)

Figure F-6: Top and side views of a hole that was etched around the perimeter but had too much unexposed (and therefore undeveloped) photoresist blocking the etch. This physical phenomenon is known as "grass" and is a result of micromasking which can occur from photoresist or from heavy passivation.

Etch #4

In this etch the recipe is given in Table F-4, followed by a brief statement of procedure, results, and conclusion (with any other pertinent information added as well), after which the results in Figure F-7 can be seen.

Table F-4: Recipe used in etch #4

	SF6	C4F8	cycle time	overrun	coil	platen	APC	total time
Etch	130	0	8	0	600	15	84.2	3 hr 30 min
Passivate	0	85	6	0	600	0		

Procedure: increased exposure in the Karl Suss to 50 seconds, accidental misalignment with nitride mask (below photoresist) required a second exposure so there are double channels side by side at every location there should be only one channel.
Results: Two channels, one is shorter than the other because of the nitride mask that had to be etched through before etching of the silicon wafer could begin
Conclusion: need a longer etch time to break through the wafer and caution should be exercised when exposing the photoresist

(a) (b)

(c) (d)

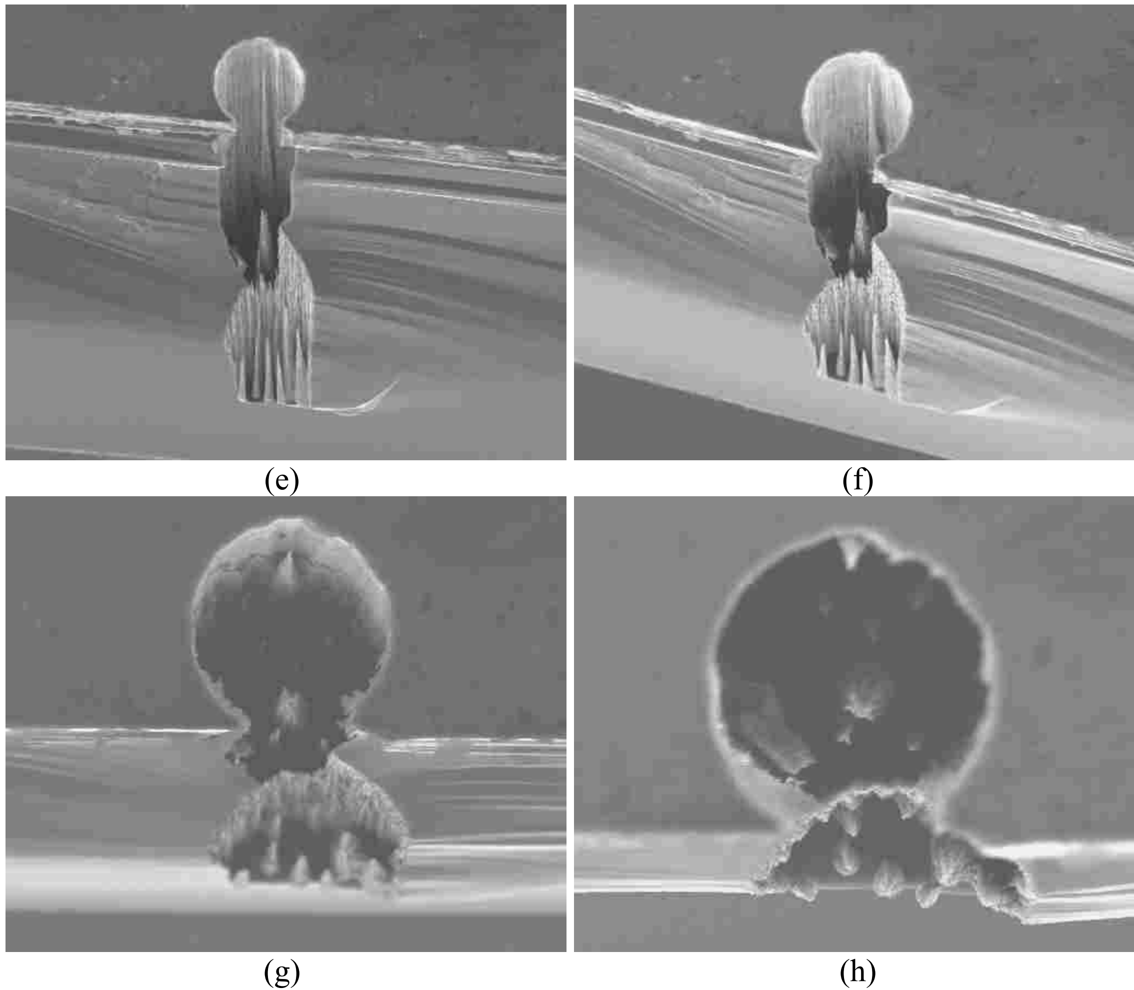

Figure F-7: A series of images shows the same double hole progressing from a side to a top view. As can be determined from the stalagmite looking structures at the base of this hole, there was slight micromasking during the etch.

Etch #5

In this etch the recipe is given in Table F-5, followed by a brief statement of procedure, results, and conclusion (with any other pertinent information added as well), after which the results in Figure F-8 – Figure F-9 can be seen.

Table F-5: Recipe used in etch #5

<table>
<tr><th></th><th>SF6</th><th>C4F8</th><th>cycle time</th><th>overrun</th><th>coil</th><th>platen</th><th>APC</th><th>total time</th></tr>
<tr><td>Etch</td><td>130</td><td>0</td><td>8</td><td>0</td><td>600</td><td>15</td><td rowspan="2">84.2</td><td rowspan="2">4 hr 30 min</td></tr>
<tr><td>Passivate</td><td>0</td><td>85</td><td>6</td><td>0</td><td>600</td><td>0</td></tr>
</table>

Procedure: increased etch time
Results: successful through-wafer etch, the channel tapers at the bottom and there is significant grass, stalagmites coming from the bottom, and striations on the walls
Conclusion: recipe needs to change a little bit to reduce effects on the feature characteristics

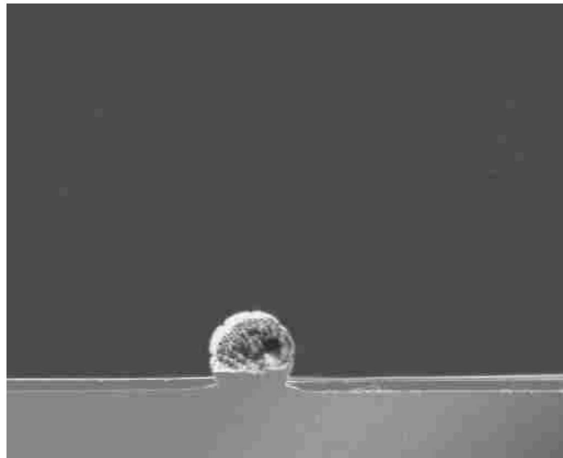
(a)

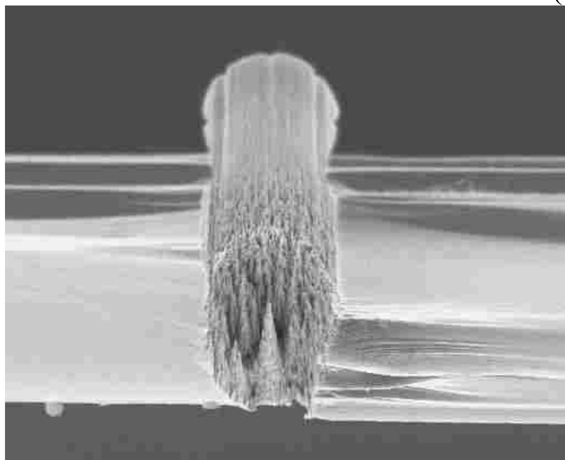
(b)

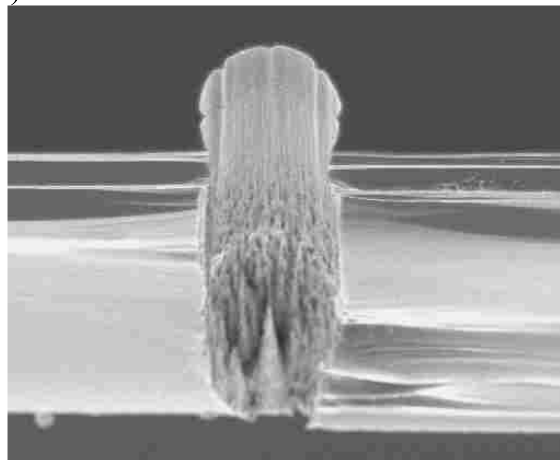
(c)

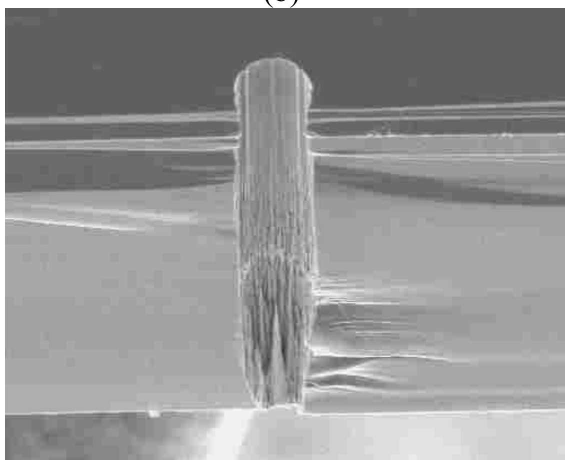
(d)

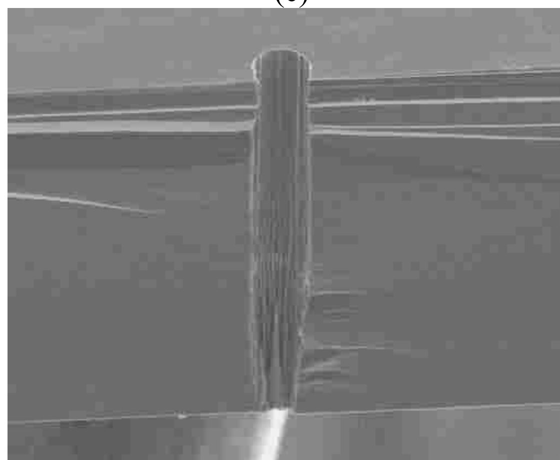
(e)

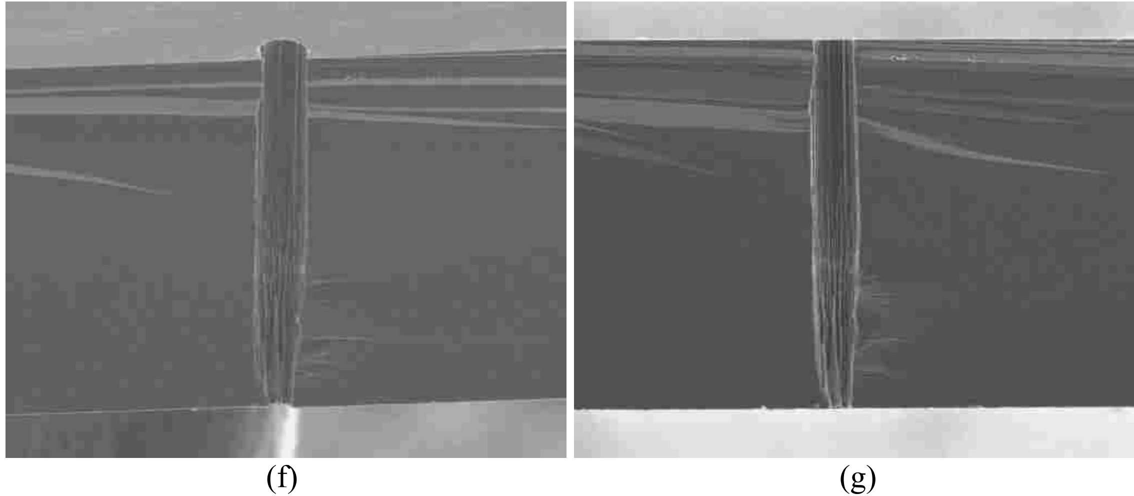

(f) (g)

Figure F-8: A series of angles reveals the quality of the etch recipe on a single channel. The channel tapers at the bottom and heavy striations on the side wall are revealed.

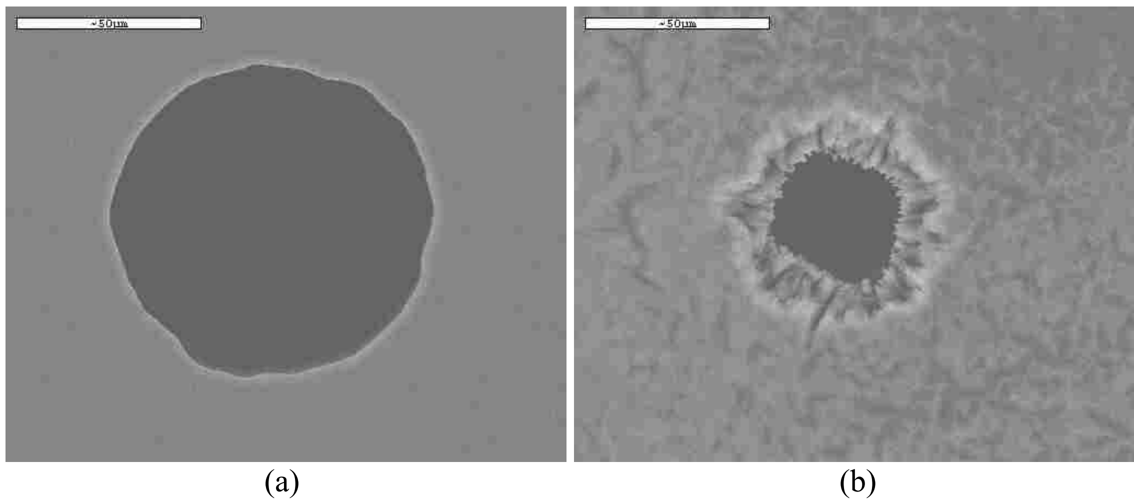

(a) (b)

Figure F-9: These two images were taken at the same magnification and show the difference in diameter of the same size hole between the top and the bottom side of a wafer. The image on the right shows the "blowout" that occurs at the bottom of the wafer due to the nitride mask on the backside of the wafer.

Etch #6

In this etch the recipe is given in Table F-6, followed by a brief statement of procedure, results, and conclusion (with any other pertinent information added as well), after which the results in Figure F-10 can be seen.

Table F-6: Recipe used in etch #6

	SF6	C4F8	cycle time	overrun	coil	platen	APC	total time
Etch	120	0	15	0.5	600	12	65	60 min
Passivate	0	85	7	0	600	0		

Procedure: new ICP recipe based on conclusions from literature review
Results: while viewing chamber, when the plasma gasses change from C4F8 to SF6 there is a bright green flash followed by a moment of darkness before the new plasma is seen. Furthermore, the photoresist was applied poorly showing many thin spots on the wafer. The etch was stopped prematurely after 1 hour.
Conclusion: after subsequent testing it was found that an increase in the overrun time for the passivation cycle solved the problem of the flashes but it is also expected that low pressure may have also contributed to the problem

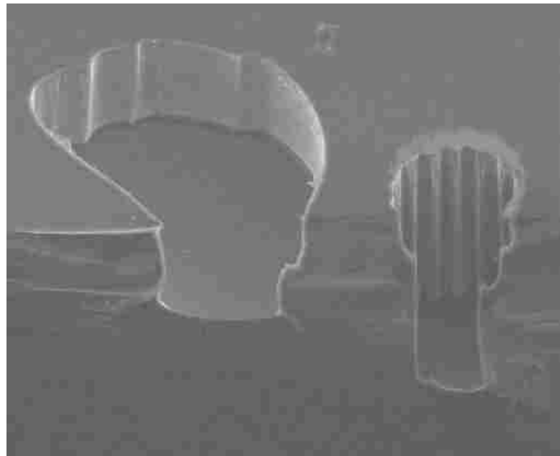

Figure F-10: This image shows an intentional hole (on the right) next to a "burnt" hole (on the left). The accidental hole has a different sidewall profile from that in etch #2 and is most likely due to a poor application of photoresist.

Etch #7

In this etch the recipe is given in Table F-7, followed by a brief statement of procedure, results, and conclusion (with any other pertinent information added as well), after which the results in Figure F-11 can be seen.

Table F-7: Recipe used in etch #7

<table>
<tr><th></th><th>SF6</th><th>C4F8</th><th>cycle time</th><th>overrun</th><th>coil</th><th>platen</th><th>APC</th><th>total time</th></tr>
<tr><td>Etch</td><td>120</td><td>0</td><td>15</td><td>0</td><td>600</td><td>12</td><td rowspan="2">65</td><td rowspan="2">3 hr 50 min</td></tr>
<tr><td>Passivate</td><td>0</td><td>85</td><td>7</td><td>0.4</td><td>600</td><td>0</td></tr>
</table>

Procedure: an overrun time of 0.4 sec is added to the passivation cycle
Results: the photoresist mask on the wafer was completely etched through, as well as most of the nitride mask. Channels are very non-anisotropic although they do have a flat bottom. Literature indicates that low pressure (low APC setting) and high etch cycle times will both increase resist etching, when these parameters are combined the problem escalates
Conclusion: decrease etch cycle time relative to passivation cycle time and increase the pressure (APC setting)

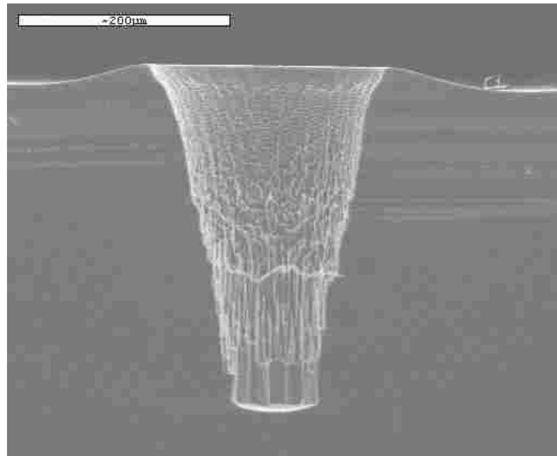

Figure F-11: The image of this channel reveals how a poor recipe can give disappointing results. It is interesting to note that the top surface of the wafer rises a little at the mouth of the hole. This is the way the photoresist settles on top of the wafer but as the photoresist is burned through, as happened on this etch, it elevation differences are magnified onto the substrate.

Etch #8

In this etch the recipe is given in Table F-8, followed by a brief statement of procedure, results, and conclusion (with any other pertinent information added as well), after which the results in Figure F-12 can be seen.

Table F-8: Recipe used in etch #8

<table>
<tr><th></th><th>SF6</th><th>C4F8</th><th>cycle time</th><th>overrun</th><th>coil</th><th>platen</th><th>APC</th><th>total time</th></tr>
<tr><td>Etch</td><td>120</td><td>0</td><td>9</td><td>0</td><td>600</td><td>14</td><td rowspan="2">84.2</td><td rowspan="2">4 hr 30 min</td></tr>
<tr><td>Passivate</td><td>0</td><td>85</td><td>6</td><td>0</td><td>600</td><td>0</td></tr>
</table>

Procedure: ratio of etch to passivation cycle time is reduced, pressure is increased and the total etch time is also increased to compensate for reduction of etch cycle time. The overrun time is also dropped as it is not needed (it was there to keep the plasma gas transitions stable) with the higher pressure settings
Results: successful through etch, there is some slight necking and bowing throughout the channel, and there is some extreme "blowout" at the bottom of the channel, also the channel is generally to wide
Conclusion: the blowout comes from the existence of a nitride mask on the wafer backside, wide channels indicates the poor selectivity ratio of the photoresist to the silicon, tweak the recipe

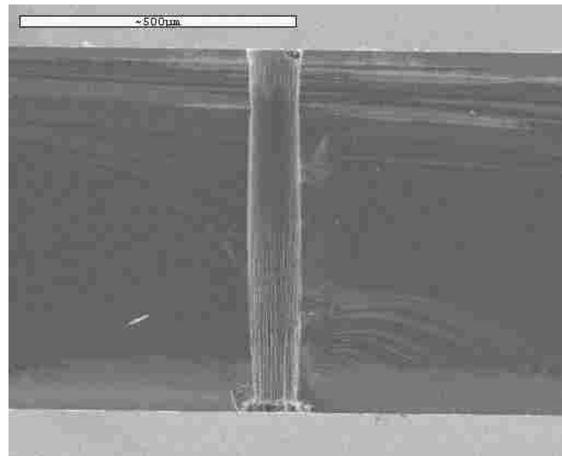

Figure F-12: A fairly anisotropic channel going all the way through the wafer is shown.

Etch #9

In this etch the recipe is given in Table F-9, followed by a brief statement of procedure, results, and conclusion (with any other pertinent information added as well), after which the results in Figure F-13 can be seen.

Table F-9: Recipe used in etch #9

<table>
<tr><th></th><th>SF6</th><th>C4F8</th><th>cycle time</th><th>overrun</th><th>coil</th><th>platen</th><th>APC</th><th>total time</th></tr>
<tr><td>Etch</td><td>120</td><td>0</td><td>9</td><td>0</td><td>600</td><td>15</td><td rowspan="2">84.2</td><td rowspan="2">4 hr 20 min</td></tr>
<tr><td>Passivate</td><td>0</td><td>85</td><td>6</td><td>0</td><td>600</td><td>0</td></tr>
</table>

Procedure: slight changes in recipe
Results: channels look good except for some slight signs of photoresist depletion around the edges of the mouth of the channel. Could not get a good cross-sectional view of an entire channel but generally it appears that the necking and bowing problem has been reduced. Ran out of nitride when starting etch so re-ran the etch, total time is probably closer to 4 hour 30 minutes
Conclusion: perform a second trial with this recipe

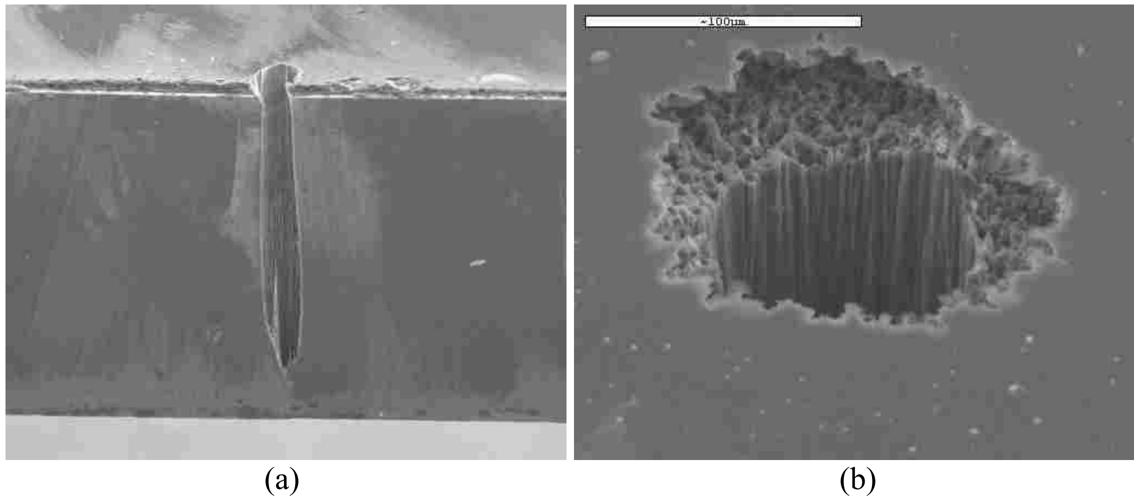

(a) (b)

Figure F-13: Although a perfect cross-section of this channel hasn't been made yet, surveying this channel gives good indications of decent anisotropy. The image on the right shows a close-up view of the blowout that has occurred.

Appendix G - ICP Operation Instructions

Steps for using the ICP RIE for the Bosch Process

Startup

1. Check that the RF power counsel and chiller is on.
2. Check to make sure power is on main controller
3. Turn on nitrogen. (You may need to turn on the green and black valves.) After the nitrogen has been turned on, all the green lights except for the process light should be on.
4. For Bosche etch turn on C_4F_8, SF_6, and He gases in the back room. The O_2 should also be on, but that is usually always on.
5. Make sure main controller is set to 600 Hz.

Processing Wafers

1. Click on edit tab. Change from Operator Mode to Development mode. Password is **dev**. Hit enter.
2. Change mode to active by clicking on mode on main screen. At this point the machine will go through some steps to make sure everything is ready. Wait until you receive the ready prompt at the bottom of the screen.
3. Fill in Log book. He value will need to be added when taking data. Mask is the type of photo resist or oxide layer you are using to mask the path of the RIE.
4. Click on the recipe button to change or create a new recipe. SIBOSCH.set is a good starting point.
    - With the recipe do not change first two steps.
    - The third step is where you want to change your parameters
        - Do not change anything in the back cooling, leak test and pressure .
    - For Bosch etch make sure SF6 is set to etch and C4F8 is set to passivation. The passivation step deposits material onto wafer
    - Save your recipe and close
6. On main console click on Vent
7. When there are no alarms and it says ready put your wafer in the holder. Align flat with mark on wafer holder.
8. Click on Load button and put manual hand pressure on top lid to seal tight.
9. Following the Load step visually inspect to make sure that the clamps are holding the wafer. This might require the use of a flashlight. Also wait for status prompt to say ready.
10. Now go to select button click on it and select the recipe that you want to use.
11. Wait until status prompt says ready
12. Click on Process button, following the process of etching the wafer it will pump out the gases out of the chamber. When this is done the status prompt should say ready.
13. Click on unload

14. Following the **unload** step, click on **vent**.
15. Remove the processed wafer.
16. Click on load. (We are making the machine believe that a new wafer has been loaded and unloaded so that we can keep the lid sealed) *If you did have another wafer that needed to be processed it would be loaded back in at this time and you would start at step seven.*
17. Click on unload

Shut down

1. Change mode back to inactive, by clicking on mode button and selecting inactive.
2. Edit tab and change back to monitor mode.
3. Turn off the gases that were turned on.

Appendix H - Human Pain Testing Draft for IRB Committee Approval

The following document is a draft written to the IRB committee in attempt to attain approval for human pain testing with the microneedles. The approval was denied because at the time no proof of fabricated needles yet existed. It was also requested that only one needle array be tested per person per location unless possibility of "prion" contamination could be controlled without question during needle sterilization.

Specific Aims

The purpose of this research is to design and fabricate silicon microneedles with the capability of penetrating the skin deep enough to deliver some types of medication with out penetrating so deep that they cause pain to the patient.

Hypothesis

Primary hypothesis: The 400 μm microneedles in this research do not penetrate the human arm, hand, and abdominal skin deep enough to cause pain to the research subject.

Secondary hypothesis: The microneedles that have fluid channels maintain their structural integrity when inserted into the human skin.

Background and Significance

Out-of-plane silicon microneedles are micro-sized silicon needles that project from the surface of a silicon substrate and contain channels through the center that allow for administration of medication when inserted into the skin. Microneedles are so advantageous because they allow for the transdermal administration of medication

without the accompanying pain that we commonly experience when receiving a typical injection with, say, a hypodermic needle. Microneedles also deliver more types of medication at a faster delivery rate than do other forms of transdermal medical administration like a skin absorption patch.

The technology to create microneedles has existed for about five years now and companies and industries across the globe are researching microneedle designs in order to prepare them for clinical use. Some of the existing designs that have been made (not from BYU) are shown in Figure H-1.

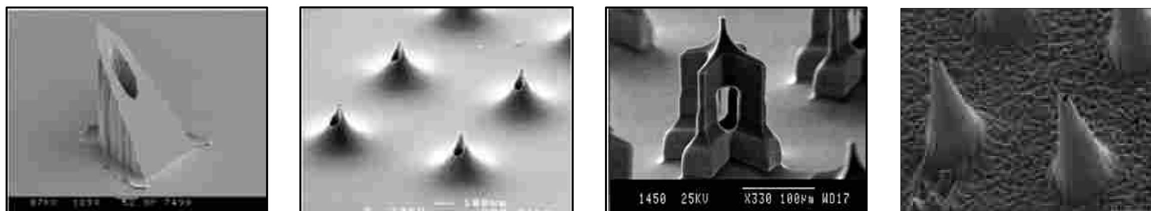

Figure H-1: Images of microneedles from other research groups (Gardeniers 2003, Stoeber 2005, Griss 2003, McAllister 1999)

The purpose of this research is to test a similar microneedle design created at BYU. The microneedles will look something like those in Figure H-2.

These microneedles will be 400 μm high and will be in arrays of 64 needles each filling an area of about 1.5 X 2.0 cm^2. The purpose of the structure channels, as seen in some of the images in Figure H-2, is to give a hydrophobic or water repellent effect to the channels. The application of hydrophobic channels has not been seen in other microneedle studies and is considered to be one of the more original portions of the research.

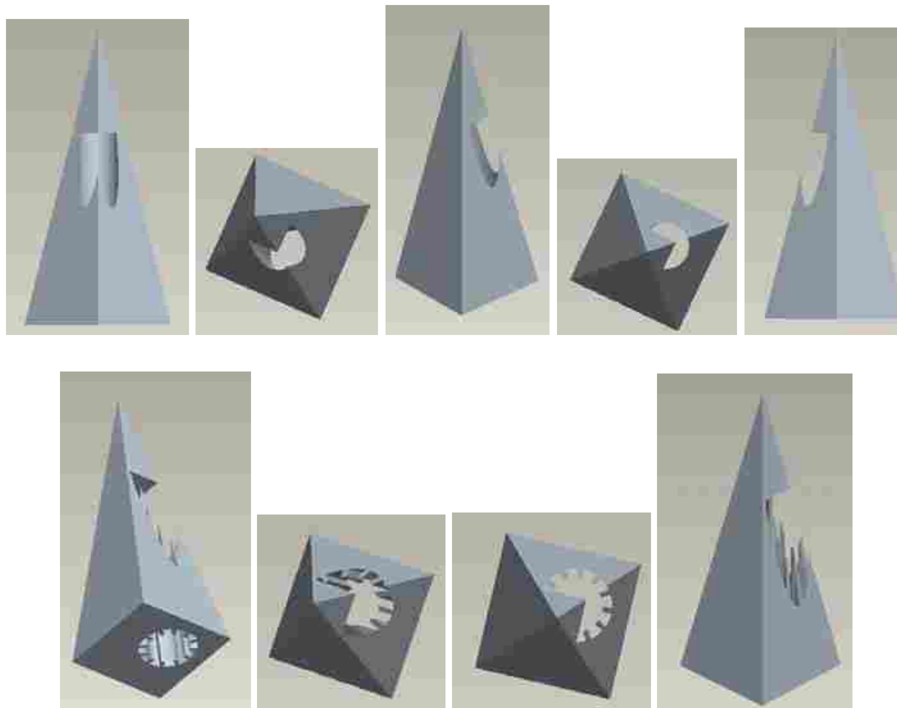

Figure H-2: CAD images of the BYU microneedle designs with and with out channel structures. (Diehl 2005)

Silicon, from which the microneedles are made, is a safe material to use in dermal medical procedures. Studies of human skin have shown that the epidermal layer of the skin, which is the topmost layer of skin, is typically between 200 and 300 µm. (Alper 2004) Below the first layer of skin is the dermis, where blood vessels and nerve endings reside. A needle that is inserted only as deep as or a little deeper than the epidermal layer of skin should not cause any painful sensation to the patient because it will not penetrate deeply enough to disturb the pain sensitive nerve endings. Testing of other microneedle designs has shown that microneedles up to 900 µm long can be inserted into the skin without causing any noticeable pain to research subjects. (Moon 2005)

The testing of human subjects in this research is primarily to validate the design of the microneedles to ensure that they are not too long. A microneedle that is too long will

cause minimal localized pain and nullify the advantage of microneedles as a painless form of injection. A limited amount of testing on human research subjects will also be done to verify the needle integrity after several punctures. The needles are expected to be able to withstand the forces associated with a puncture through human skin without being damaged. However, testing will be done to verify this as well.

The test chips used to study the possible pain associated with microneedles will contain needles without flow channels going through them and will look something like the image in Figure H-3. The test chips that will be used for the study of needle integrity will contain flow channels and will look like the chip in the image in Figure H-4. If there is any pain associated with insertion it should not vary between chips with or without channels due to the fact that pain is primarily a function of the length of the needle and not of the existence of a channel.

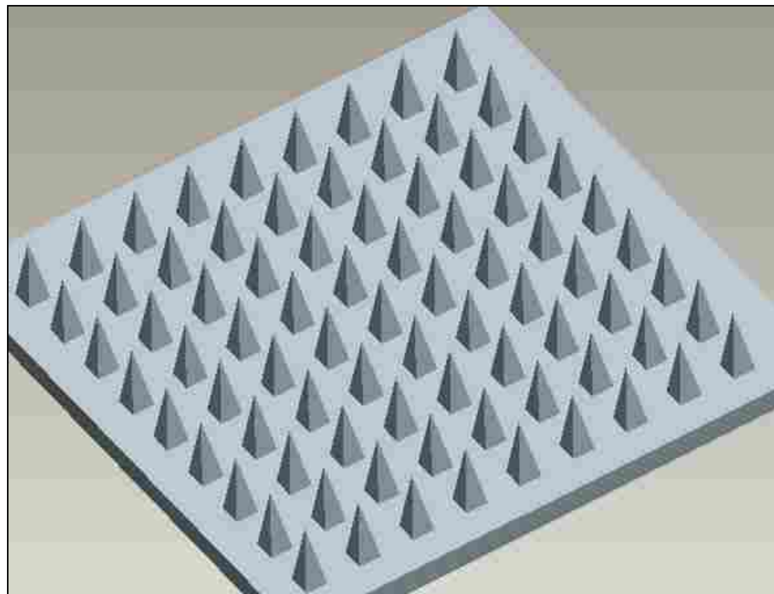

Figure H-3: Computer rendering of a silicon chip of an array of microneedles without channels. This would be used for the testing of pain associated with needle insertion.

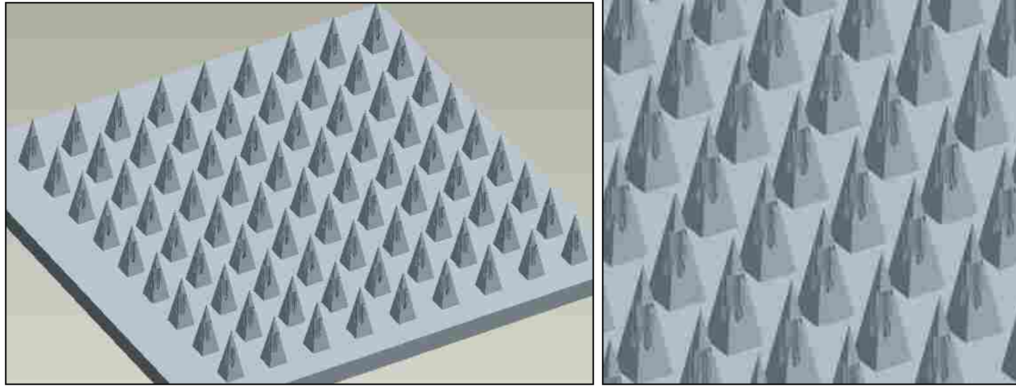

Figure H-4: Computer renderings of a silicon chip of an array of microneedles with channels. This would be used for the testing of needle structure integrity associated with insertion.

Description of Subjects

The research subjects in this testing will be adults 18 years and older. There will be an even mix of male and female research subjects that will be selected through convenience sampling. Research subjects will be screened to avoid anyone who is pregnant, has had nerve or spinal damage, has had a history of uncontrollable bleeding, or who is currently experiencing any unusual epidermal conditions in the areas of the body that are intended for testing. Any testing of the research subject will be conditional upon the signing of a consent form.

Confidentiality

The data that is collected in this experiment will not be linked to a name or any identification number associated with the research subject. Only research specific information, such as gender, will be recorded.

Method and Procedures

The research subject will be administered to by either a nurse or a student nurse (hereafter referred to as the "nurse"). The nurse and the research subject will both be behind a curtain or solid partition where they cannot be seen by anyone else. This is to give a comfortable level of privacy to the research subject. The same nurse will perform all the tests for all research subjects. This will reduce the variation in administration styles.

As the research subject enters the testing area there will be several silicon chips that have been thoroughly soaked in rubbing alcohol for at least 60 seconds to disinfect them of any airborne contaminants. Some of these chips will have microneedles fabricated on them and some will be blank to serve as control chips in the experiment. The nurse will apply these chips in a predetermined random order (mixing use of the control chips with the real chips) to different parts of the body including the top side of the forearm, the under side of the forearm, the back side of the hand, and the abdomen (at least 2 inches away from the belly button). The research subject will not be aware of whether the chip is a blank or contains microneedles. The nurse will apply the chips by pressing the chips against the skin with her fingers for at least 2-3 seconds after which she will ask the patient for a response regarding any pain or other sensation that is felt. The temperature of these chips will be kept at room temperature or higher to avoiding confusing the research subject as to whether they are feeling pain or a temperature sensitive sensation.

The primary investigator will be outside the curtain or partition recording the responses of the research subjects. Since the research subjects will be both male and female the

nurse performing the administration will be female, the biggest concern, of course, being the privacy of female research subjects as their abdomen is tested. After the test has been administered, all areas where a chip has been placed will receive an application of antibiotic ointment to help prevent infection. After the testing has been completed the silicon chips will be put into an autoclave where they will undergo sterilization for 30 minutes to an hour at a temperature of 121 °C and a pressure of 15-18 psi (a little higher than atmospheric pressure). This is to ensure a completely sterile needle that can be reused for further testing.

The testing of microneedles that contain flow channels will be done in a similar manner as those mentioned above except that they will be examined by either an optical microscope or a scanning electron microscope to view if any damage has been done to the needle.

Data Analysis

The data analysis will simply be a statistical analysis to find if any of the variables in the tests show increased probability of any pain in the microneedle administration. These variables will include gender, race/ethnicity (this variable is added in case race and skin thickness are related in any way), location on the body, and perception of a pain sensation by the research subject.

Risks

Risks include possible minimal site infection and minimal localized pain. As stated previously, an antibiotic ointment will be applied to all sites on the skin where testing was performed to reduce the risk of infection.

Benefits

There are no direct benefits to the research subjects. The benefit to society is the development of an effective and painless form of transdermal drug delivery for some types of drugs.

Compensation

There will be no compensation for participation.

References

Moon, Sang Jun and Lee, Seung S.; "A novel fabrication method of a microneedle array using inclined deep x-ray exposure". Journal of Micromechanics and Microengineering, March 2005, p.903-911.

Diehl, Michael S.; "Increased Flow Rate in Microneedles Using Hydrophobic Microchannels". Brigham Young University, Ira A. Fulton College of Engineering and Technology, Department of Mechanical Engineering, Thesis Proposal, September 2005.

Alper, M.; Kavak, A.; Parlak, A. H.; Demirci, I. Belenli; and Yesilda N.; "Measurement of epidermal thickness in a patient with Psoriasis by computer-supported image analysis". Brazilian Journal of Medical and Biological Research, January 2004, p.111-117.

Gardeniers, H. J. G. E.; Luttge, R.; Berenschot, E. J. W.; de Boer, M. J.; Yeshurun, S. Y.; Hefetz, M.; van't Oever, R.; and van den Berg, A.; "Silicon Micromachined hollow microneedles for transdermal liquid transport". Journal of Microelectromechanical Systems, December 2003.

Stoeber, B. and Liepmann, D.; "Arrays of hollow out-of-plane microneedles fro drug delivery". Journal of Microelectromechanical Systems, June 2005.

Griss, P. and Stemme, G.; "Side-opened out-of-plane microneedles for microfluidic transdermal liquid transfer". Journal of Microelectromechanical Systems, June 2003.

McAllister, D. V.; Cros, F.; Davis, S. P.; Matta, L. M.; Prausnitz M. R.; and Allen M. G.; "Three-dimensional hollow microneedle and microtube arrays". Transducers 99, Int. Conf. Solid-State Sens. Actuators, 10th, Sendai, Japan, 1999.

Qualifications

An individual who knows how to perform statistical analysis of the data collected is needed. This person will be the primary investigator who has knowledge and experience in this field based from some statistics classes which focus on statistical methods and design of experiments. The primary investigator has also had experience executing experimental designs in other former research work.